Receive Soft Antenna Selection for Noise-Limited/Interference MIMO Channels

by

Javad Ahmadi Shokouh

A thesis
presented to the University of Waterloo
in fulfillment of the
thesis requirement for the degree of
Doctor of Philosophy
in
Electrical and Computer Engineering

Waterloo, Ontario, Canada, 2008

© Javad Ahmadi Shokouh 2008

Declaration

I hereby declare that I am the sole author of this thesis. This is a true copy of the thesis, including any required final revisions, as accepted by my examiners.

I understand that my thesis may be made electronically available to the public.

Abstract

Although the Multi-Input and Multi-Output (MIMO) communication systems provide very high data rates with low error probabilities, these advantages are obtained at the expense of having high signal processing tasks and the hardware cost, e.g. expensive Analog-to-Digital (A/D) converters. The increased hardware cost is mainly due to having multiple Radio Frequency (RF) chains (one for each antenna element). Antenna selection techniques have been proposed to lower the number of RF chains and provide a low cost MIMO system. Among them, due to a beamforming capability Soft Antenna Selection (SAS) schemes have shown a great performance improvement against the traditional antenna sub-set selection methods for the MIMO communication systems with the same number of RF chains. A SAS method is basically realized by a pre-processing module which is located in RF domain of a MIMO system. In this thesis, we investigate on the receive SAS-MIMO, i.e. a MIMO system equipped with a SAS module at the receiver side, in noise-limited/interference channels. For a noise-limited channel, we study the SAS-MIMO system for when the SAS module is implemented before Low Noise Amplifier (LNA), so-called pre-LNA, under both spatial multiplexing and diversity transmission strategies. The pre-LNA SAS module only consists of passive elements. The optimality of the pre-LNA SAS method is investigated under two different practical cases of either the external or internal noise dominates. For the interference channel case, the post-LNA SAS scheme is optimized based on Power Angular Spectrum (PAS) of the received interference signals. The analytical derivations for both noise-limited and interference channels are verified via the computer simulations based on a general Rician statistical MIMO channel model. The simulation results reveal a superiority of the post-LNA SAS to the post-LNA SAS at any condition. Moreover, using the simulations performed for the interference channels we show that the post-LNA SAS is upper bounded by the full-complexity MIMO.

Since in both above-mentioned channels, noise-limited and interference, the channel knowledge is needed for the SAS optimization, in this thesis we also propose a two-step channel estimation method for the SAS-MIMO. This channel estimation is based on an Orthogonal Frequency-Division Multiplexing (OFDM) MIMO system. Two different estimators of Least-Square (LS) and Minimum-Mean-Square-Error (MMSE) are applied. Simulation results show a superiority of the MMSE method to the LS estimator for a MIMO system simulated under the 802.16 framing strategy. Moreover, a 802.11a framing based SAS-MIMO is simulated using MATLAB SIMULINK to verify the two-step estimation procedure.

Furthermore, we also employ a ray-tracing channel simulation to assess different SAS configurations, i.e. realized by active (post-LNA) and/or passive (pre-LNA) phased array, in terms of signal coverage. In this regard, a rigorous Signal to Noise Ratio (SNR) analysis is performed for each of these SAS realizations. The results show that although the SAS method performance is generally said to be upper-bounded by a full-complexity MIMO, it shows a better signal coverage than the full-complexity MIMO.

Acknowledgements

I would like to thank Ministry of Science and Research Technology (MSRT) of IRAN, Ontario government of Canada and University of Waterloo which sponsored me for my PhD program. Moreover, I would also like to thank all the people who made this possible.

Dedication

To my wife, **Hengameh**, and my lovely son, **Kian**.

Contents

List of Tables **ix**

List of Figures **x**

1 Introduction **1**

1.1 MIMO Technology 2

1.1.1 MIMO Data Transmission Techniques 3

1.1.2 Adaptability in MIMO 4

1.1.3 RF Processing Techniques 6

1.2 Antenna Selection 6

1.2.1 Pure Antenna Selection/Antenna Subset Selection 7

1.2.2 Hybrid Antenna Selection 8

1.3 Thesis Organization 9

2 *Soft* (Adjustable Hybrid) Antenna Selection (SAS) **12**

2.1 Soft Antenna Selection Module Built by a Linear Network 12

2.1.1 Post-LNA Soft Antenna Selection (Active Phased Array): . . 13

2.1.2 Pre-LNA Soft Antenna Selection (Passive Phased Array): . . 14

2.2 Noise in MIMO Receivers 14

2.2.1 Mathematical Model for Noise Sources 15

2.2.2 Noise Model in SAS 16

3 SAS-MIMO for Noise-Limited Channels **20**

3.1 BaseBand Noise Model 20

3.2 MIMO Spatial Multiplexing System 21

3.2.1 Optimum Pre-LNA SAS for Spatial Multiplexing Transmission 23

3.3 MIMO Diversity System 25
3.3.1 Optimum vector $\mathbf{v}$ 26
3.3.2 Optimum vector $\mathbf{u}$ 27
3.3.3 Optimum Pre-LNA SAS for Diversity Transmission 29
3.4 Computer Simulations 31
3.4.1 Channel Model 31
3.4.2 Systems under the test 32
3.4.3 Simulation Results 33

4 SAS-MIMO for Interference Channels 36
4.1 Baseband Interference-plus-Noise Model 37
4.2 SAS-MIMO for Spatial Multiplexing Transmission 38
4.2.1 Optimum Pre-processing Matrix $\mathbf{W}$ 39
4.2.2 Optimum Transmit Covariance Matrix $\mathbf{K}_x$ 41
4.3 SAS-MIMO for Diversity Transmission 44
4.3.1 Optimum vector $\mathbf{v}$ 45
4.3.2 Optimum vector $\mathbf{u}$ and SAS matrix 47
4.4 Full-Complexity MIMO System in an Interference Channel 49
4.4.1 Spatial Multiplexing Transmission 49
4.4.2 Diversity Transmission 50
4.5 Computer Simulations 51
4.5.1 Interference Dominance Effect on Mutual Information/SNR Gain 51
4.5.2 Signal to Interference-plus-Noise Ratio Effect on Mutual Information 55
4.5.3 Number of Interferers Effect on Mutual Information/SNR Gain 55
4.5.4 Rician K-Factor Effect on Mutual Information/SNR Gain . 57
4.5.5 Number of RF chains Effect on Mutual Information/SNR Gain 58

5 Channel Estimation for SAS-MIMO System 61
5.1 Frequency Domain Representation of OFDM based SAS-MIMO System 62
5.2 Channel Estimation Method 62
5.2.1 Measurement Approach 63

5.2.2 **H** Estimation 69
5.3 Proposed Method Evaluation via Simulation 69
5.3.1 Performance Evaluation Results 70

6 Signal Coverage **72**
6.1 SNR Analysis 72
6.1.1 Reference Single RF Channel Receiver 73
6.1.2 Active Phased Array Receiver 74
6.1.3 Passive Phased Array Receiver 76
6.1.4 Discussion on Analytical Derivations 77
6.2 Ray-tracing Modeling 78
6.2.1 Propagation Environment 79
6.3 Wireless Communication Link Settings 80
6.4 Simulation Results 84

7 Conclusion and Future Work **86**

References **89**

List of Tables

1.1 Acronyms 11

6.1 A Typical Receiver for WLAN 802.11b Standard [62] 72
6.2 SAS Module Components 73
6.3 Measured Permittivity of Indoor Materials at 2.4 GHz 80

List of Figures

1.1 MIMO communication system model. 2

1.2 A schematic of the adaptive transceiver design of a MIMO system. . 5

1.3 MIMO diversity system structure equipped with the hybrid antenna selection scheme. 8

2.1 MIMO communication system model equipped with the receive soft antenna selection scheme. 13

2.2 The circuit equivalent model of $[\mathbf{W}]_{i,j}$ for a full adjustable post-LNA SAS (or active phased array). 13

2.3 The circuit equivalent model of $[\mathbf{W}]_{i,j}$ for a phase only adjustable post-LNA SAS (or active phased array). 14

2.4 The circuit equivalent model of $[\mathbf{W}]_{i,j}$ for a phase only adjustable pre-LNA SAS (or passive phased array). 15

2.5 Single RF channel Receiver. 16

2.6 Active phased array of ith (out of N_r) receiver input. 18

2.7 Passive phased array of ith (out of N_r) receiver input. 19

3.1 Baseband Models with $\mathbf{H}_a = \mathbf{WH}$ for (a) MIMO spatial multiplexing system (b) MIMO diversity system. 22

3.2 Mean mutual information versus the receiver/channel noise power ratio for different MIMO configurations. 34

3.3 Mean mutual information versus the SNR for different MIMO configurations. 35

4.1 Interference Model. 38

4.2 Baseband Models with $\mathbf{H}_a = \mathbf{WH}$ for (a) MIMO spatial multiplexing system (b) MIMO diversity system. 39

4.3 MI versus IDR when $\mathrm{SINR}_0 = 10dB$, the number of interferers is 2 and $K_f = 5dB$. 53

4.4 SINR gain versus IDR when the number of interferers is 2 and $K_f = 5dB$. 54

4.5 MI versus nominal Signal to Nominal Interference-plus-Noise Ratio (SINR_0) when the number of interferers is 2, IDR $= 10dB$ and $K_f = 5dB$. 55

4.6 MI and SNIR gain versus Number of Interferers when IDR $= 10dB$, $K_f = 5dB$ and CSIR case. For MI plot $\text{SINR}_0 = 10dB$. 56

4.7 MI and SNIR gain versus Rician K factor (K_f) when IDR $= 10dB$, the number of interferers is 2 and CSIR case. For MI plot $\text{SINR}_0 = 10dB$. 57

4.8 MI versus number of receive RF chains (N_r) when $\text{SINR}_0 = 10dB$, the number of interferers is 2, IDR $= 10dB$ and $K_f = 5dB$. 58

4.9 SNIR gain versus number of receive RF chains (N_r) when the number of interferers is 2, IDR $= 10dB$ and $K_f = 5dB$. 59

5.1 Framing structure for SAS-MIMO channel estimation. 64

5.2 OFDM-based 4×4 SAS-MIMO with $N_s = 8$ simulation model. . . . 68

5.3 BER versus different nominal SNRs. 71

6.1 Single RF chain Transceiver. 73

6.2 Low/Full complexity MIMO RF chain Transceiver. 74

6.3 ith (out of N_r) receiver input for a SAS-MIMO with active phased array. 75

6.4 ith (out of N_r) receiver input for a SAS-MIMO with passive phased array. 76

6.5 RPS software appearance. 79

6.6 The third floor map of EIT building, University of Waterloo. 81

6.7 A 3D view of simulated environment (the third floor of EIT building, University of Waterloo). 82

6.8 The overall settings for each transmitter elements. 83

6.9 Beam pattern of the transmitter (a) and the receiver (b) antenna elements. 83

6.10 The overall settings for each transmitter elements. 84

6.11 Signal coverage from A to B points. 85

Chapter 1

Introduction

Wireless communications is, by any criterion, the fastest growing part of the communications industry. As it has captured the attention of the media and the imagination of the public, wireless systems continue to strive for higher data rates. This goal is particularly challenging for systems which are power, bandwidth, and complexity limited. There are two fundamental aspects of wireless communication that make the problem interesting and challenging. First is *fading* phenomenon which is classified into large and small scale fading. The large-scale fading is mainly due to path loss via distance attenuation and shadowing by obstacles. The time-variation of the channel strengths due to the small-scale effect of multipath fading cause the small scale fading. The second one is *interference* issue. Unlike in the wired world where each transmitter-receiver pair can often be thought of as an isolated point-to-point link, in a wireless network users communicate over the air and therefore there must be significant interference between them. To improve the performance of a transmission in the fading and interference channels, there exist various diversity techniques over time, frequency or space. In a typical diversity method, the signals carrying the same information are sent through different paths; therefore, multiple independently faded replicas of data symbols are obtained at the receiver end and more reliable detection can be achieved. To exploit time diversity, interleaving and coding over several coherence time periods is necessary. When there is a strict delay constraint and/or the coherence time is large, e.g. in an indoor environment where usually the large-scale fading exists, this achievement may not be possible. The second one, i.e. the frequency diversity, also has its own problems, e.g. it is useful when the transmission bandwidth is greater than the coherence bandwidth of the channel. The third domain which can be exploited to significantly increase channel capacity is *spatial domain*. The spatial diversity can be obtained by placing multiple antennas at the transmitter and/or the receiver.

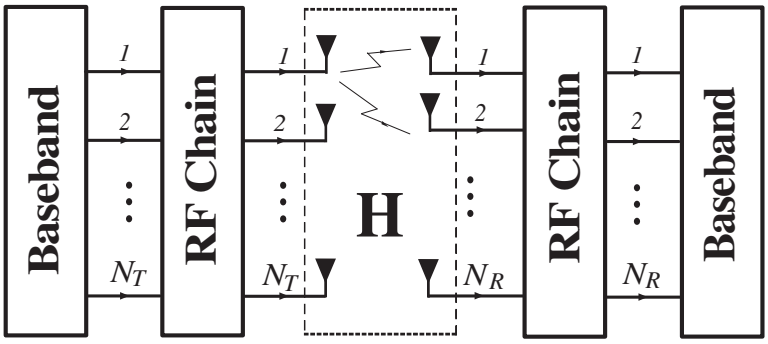

Figure 1.1: MIMO communication system model.

1.1 MIMO Technology

Multiple-Input-Multiple-Output (MIMO) wireless systems (see Fig. 1.1), characterized by multiple antenna elements at the transmitter and receiver, operate by exploiting the spatial properties of the multipath channel, thereby offering a new dimension which can be used to enable enhanced communication performance. Such systems have demonstrated the potential for increased capacity in rich multipath environments [1]-[5]. The performance improvements resulting from the use of MIMO systems are due to the following:

- *Array Gain:* Array gain is available on both the transmitter and the receiver, and results in an increase in the average received Signal to Noise Ratio (SNR) due to coherent combining. Transmit/receive array gain requires the Channel State Information (CSI) at the transmitter and receiver, respectively, and depends on the number of transmit and receive antennas. Channel knowledge at the receiver side is typically available via channel characterization, e.g. the channel estimation, whereas CSI at the transmitter is based on the information fed back from the receiver and generally difficult to maintain.

- *Diversity Gain:* Spatial diversity obtained from multiple antennas helps combat channel fluctuations, i.e. fading. Diversity techniques rely on transmitting the signal over multiple (ideally) independently fading paths (in time/frequency/space). Spatial (or antenna) diversity is preferred over time and frequency diversities as it does not incur an expenditure in transmission time or bandwidth. Denoting N_T and N_R as the number of transmit and receive antenna elements respectively, if the $N_R N_T$ links composing the MIMO channel fade independently and the transmitted signal is suitably constructed, the receiver can combine the arriving signals such that the resultant signal exhibits considerably reduced amplitude variability in comparison to a Single-Input-Single-Output (SISO) link and we get $N_R N_T$th-order diversity. Extracting spatial diversity gain in the absence of channel knowledge at the transmitter is possible using suitably designed transmit signals which is known as spacetime coding.

- *Spatial Multiplexing Gain:* This multiplexing employs the multiple antennas at both ends to create multiple channels, and improves the spectrum efficiency. Under conducive channel conditions, such as rich scattering, the receiver can separate the different streams, yielding a linear increase in capacity.

- *Co-Channel Interference Suppression:* The interference arises due to frequency reuse in wireless channels particularly when the multiuser MIMO system are used. Interference suppression requires knowledge of the desired signals channel. Exact knowledge of the interferers channel may not be necessary. Interference reduction (or avoidance) can also be implemented at the transmitter, where the goal is to minimize the interference energy sent toward the co-channel users while delivering the signal to the desired user. Interference reduction allows aggressive frequency reuse and thereby increases multicell capacity. We note that in general it is not possible to exploit all the leverages of MIMO technology simultaneously due to conflicting demands on the spatial degrees of freedom (or number of antennas). The degree to which these conflicts are resolved depends upon the signaling scheme and transceiver design.

1.1.1 MIMO Data Transmission Techniques

To evaluate different MIMO systems, we study two cases of the transmission methods in this thesis: spatial multiplexing, to enhance the data rate, and diversity, to improve the reliability. As mentioned earlier, MIMO channels, having both multiple transmit and multiple receive antennas provide an additional spatial dimension for communication and yield a *degree-of-freedom* gain. These additional degrees of freedom can be exploited by spatially multiplexing several data streams onto the MIMO channel, and lead to an increase in the capacity. Hence, with spatial multiplexing, different data streams can be applied on the transmitting antenna elements to provide a maximal data rate. Diversity in a MIMO system can be obtained through the use of spacetime codes, e.g. Alamouti scheme [6]) or via intelligent use of CSI at the transmitter, e.g. Maximum Ratio Transmission (MRT) [7], which is the one we consider in this thesis. Transmit beamforming with receive combining is one of the simplest approaches to achieving full diversity and has been of interest recently [8]. According to this system, the original source stream is multiplied by the a complex weighting vector (baseband beamforming), before it is modulated to the passband and applied to each of the transmitting antennas. Then through a combining approach the received signal vector after demodulation is multiplied by another complex weighting vector, so-called combining vector, to provide the output stream of data (as a scalar). In this thesis, we consider an uncoded transmission under both the above-mentioned transmission strategies in a narrowband fading channel.

1.1.2 Adaptability in MIMO

An adaptive MIMO system design can enable robust and spectrally-efficient transmission over time-varying channels. The basic premise is to estimate the channel at the receiver and feed this estimate back to the transmitter, so that the transmission scheme can be adapted relative to the channel characteristics. Transceiver design techniques which do not adapt to the fading conditions require a fixed link margin to maintain acceptable performance when the channel quality is poor. Hence, these transceivers are effectively designed for the worst-case channel conditions. Since Rayleigh fading can cause a signal power loss of up to $30dB$ [2], designing for the worst case channel conditions can result in very inefficient utilization of the channel. Adapting to the channel fading can increase average throughput, reduce required transmit power, or reduce average probability of bit error by taking advantage of favorable channel conditions to send at higher data rates or lower power, and reducing the data rate or increasing power as the channel degrades. An adaptive design can be based on different criteria; however, here in thesis, we focus on the information theoretic aspect of the MIMO systems. Moreover, in this thesis we consider the system adaptivity only at the physical-layer which spreads from antenna front end to the input of Medium Access Control (MAC) layer. Fig. 1.2 represents a schematic design of the adaptive MIMO system.

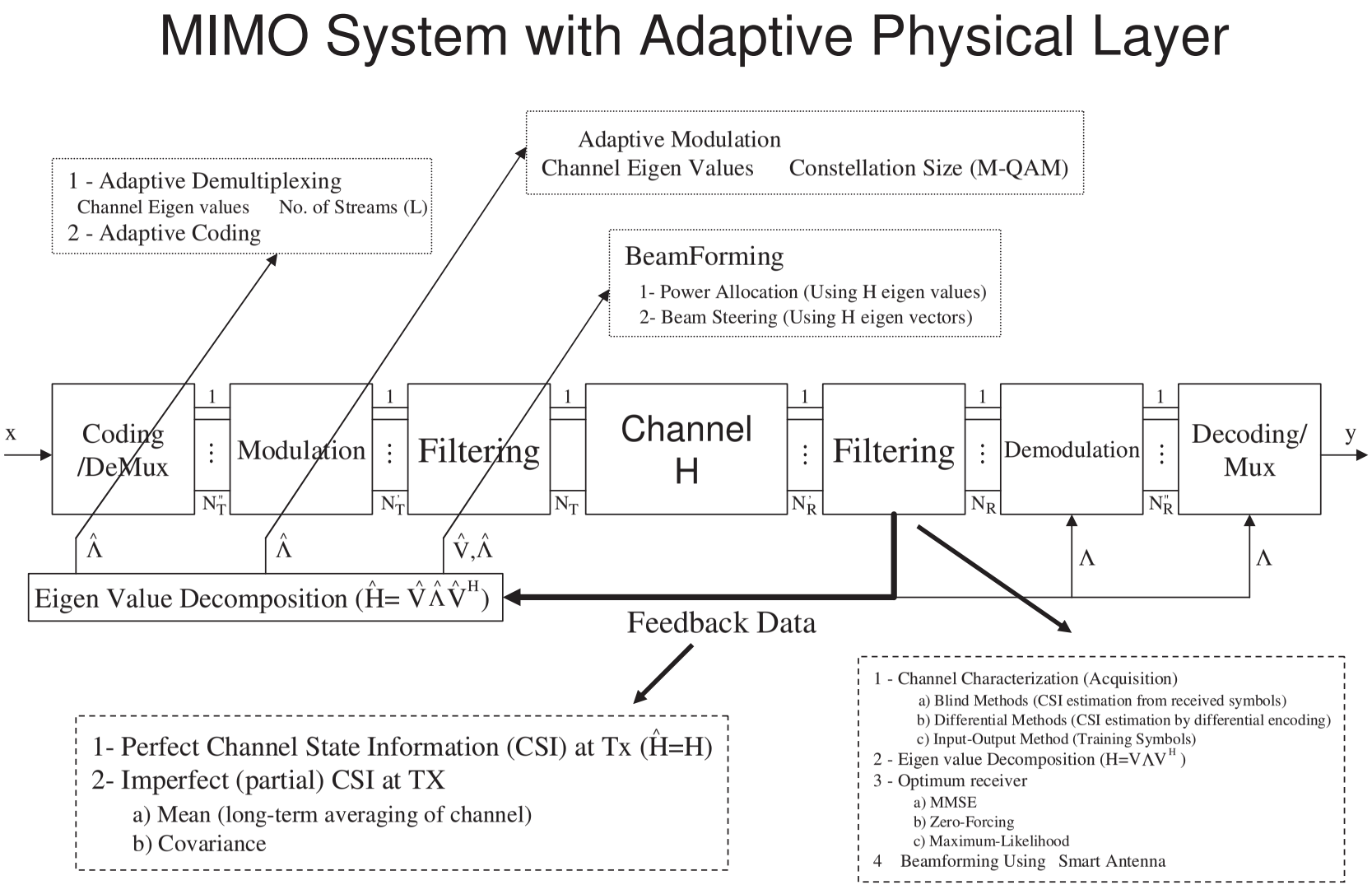

Figure 1.2: A schematic of the adaptive transceiver design of a MIMO system.

1.1.3 RF Processing Techniques

The multiple antennas are exploited to improve the data rate and/or signal-to-noise ratio of the communication channel, as demonstrated by analytical and simulation studies [2] and [4]. Despite the significant gains, an important factor limiting the widespread adoption of MIMO systems is their increased hardware complexity. This complexity results in the increased fabrication cost and energy consumption of the RF chains including the microwave/baseband frequency translation and the Digital-to Analog (D/A) and Analog-to-Digital (A/D) conversions. In a regular MIMO system, at the transmitter side we need a separate RF chain that comprises a Power Amplifier (PA), modulator, and a D/A converter for each antenna element. On the other hand, the signal received at each antenna element requires a separate RF chain that comprises a Low Noise Amplifier (LNA), demodulator, and an A/D converter. All these electronic components are expensive. The cost and complexity obviously increase linearly with the number of antenna elements. These factors motivate the recent popularity of RF processing techniques. One of these methods is known as *Antenna Selection*. Although the RF chain components are expensive, additional antenna elements, e.g. patch or dipole antennas, are usually inexpensive, and therefore using a cheap but adaptive selection technique we can achieve a good performance improvement. Different kinds of antenna selection schemes have been proposed in the literature [9]-[14]. These techniques can be applied at both transmitter and receiver sides; however, in this thesis the receiver side is only considered to apply such RF processing techniques, thus so-called RF pre-processing methods.

1.2 Antenna Selection

From communications point of view, the antenna is usually assumed as a part of the channel which means that the channel matrix includes the antenna characteristics. In this case, the transfer matrix $\mathbf{H}$ depends not only on the propagation environment but also on the array properties such as pattern, polarization, array configuration, and mutual coupling [15] and [16]. The question now is how someone can change some, and not necessarily all, of these properties through a RF pre-processing method to maximize the system capacity (perhaps in an average sense over a variety of propagation channels) or minimize symbol error rates. This is difficult to answer definitively, since the optimal array shape depends on the site-specific propagation characteristics, although some general observations are possible. In fact, by changing the array properties we are somehow *forming* the "channel" which is seen from the baseband.

In the following, we explain the RF pre-processing techniques in which the received signals to a N_s-element array are mapped to $N_r < N_s$ RF chains. The transceiver antenna array in this thesis is considered Uniform Linear Array (ULA)

of iso-tropic antenna[1] elements. However, other configurations can be also applied, e.g. a Rectangular Linear Array (RLA) antenna. Throughout the thesis, the pre-processing techniques are compared with two standard configurations of a MIMO system in terms of performance. These two configurations are as follows:

- A MIMO system with N_s receive antennas and N_s receive RF chains is called *receiver full-complexity* MIMO system (see Fig. 1.1 when $N_R = N_s$).
- A MIMO system with N_r receive antennas and N_r receive RF chains is called *receiver low-complexity* MIMO system (see Fig. 1.1 when $N_R = N_r$).

It is shown in the literature [17]-[20] and also in this thesis that the antenna selection methods (of any) outperform low-complexity MIMO and some of them are upper-bounded by the full-complexity MIMO at their optimum condition. Note that we assume all configurations are using the same antenna geometry, i.e. ULA, and the same aperture size, i.e. not necessarily the same antenna element spacing.

1.2.1 Pure Antenna Selection/Antenna Subset Selection

A conventional antenna selection method is to consider an adaptive system that selectively connects a subset of available antennas to the electronic modules according to CSI [9]. Studies have shown that an intelligently-selected sub-array can provide improved capacity [17]-[20] or lower probability of symbol error [11] relative to the performance of fixed arrays (low-complexity MIMO). Moreover, the antenna subset selection strategy is a powerful solution that reduces the need for multiple analog chains yet retains many diversity benefits. The antenna selection core idea is to use a limited number of the analog chains that is adaptively switched to a subset of the available antennas. An appropriate subset of antennas can be identified, e.g., within the training phase, by probing all receive antennas with the available set of the receive chains. This general approach provides certain diversity benefits at a low additional cost that is mainly determined by low-cost RF switches rather than by expensive analog chains.

To make this approach practical, however, efficient and effective methods for choosing the appropriate antenna element subset are required. Each of the proposed methods in the literature ([17]-[20]) employs an exhaustive search to identify the optimal element set, an approach that becomes prohibitive for large arrays. Further, [21] studies alternate suboptimal efficient antenna-selection algorithms with low computational complexity, suitable for application to large antenna arrays, based upon metrics derived from Mutual Information (MI) considerations.

[1]Though in some simulations without losing any generality - as the antenna array element are assumed to be a part of channel - we use dipole or patch antennas.

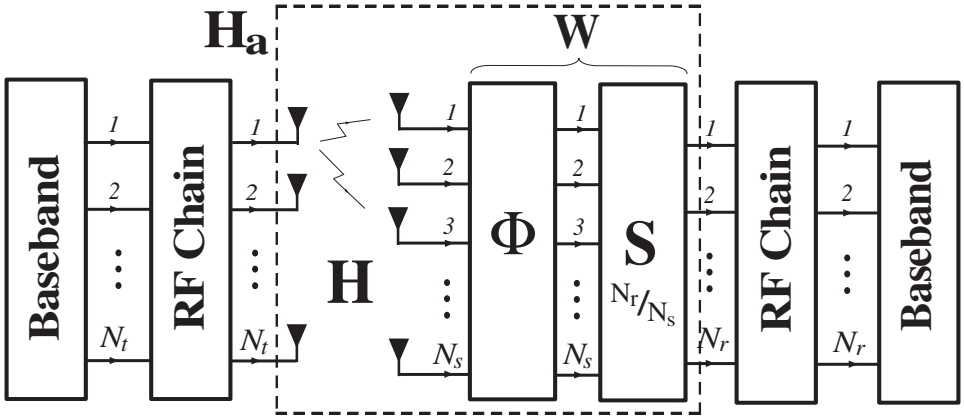

Figure 1.3: MIMO diversity system structure equipped with the hybrid antenna selection scheme.

1.2.2 Hybrid Antenna Selection

The antenna selection schemes work well for the uncorrelated MIMO channels (e.g., independent and identically distributed (i.i.d.) Rayleigh fading at each antenna element) [10] and [22]. However, despite the great advantages of the pure antenna selection approaches in terms of cost reduction, they suffer from severe performance degradation. In most practical MIMO channels, due to the directional nature of the multipath propagation, the signals at the antenna array are highly correlated dependent on the arriving angles [23]. Moreover, this correlation can arise from the mutual coupling between the transmit and/or receive antenna elements [24]. In such channels, the antenna selection schemes performs considerably worse than full-complexity MIMO systems [25], and the performance of conventional selection reduces to that of a N_r-antenna system, i.e. a low-complexity MIMO, losing all advantages of having additional antenna elements.

An alternative method to overcome this shortcoming is Hybrid Antenna Selection (HAS) scheme [13], [26], [27]. The idea originally comes from the Hybrid Selection Maximum Ratio Combining (HS-MRC) schemes [25]. Fig. 1.3 shows the MIMO system structure equipped with the HAS method used in [13], [26], [27]. To implement the HAS method, Fast Fourier Transformation (FFT) and Discrete Fourier Transformation (DFT) of the (spatial) received signal vector in the RF domain are respectively used in [13] and [26], i.e. $\mathbf{\Phi}$ in Fig. 1.3. This implementation (DFT/FFT) can be electronically realized simply by placing a Butler matrix (a butterfly structure consisting of phase shifters, adders and power splitters) between the antenna elements and the receiver switch. Then a switch matrix, i.e. $\mathbf{S}$ in Fig. 1.3, selects the best outputs from the fixed beamformer $\mathbf{\Phi}$ based on the assigned criterion, which is capacity in [13] and [26]. The DFT (FFT) matrix gives reasonable performance for a wide range of channel configurations, does not need adaptive elements, and is very simple to implement. However, the used Fourier transformation based phase-shifter is not the optimum transformation matrix; rather, a matrix

that adapts to the instantaneous channel realization is required to give the best performance for the fading channels.

To exploit the transmitted/received signal correlation benefits in a multipath propagation environment, a controllable RF pre-processing method, so-called *Soft* Antenna Selection (SAS), is introduced in [27]. This method is basically known as a controllable/adjustable HAS scheme. Indeed, in contrast to the DFT (FFT) operation proposed in [13] and [26], the variable - in amplitude and phase - phase shifter method used in [27] adapts to the channel characteristics. However, the proposed method in [27], instead of the capacity, tries to maximize the received SNR, and therefore, it is a Phase-Shift and Selection Maximum Ratio Combining (PSS-MRC) scheme. Later in [14], the authors extend the results for both diversity and spatial multiplexing transmissions. Their RF pre-processing method uses a transformation which adapts to the instantaneous channel state. A similar architecture is also used in [28]; however, in which the linear RF pre-processing matrix is tuned based on only the large-scale statistics of the channel. In none of [14] and [28], an exact noise analysis for the MIMO system equipped with the SAS module, called SAS-MIMO system, is provided. In fact, in both these references the SAS module is applied on signal and noise without any explanation where the SAS module is located in the RF domain, after and/or before LNA, and how the vector noise is modeled. Moreover, authors in [14] and [28] never investigate the SAS-MIMO in an interference channel, i.e. where both interference and noise exist. The main contribution of this thesis is to address these shortcomings and clarify how much performance improvement we will achieve with different SAS configurations in both noise-limited and interference channels.

1.3 Thesis Organization

The rest of this thesis is organized as follows. In Chapter 2, we introduce the SAS-MIMO system model implemented using the active phased array (post-LNA) and passive phased array (pre-LNA). In this model, the SAS method is realized via a linear processing network. In the same section, we show how the two major noise sources, external (sky) and internal (amplifier), contribute in the noise model. In Chapter 3, the optimality of the pre-LNA SAS method is investigated under the spatial multiplexing and diversity transmission strategies for when either the sky noise and/or the amplifier noise dominates. We also find an upper-bound for the maximized mutual information/SNR gain in the same section followed by a procedure which provides the sub-optimal solution for the pre-LNA processing matrix. In Chapter 4, the post-LNA SAS-MIMO is optimized under the aforementioned transmission strategies when the interferers exist in the channel. A mathematical representation of the interference model introduced in this regards in the same chapter. Each of Chapters 3 and 4 is supported with a computer simulation to verify the mathematical derivations. In Section V, an OFDM-based channel estimation method is proposed for the SAS-MIMO system. We verify the estimator

via two series of simulations, under 802.11a/802.16 framing based MIMO, in this chapter. A signal coverage evaluation is performed in Chapter 6. In this chapter, a rigorous SNR analysis is done for pre/post-LNA SAS-MIMO. Moreover, a deterministic ray-tracing simulation is used to realize a typical example set based on a 802.11b wireless link in the same chapter. Finally, Section 7 concludes the paper and gives some directions for future work.

The following notations will be used throughout the thesis.

- Superscripts ^{T}, $'$ and * represent the transpose, the conjugate and the conjugate transpose, respectively.
- $I(\bullet)$, $\mathcal{E}(\bullet)$, $\det(\bullet)$, $\log(\bullet)$ and $\mathrm{tr}(\bullet)$ denote MI, the expectation, the determinant, the natural logarithm and the trace, respectively.
- $\mathbf{K}_x = \mathcal{E}(\mathbf{x}\mathbf{x}^*)$ shows the covariance matrix of the signal vector $\mathbf{x}$.
- $\mathbf{I}_N$, $\mathbf{1}_{M\times N}$ and $\mathbf{1}_N$ are respectively an identity matrix of size N, a $M \times N$ all-ones matrix and a N-long all-ones vector.
- $\mathcal{C}^{M\times N}$ and $\mathcal{C}^N$ are respectively a set of $M \times N$ matrices and N-long vectors with complex valued entries, and $\mathcal{R}$ and $\mathcal{C}$ represent a set of real and complex scalars, respectively.
- $\mathbf{u}_{i,\bullet}$ and $\mathbf{v}_{i,\bullet}$ respectively denote the left and right singular vector associated with the ith eigenvalue, $\lambda_{i,\bullet}$, of a matrix for $i \in \{1, 2, ...\}$; $\|\cdot\|_1$ and $\|\cdot\|_2/\|\cdot\|$ represent respectively the l_1 and l_2 norms [42].
- $\lceil\bullet\rceil$ represents the ceiling function.

Acronyms used throughout the thesis are also given in Table 1.1.

Table 1.1: Acronyms

2D	Two Dimensional
3D	Three-Dimensional
A/D	Analog-to-Digital
AOA	Angle of Arrival
AOD	Angle of Departure
AWGN	Additive White Gaussian Noise
CP	Cyclic Prefix
CSI	Channel State Information
CSIR	Channel State Information at Receiver
CSIT	Channel State Information at Transmitter
D/A	Digital-to Analog
DFT	Discrete Fourier Transformation
EGT	Equal Gain Transmission
EGTS	Equal Gain Two-Step
FFT	Fast Fourier Transform
GSS	Generalized Subset Selection
HAS	Hybrid Antenna Selection
IDR	Interference Dominance Ratio
IFFT	Inverse Fast-Fourier Transform
i.i.d.	independent and identically distributed
iMARS	Intelligent Multi-Antenna radio Systems
ISI	Inter-Symbol Interference
LN	Linear Network
LNA	Low Noise Amplifier
LOS	Line of Sight
LS	Least-Square
MAC	Medium Access Control
MEMS	Micro-Electro-Mechanical Systems
MI	Mutual Information
MIMO	Multiple Input Multiple Output
MMSE	Minimum-Mean-Square-Error
MRC	Maximum Ratio Combining
MRT	Maximum Ratio Transmission
NF	Noise Figure
NLOS	Non Line of Sight
OFDM	Orthogonal Frequency-Division Multiplexing
OPSD	Optimum Pre-LNA SAS for Diversity transmission
OPSSM	Optimum Pre-LNA SAS for Spatial Multiplexing transmission
OSD	Optimum SAS for Diversity
OSSM	Optimum SAS for Spatial Multiplexing
OTSD	Optimum Trace-bounded SAS for Diversity transmission
OTSSM	Optimum Trace-Bounded SAS for Spatial Multiplexing transmission
PA	Power Amplifier
PAS	Power Angular Spectrum
PLN	Passive Linear Network
PP	Preamble-Patterns
PSB	Phase Shift Based
RCB	Receiver Chain Block
RLA	Rectangular Linear Array
RF	Radio Frequency
RPS	Radiowave Propagation Simulator
SAS	Soft Antenna Selection
SDT	Selection Diversity Transmission
SINR	Signal to Interference-plus-Noise Ratio
SISO	Single Input Single Output
SNR	Signal to Noise Ratio
SVD	Singular Value Decomposition
ULA	Uniform Linear Array
WLAN	Wireless Local Area Networks
WMAN	Wireless Metropolitan Area Network

Chapter 2

Soft (Adjustable Hybrid) Antenna Selection (SAS)

By definition [14] and [28], a SAS scheme is a controllable/adjustable HAS which has a beamforming capability. In this type of HAS, the phase shift components are assumed to be fully adjustable at phase and magnitude, or only at phase for the phase-only controllable HAS.

2.1 Soft Antenna Selection Module Built by a Linear Network

The MIMO system equipped with a receive soft antenna selection module, so-called SAS-MIMO for the rest of this thesis, is depicted in Fig. 2.1. It consists of N_t transmit and N_s receive antennas. In this framework the physical channel, consisting of the radio propagation environment and transmit and receive antennas, is modeled by a $N_s \times N_t$ matrix $\mathbf{H}$. There exist N_t transmit RF chains including PAs and $N_r < N_s$ receive RF chains. Two different SAS configurations are investigated in this thesis. First, the SAS module $\mathbf{W}$ is applied after LNA, i.e. post-LNA SAS. This configuration can be also called SAS realized with an active phased array since the structure is very similar to the well-known active phased arrays, i.e. LNA as a part of the phased array, in the literature [29]. The other configuration is the pre-LNA SAS in which the SAS module $\mathbf{W}$ is applied before LNA. Since we only use passive elements in this configuration, we also call this architecture SAS realized with a passive phased array.

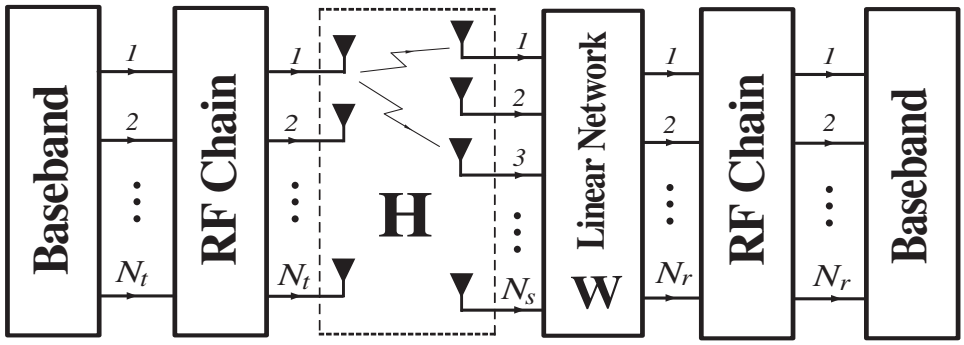

Figure 2.1: MIMO communication system model equipped with the receive soft antenna selection scheme.

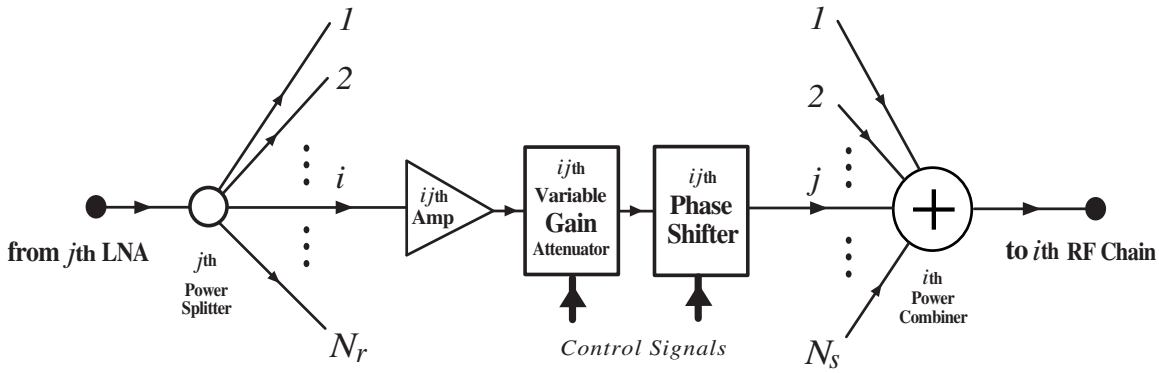

Figure 2.2: The circuit equivalent model of $[\mathbf{W}]_{i,j}$ for a full adjustable post-LNA SAS (or active phased array).

2.1.1 Post-LNA Soft Antenna Selection (Active Phased Array):

The receive post-LNA SAS module represented by a $N_r \times N_s$ matrix $\mathbf{W}$ is practically made by a Linear Network (LN) including power splitters/combiners and phase-shifters and variable gain amplifiers (or fixed gain amplifiers plus the variable attenuator). Fig. 2.2 shows such a structure for the SAS module.

In practice a low-cost and low complexity implementation of the post-LNA SAS module, made by Passive Linear Network (PLN) including only power splitters/combiners and phase-shifters (see Fig. 2.3), is preferred. For this implementation, $\mathbf{W} \in S_p$ where $S_p = \{\mathbf{W}| \ |[\mathbf{W}]_{i,j}| \leq \sqrt{\frac{1}{N_r N_s}}\}$ and the equality holds for lossless PLN, i.e. no insertion loss. In this definition, the factor $\sqrt{\frac{1}{N_r}}$ is due to the power splitting in the power divider. Moreover, a normalizing (dividing) to the factor $\sqrt{\frac{1}{N_s}}$ is needed to be consistent with the analog world. In other words, from the signal processing point of view when N_s channels are combined the total noise power goes up by a factor of N_s, and the signal power implicitly increases

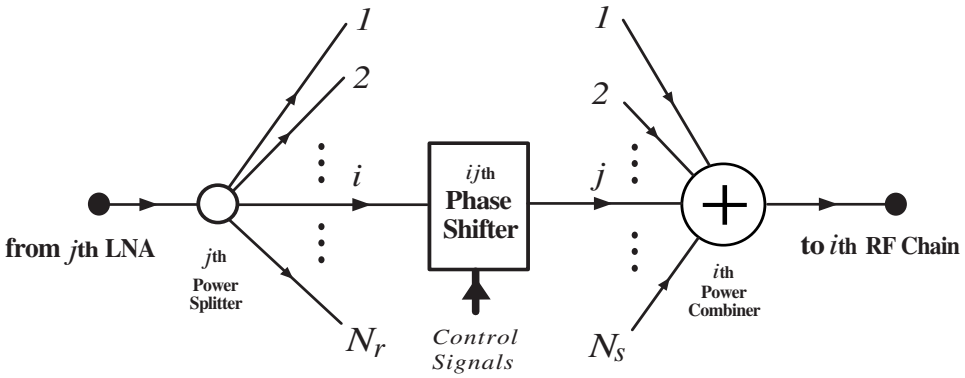

Figure 2.3: The circuit equivalent model of $[\mathbf{W}]_{i,j}$ for a phase only adjustable post-LNA SAS (or active phased array).

by a factor of N_s^2 because of amplitude combining; however, in practice when the in-phase signals of equal amplitude are combined the output signal power will go up by the factor N_s, while the noise will stay at the same level as in the input ports [29] and [30]. The lossless PLN can be somehow achieved by using the low insertion loss passive elements. One way of implementing this idea is to use Micro-Electro-Mechanical Systems (MEMS) technology. RF-MEMS switches due to their excellent switching characteristics: very low insertion loss, very low power requirements and high isolation [31], [32], have been a perfect choice in the reconfigurable antennas implementation [33]. For instance, RF-MEMS switched line phase shifters [34] make the implementation of the passive linear structure feasible. Although the RF-MEMS switches are not very fast (3 to 6 μs [31]), this speed is enough so that the SAS system can track the channel behavior, particularly for indoor areas which present a slow-fading channel.

2.1.2 Pre-LNA Soft Antenna Selection (Passive Phased Array):

The pre-LNA SAS module represented by a $N_r \times N_s$ matrix $\mathbf{W}$ is realized with a PLN, i.e. $\mathbf{W} \in S_p$. The PLN architecture consists of passive components including power splitters/combiners and phase shifters. The circuit equivalent model for the ijth entry of $\mathbf{W}$ is depicted in Fig. 2.4.

2.2 Noise in MIMO Receivers

In a MIMO system, the spatial multiplying and diversity methods are basically baseband signal processing mechanisms. Hence, an appropriate baseband noise model can lead the formulation to a more precise result. In order to present such a noise model we need to determine which noise sources have the main contributions in the model.

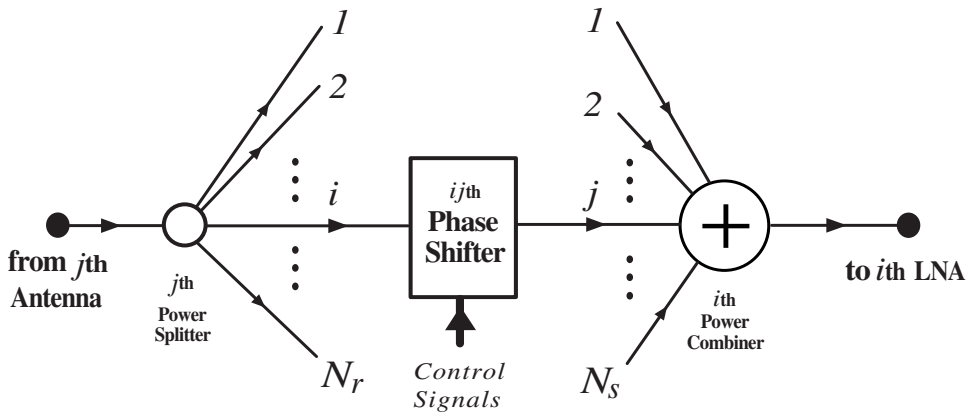

Figure 2.4: The circuit equivalent model of $[\mathbf{W}]_{i,j}$ for a phase only adjustable pre-LNA SAS (or passive phased array).

2.2.1 Mathematical Model for Noise Sources

In a wireless communication system, the system noise is made of two noise types: the external and the internal [35], regardless where it is modeled. Based on the environment type, different noise sources contribute in the former one including sky noise, man made noise and ground noise. The internal noise is essentially due to the thermal noise of electronic components. In the following, we formulate these two noise types and their contribution in the baseband noise model.

Antenna Noise

A receiving antenna receives black-body radiation emanating from the surrounding sources. This undesired power degrades the received signal SNR. The amount of black-body radiation received by an antenna depends on the antenna radiation pattern, the black-body locations and temperatures. The antenna noise temperature is indeed a measure of the received noise power from the surrounding black-bodies.

The antenna noise temprature T_A is defined by [29]

$$T_A = \frac{1}{4\pi} \iint_{\Omega} T(\Omega) G_A(\Omega) d\Omega \tag{2.1}$$

where $T(\Omega)$ and $G_A(\Omega)$ respectively represent the temperature profile of the external noise sources and the antenna gain, along the solid angle Ω. For an isotropic antenna $G_A(\Omega) = 1$. Hence, the antenna noise model at the receiver input is given by

$$N_A = K T_A B_\omega \tag{2.2}$$

where K and B_ω are Boltzman constant and frequency bandwidth, respectively.

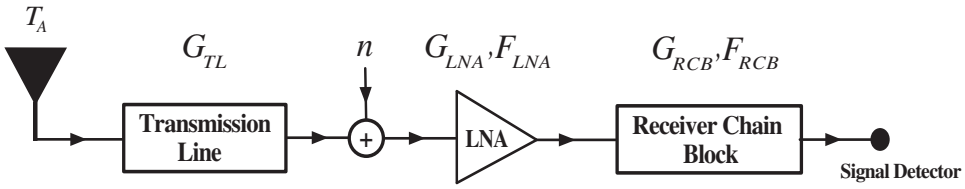

Figure 2.5: Single RF channel Receiver.

In this thesis we exclude the directional interference, i.e. dominant undesired received noise, from the external noise sources and therefore it is assumed that the rest so-called channel/sky noise is uniformly distributed along all solid angles Ω and also i.i.d. for all receiving antenna array elements [36].

Receiver Noise

There are many active and passive devices from RF front-end receiver to the signal detector. Regardless of the device type, two essential figures can state the output noise power computation: *Gain (G)* and *Noise-Figure (F)*. Accordingly, the device introduced noise, modeled at the input, is given by [35, page 457]

$$N_d \;=\; (F-1)\; K\; T_0\; B_\omega \tag{2.3}$$

where $T_0 = 290K$ denotes the room temperature. Hence, the device output noise is

$$N_o \;=\; G(N_i + N_d) \tag{2.4}$$

where N_i represents the input noise power.

In our noise power calculation, we assume that the active devices are only made of one-input one-output amplifiers with a given gain and noise-figure. Furthermore, it is assumed any other complex active device can be made by the combination of the aforementioned amplifiers and passive circuits. The noise temperature of a passive circuit with resistive elements is of importance since such circuits are utilized in several components of an array feed network, e.g. power splitters/combiners, phase shifters and attenuators.

2.2.2 Noise Model in SAS

The system noise, which is a combination of the external noise and the internal noise, can be modeled either at the antenna terminals or at the LNA input [35, page 456]. In this thesis, the system noise is modeled at the LNA input. Due to the low noise figure and high gain of the LNAs, we usually consider only the contribution of the LNA noise and the lossy components between the antenna terminals and LNA.

In the following, we introduce the system noise model for different MIMO receivers discussed in this thesis.

Single RF Channel: A Reference

Consider a regular receiver with single antenna connected to the RF chain depicted in Fig. 2.5. Such an structure is used in common MIMO structures like a full/low-complexity MIMO system simply by using multiple of them together while they are assumed to be independent. It consists of the receiving antenna at the temperature T_A, a transmission line between the antenna and LNA with the gain $G_{TL} \leq 1$, LNA with the gain G_{LNA} and noise-figure F_{LNA}, and the rest of system components from mixer to the signal detector input considered as a system block called Receiver Chain Block (RCB) with a gain G_{RCB} and noise-figure F_{RCB}. Hence, the equivalent modeled noise power is given by

$$\sigma_n^2 = (N_A + N_{TL})G_{TL} + N_{LNA} \tag{2.5}$$

where

$$\begin{aligned} N_{TL} &= (1/G_{TL} - 1)KT_0B_\omega \\ N_{LNA} &= (F_{LNA} - 1)KT_0B_\omega \end{aligned}$$

Assuming $G_{TL} = 1$ yields $\sigma_n^2 = N_A + N_{LNA}$. As seen, the major contributing noise sources will be the antenna noise and the LNA noise.

Active Phased Array Receiver

To perform a noise analysis for a SAS module with an active phased array, we consider one out of N_r input receiver branches depicted in Fig. 2.6. As shown in the figure, we have considered all components in the amplitude/phase controlling branch (from the power splitter to combiner) together and assigned a total gain G_ϕ and noise-figure F_ϕ to them. Moreover, we assume the power splitter and combiner have an insertion loss $1/G_S$ and $1/G_C$, respectively. Hence, the equivalent modeled noise power is given by

$$\sigma_{n_j}^2 = (N_{A_j} + N_{TL_j})G_{TL_j} + N_{LNA_j} \quad \text{for } j \in \{1, 2, , ..., N_s\} \tag{2.6}$$

Assuming $G_{TL_j} = 1$, and uniform array elements and LNAs yields

$$\sigma_{n_j}^2 = N_A + N_{LNA} \quad \text{for } i \in \{1, 2, , ..., N_s\} \tag{2.7}$$

In other words, the major contributing noise sources will be still the antenna noise and the LNA noise. The same procedure is applied for the noise analysis

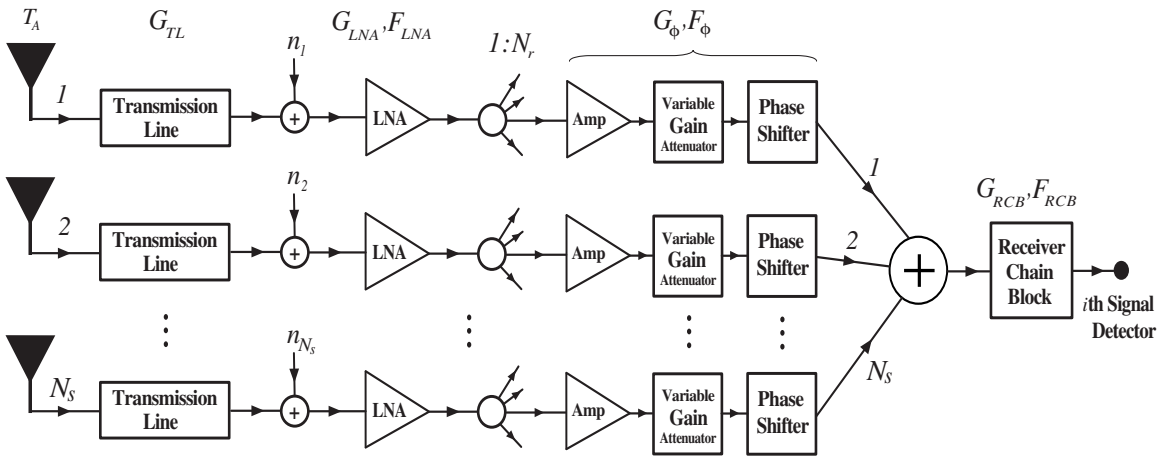

Figure 2.6: Active phased array of ith (out of N_r) receiver input.

of a phase only controlled post-LNA SAS module. In this case, the gain G_ϕ and noise-figure F_ϕ only demonstrate the phase shifter characteristics.

Passive Phased Array Receiver

A noise analysis for a pre-LNA SAS module is herein investigated by considering one out of N_r input receiver branches depicted in Fig. 2.7. As shown in the figure, we only have a phase adjusting method using a phase shifter and therefore a gain G_ϕ and noise-figure $F_\phi = 1/G_\phi$ are assigned for the phase shifter which is assumed to be passive. Hence, the equivalent modeled noise power is given by

$$\begin{aligned}\sigma_{n_i}^2 &= \frac{G_{C_i}}{N_s}\sum_{j=1}^{N_s}\left(N_{A_j}\frac{G_{TL_j}G_{S_j}G_{\phi_{ij}}}{N_r} + N_{TL_j}\frac{G_{TL_j}G_{S_j}G_{\phi_{ij}}}{N_r} + N_{S_j}\frac{G_{S_j}G_{\phi_{ij}}}{N_r}\right.\\ &\quad \left. + N_{\phi_{ij}}G_{\phi_{ij}} + N_{C_j}\right) + N_{LNA_i} \quad \text{for } i \in \{1, 2, , ..., N_r\} \qquad (2.8)\end{aligned}$$

where

$$\begin{aligned}N_{S_j} &= (N_r/G_{S_j} - 1)KT_0B_\omega\\ N_{\phi_{ij}} &= (1/G_{\phi_{ij}} - 1)KT_0B_\omega\\ N_{C_i} &= (1/G_{C_i} - 1)KT_0B_\omega\end{aligned}$$

As seen, to obtain the above-mentioned noise power it is assumed that the antenna noise on each antenna element is uncorrelated with the others and therefore the antenna noise power contribution in (2.8) is also normalized to N_s. This case is considered in Chapter 3.

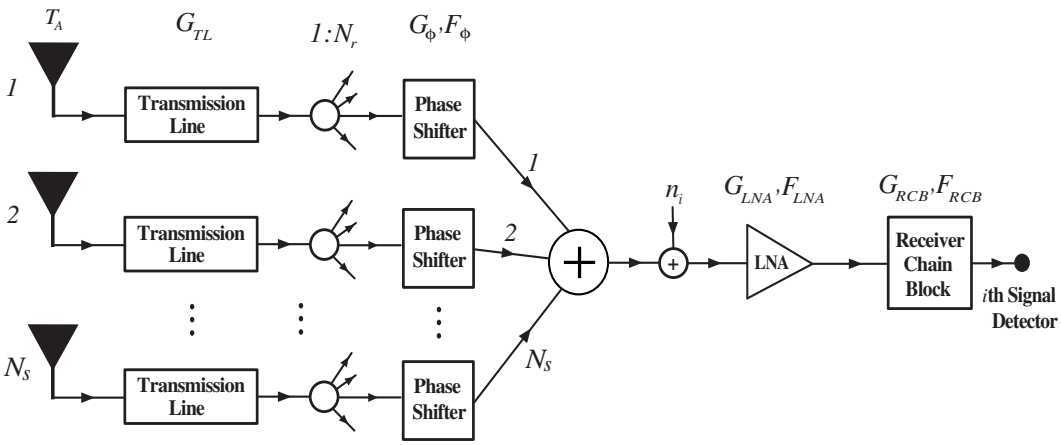

Figure 2.7: Passive phased array of ith (out of N_r) receiver input.

Now, assuming an ideal lossless SAS module

$$\sigma_{n_i}^2 = N_{LNA_i} + \sum_{j=1}^{N_s} \frac{N_{A_j}}{N_r N_s} \tag{2.9}$$

Hence, one can say that the major noise sources contributing in the modeled noise are the antenna noise and the LNA noise. In the next chapter the pre-LNA SAS-MIMO system is analyzed for when only these two noise sources exist in the system.

Chapter 3

SAS-MIMO for Noise-Limited Channels

It is shown in [14] and [28] that the SAS method outperforms the traditional antenna selection methods, but its performance is upper-bounded by a full-complexity MIMO system. From an implementation point of view, a post-LNA SAS is introduced in [14] while the SAS structure used in [28] is performed before LNA and therefore it uses a lower number of LNAs. In both [14] and [28], the noise is modeled at the antenna terminals. However, in [14] the receiver noise is considered as a dominant noise while in [28] it is assumed that the sky noise dominates. Hence, the receiver noise dominance, which is usually the only case considered in literature [35, page 662] for communication systems, is not discussed in [28]. Similar to [28], in this chapter we investigate the performance of the SAS method for MIMO spatial multiplexing/diversity transmission systems when the RF pre-processing is performed between the antenna elements and LNA. However, our approach is different from [28] in two aspects: first, the SAS solution adapts to the instantaneous behavior of the channel. Second, the SAS analysis and design is performed for the two cases when the receiver or the sky noise dominates.

3.1 BaseBand Noise Model

As seen in the previous chapter, in a noise-limited wireless communication system, i.e. when there is no dominant interference, only two noise sources *sky/channel/antenna* and *amplifier* contribute in the baseband system modeled noise. Assuming both of these noise sources are zero-mean, i.i.d. circularly symmetric Gaussian random processes, yields

$$\mathbf{n} = \mathbf{W}\mathbf{n}_s + \mathbf{n}_a \tag{3.1}$$

where Additive White Gaussian Noise (AWGN) $\mathbf{n}_s \sim \mathcal{CN}(0, \sigma^2_{\mathbf{n}_s}\mathbf{I}_{N_s})$ and $\mathbf{n}_a \sim \mathcal{CN}(0, \sigma^2_{\mathbf{n}_a}\mathbf{I}_{N_r})$ respectively represent the sky noise and the amplifier noise. Although both the sky noise and the amplifier noise sources can contribute in the noise vector $\mathbf{n}$ as shown in (3.1), in practice either the sky noise [36] or the amplifier noise [38] dominates. This dominance highly depends on the operating frequency. In low frequencies, e.g. below 1GHz, the sky noise is basically dominant; however, when the frequency increases above that the receiver noise dominates [39, Fig. 3.1, page 37]. In addition to the frequency band, the man made part of the sky noise has a major contribution in the above noise type dominance. For instance, due to different man made noise powers for urban and sub-urban areas either the sky noise or receiver noise can dominate in a particular frequency carrier [39, Fig. 3.1, page 37]. In an indoor area, due to the high frequency applications like Wireless Local Area Networks (WLAN) the dominant noise is typically the receiver noise. Although, there can exist a various man made noise sources in a normal indoor environment like office areas, the low cost commercial receivers consist of many electronic noisy components particularly high noise figure front end amplifiers and this makes the receiver noise dominant.

3.2 MIMO Spatial Multiplexing System

Fig. 3.1-a shows the MIMO spatial multiplexing system. The $N_r \times 1$ received signal vector $\mathbf{y}$ is written as

$$\mathbf{y} = \mathbf{H}_a\mathbf{x} + \mathbf{n} \tag{3.2}$$

where $\mathbf{x}$ is an $N_t \times 1$ transmitted signal and $\mathbf{H}_a = \mathbf{WH}$. In this system the achieved mutual information for a transmitter without CSI case but the receiver fully knows CSI, where the signals transmitted from individual antennas are independent and equi-powered, is given by [40]

$$I_u(\mathbf{x}; \mathbf{y}, \mathbf{H}_a) = \log\left[\det\left(\frac{P_t}{N_t}\mathbf{WU\Lambda\Lambda^*U^*W^*}(\sigma^2_{\mathbf{n}_s}\mathbf{WW^*} + \sigma^2_{\mathbf{n}_a}\mathbf{I}_{N_r})^{-1} + \mathbf{I}_{N_r}\right)\right] \tag{3.3}$$

where P_t is the total average energy available at the transmitter over a symbol period, and the channel matrix has a Singular Value Decomposition (SVD) of $\mathbf{H} = \mathbf{U\Lambda V}^*$. $\mathbf{U}$, $\mathbf{V}$ and $\mathbf{\Lambda}$ are respectively a $N_s \times N_s$ unitary matrix, a $N_t \times N_t$ unitary matrix and a $N_s \times N_t$ diagonal matrix.

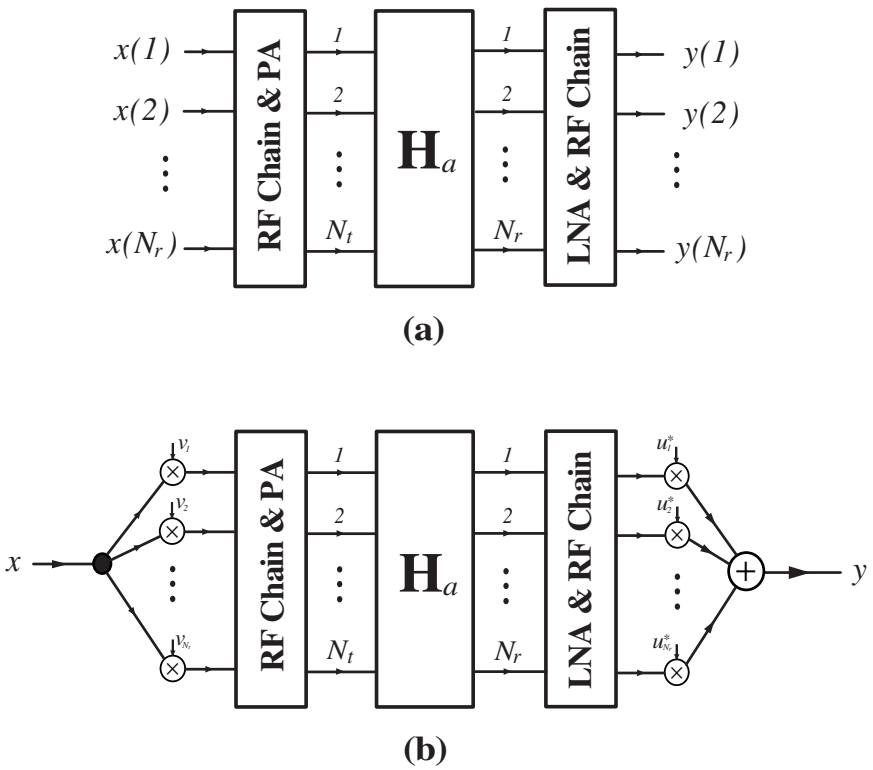

Figure 3.1: Baseband Models with $\mathbf{H}_a = \mathbf{WH}$ for (a) MIMO spatial multiplexing system (b) MIMO diversity system.

3.2.1 Optimum Pre-LNA SAS for Spatial Multiplexing Transmission

For a given channel matrix $\mathbf{H}$ the Optimum Pre-LNA SAS for Spatial Multiplexing transmission (OPSSM) is given by

$$\mathbf{W}_{opssm} = \arg \max_{\mathbf{W} \in S_p} I_u(\mathbf{x}; \mathbf{y}, \mathbf{H}_a) \tag{3.4}$$

where the PLN constraint $\mathbf{W} \in S_p$ is defined in Section 2.1.1.

To the best of our knowledge, there is no closed-form solution for the OPSSM. However, $\mathbf{W}_{opssm}$ can be instead numerically found using an exhaustive search. Since we are designing an adaptive system where the OPSSM is calculated based on each channel realization, such an exhaustive search may not be feasible as it is time consuming. In the following we propose an alternative method which provides a sub-optimal solution for the pre-LNA SAS. To proceed, we adopt a trace-bounding approach in which the constraint $\mathbf{W} \in S_p$ is relaxed and a less stringent condition is applied. The new condition is a trace-bounded constraint $\mathbf{W} \in S_t$ where $S_t = \{\mathbf{W} | tr(\mathbf{W}^*\mathbf{W}) \leq 1\}$. Hence, the Optimum Trace-Bounded SAS for Spatial Multiplexing transmission (OTSSM), $\mathbf{W}_{otssm}$, is found by solving the maximization problem (3.4) when the constraint $\mathbf{W} \in S_t$ is applied. Since[1] $S_p \subset S_t$, the OTSSM provides an upper-bound on the pre-LNA SAS performance. $\mathbf{W}_{otssm}$ is found for two practical cases of noise as defined in Section 3.1. Then, we use the calculated OTSSM to obtain a practical sub-optimal solution for the pre-LNA SAS.

Sky Noise $\mathbf{n}_s$ Dominates

In this case, (3.2) is represented as $\mathbf{y} = \mathbf{WHx} + \mathbf{Wn}_s$. Thus, using the equality $\det(\mathbf{I} + \mathbf{AB}) = \det(\mathbf{I} + \mathbf{BA})$ in (3.3) the OTSSM is given by

$$\mathbf{W}_{otssm,s} = \arg \max_{\mathbf{W} \in S_t} \log \left[\det \left(\frac{P_t}{N_t \sigma^2_{\mathbf{n}_s}} \mathbf{\Lambda}^* \mathbf{U}^* \mathbf{W}^* (\mathbf{W}\mathbf{W}^*)^{-1} \mathbf{W}\mathbf{U}\mathbf{\Lambda} + \mathbf{I}_{N_t} \right) \right] \tag{3.5}$$

Theorem 1 *For a given $N_s \times N_t$ channel matrix $\mathbf{H}$, the $N_r \times N_s$ OTSSM matrix, $\mathbf{W}_{otssm,s}$, represented in (3.5) is given by*

$$\mathbf{W}_{otssm,s} = \mathbf{M}\mathbf{\Omega}\mathbf{U}^* \tag{3.6}$$

where $\mathbf{M}$ is any $N_r \times N_r$ matrix with the constraint $tr(\mathbf{M}^*\mathbf{M}) \leq 1$, and $\mathbf{\Omega} = [\mathbf{I}_{N_r} | \mathbf{0}_{N_r \times (N_s - N_r)}]$.

proof 1 *Define*

$$\mathbf{W}_{osm,s} = \arg \max_{\mathbf{W}} \log \left[\det \left(\frac{P_t}{N_t \sigma^2_{\mathbf{n}_s}} \mathbf{\Lambda}^* \mathbf{U}^* \mathbf{W}^* (\mathbf{W}\mathbf{W}^*)^{-1} \mathbf{W}\mathbf{U}\mathbf{\Lambda} + \mathbf{I}_{N_t} \right) \right] \tag{3.7}$$

[1] This can be obtained using $tr(\mathbf{W}^*\mathbf{W}) = \|\mathbf{W}\|_2^2$.

Then, from [14, Appendix B] $\mathbf{W}_{osm,s} = \mathbf{B\Omega U}^*$ *where* $\mathbf{B}$ *can be any* $N_r \times N_r$ *matrix. Now assume* $S_1 = \{\mathbf{W}|\mathbf{W} = \mathbf{W}_{osm,s}\}$*, then* $\mathbf{W}_{otssm,s} \in S_1 \cap S_t$ *which implies*

$$\mathbf{W}_{otssm,s} \;=\; \mathbf{M\Omega U}^* \tag{3.8}$$

Amplifier Noise $\mathbf{n}_a$ Dominates

In this case, (3.2) is represented as $\mathbf{y} = \mathbf{WHx} + \mathbf{n}_a$ and therefore the OTSSM is given by

$$\mathbf{W}_{otssm,a} \;=\; \arg \max_{\mathbf{W} \in S_t} \log \left[\det \left(\frac{P_t \mathbf{WU\Lambda\Lambda}^* \mathbf{U}^* \mathbf{W}^*}{N_t \sigma^2_{\mathbf{n}_a}} + \mathbf{I}_{N_r} \right) \right] \tag{3.9}$$

Theorem 2 *For a given* $N_s \times N_t$ *channel matrix* $\mathbf{H}$*, the* $N_r \times N_s$ *OTSSM matrix,* $\mathbf{W}_{otssm,a}$*, represented in (3.9) is given by*

$$\mathbf{W}_{otssm,a} \;=\; \tilde{\mathbf{U}}\mathbf{\Pi U}^* \tag{3.10}$$

where $\tilde{\mathbf{U}}$ *can be any* $N_r \times N_r$ *unitary matrix, and* $\mathbf{\Pi} = [\mathbf{\Psi}|\mathbf{0}_{N_r \times (N_s - N_r)}]$*.* $\mathbf{\Psi}$ *is a* $N_r \times N_r$ *diagonal matrix with* $tr(\mathbf{\Psi}) \leq 1$*. The diagonal entries of* $\mathbf{\Psi}$ *are given by*

$$[\mathbf{\Psi}]^2_{i,i} \;=\; \left(\gamma - \frac{N_t \sigma^2_{\mathbf{n}_a}}{P_t \lambda^2_{i,\mathbf{H}}} \right)^+$$

with γ *chosen to satisfy the following condition* $\sum_{i=1}^{N_{min}} (\gamma - \frac{N_t \sigma^2_{\mathbf{n}_a}}{P_t \lambda^2_{i,\mathbf{H}}})^+ \leq 1$ *where* $N_{min} = min\{N_t, N_r\}$ *and* $x^+ = max(0, x)$*.*

proof 2 *Let singular value decomposition of* $\mathbf{W}$ *be as* $\mathbf{U}_w \mathbf{\Lambda}_w \mathbf{V}_w^*$ *where* $\mathbf{U}_w$ *and* $\mathbf{V}_w$ *are respectively* $N_r \times N_r$ *and* $N_s \times N_s$ *unitary matrices and* $\mathbf{\Lambda}_w$ *is a diagonal matrix whose non-zero elements are arranged in descending order. Now, using the equality* $det(\mathbf{I} + \mathbf{AB}) = det(\mathbf{I} + \mathbf{BA})$*, it is seen that the maximization problem (3.9) does not depend on* $\mathbf{U}_w$ *and therefore it can be any* $N_r \times N_r$ *unitary matrix like* $\tilde{\mathbf{U}}$*. Moreover, applying the approach used in [41, Section IV] yields* $\mathbf{V}_w = \mathbf{U}$*. Hence, (3.9) is simplified to*

$$\begin{aligned} \mathbf{\Lambda}_w \;&=\; \arg \max_{tr(\mathbf{\Lambda}_w^2) \leq 1} \log \left[\det \left(\frac{P_t \mathbf{\Lambda}^* \mathbf{\Lambda}_w^2 \mathbf{\Lambda}}{N_t \sigma^2_{\mathbf{n}_a}} + \mathbf{I}_{N_t} \right) \right] \\ &=\; \arg \max_{tr(\mathbf{\Lambda}_w^2) \leq 1} \sum_{i=1}^{N_{min}} \log \left(1 + \frac{P_t}{N_t \sigma^2_{\mathbf{n}_a}} \lambda^2_{i,\mathbf{H}} \lambda^2_{i,\mathbf{W}} \right) \end{aligned} \tag{3.11}$$

The water-filling approach is then employed to maximize (3.11). Hence,

$$\lambda_{i,\mathbf{W}}^2 = \left(\gamma - \frac{N_t \sigma_{\mathbf{n}_a}^2}{P_t \lambda_{i,\mathbf{H}}^2}\right)^+$$

with γ chosen to satisfy the following constraint

$$\sum_{i=1}^{N_{min}} \left(\gamma - \frac{N_t \sigma_{\mathbf{n}_a}^2}{P_t \lambda_{i,\mathbf{H}}^2}\right)^+ \leq 1$$

This concludes $\mathbf{\Lambda}_w = \mathbf{\Pi}$.

A Sub-OPSSM, $\mathbf{W}_{sopssm}$, is now found using the following Equal Gain Two-Step (EGTS) procedure:

Algorithm I: EGTS for Pre-LNA SAS in Noise-Limited Channels

1- `Find the OSSM matrix using (3.6) and (3.10) respectively for when` $\mathbf{n}_s$ `or` $\mathbf{n}_a$ `dominates.`

2- `Set the magnitude of all elements of the found matrix to` $\sqrt{\frac{1}{N_r N_s}}$.

Hence, due to $S_p \subset S_t$ the mutual information corresponding to the OPSSM, $\mathbf{W}_{opssm}$, is bounded as

$$I_u(\mathbf{W}_{sopssm}) \leq I_u(\mathbf{W}_{opssm}) \leq I_u(\mathbf{W}_{otssm})$$

which reveals an optimality-region for the mutual information $I_u(\mathbf{W}_{opssm})$.

3.3 MIMO Diversity System

The MIMO system equipped with the pre-LNA SAS for the diversity transmission is depicted in Fig. 3.1-b. We assume that both the transmitter and receiver know the channel information perfectly. Hence, the input-output relationship for the signal transmission is given by

$$y = \mathbf{u}^* \mathbf{H}_a \mathbf{v} x + \mathbf{u}^* \mathbf{n} \tag{3.12}$$

where $\mathbf{u}$ and $\mathbf{v}$ are respectively $N_r \times 1$ and $N_t \times 1$ weighting vectors determined to optimize the diversity transmission. There is no constraint on the vectors $\mathbf{u}$ and $\mathbf{v}$ but for a total average transmit power P_t, it is required that $\|\mathbf{v}\| = 1$. To find the optimum solution for the diversity gain, we maximize the SNR gain, which is

generally defined as the ratio of the combiner output SNR to a reference system SNR [35, page 556]. From (3.12), the combiner output SNR is

$$\rho_c = P_t \frac{|\mathbf{u}^*\mathbf{W}\mathbf{H}\mathbf{v}|^2}{\sigma^2_{\mathbf{n}_s}\|\mathbf{u}^*\mathbf{W}\|^2 + \sigma^2_{\mathbf{n}_a}\|\mathbf{u}^*\|^2} \tag{3.13}$$

We use the nominal receiver SNR [14], i.e. $\rho = \frac{P_t}{\sigma^2_{\mathbf{n}_s}+\sigma^2_{\mathbf{n}_a}}$ when $\mathcal{E}[|[\mathbf{H}]_{i,j}|] = 1$, as a reference. Hence, the SNR gain is given by

$$G_\rho = \frac{\rho_c}{\rho} = \frac{(1+\frac{\sigma^2_{\mathbf{n}_a}}{\sigma^2_{\mathbf{n}_s}})|\mathbf{u}^*\mathbf{W}\mathbf{H}\mathbf{v}|^2}{\|\mathbf{u}^*\mathbf{W}\|^2 + \frac{\sigma^2_{\mathbf{n}_a}}{\sigma^2_{\mathbf{n}_s}}\|\mathbf{u}^*\|^2} \tag{3.14}$$

The SNR Gain G_ρ can be maximized through the optimal vectors $\mathbf{u}$ and $\mathbf{v}$ located in the transceiver baseband, and the Optimum Pre-LNA SAS for Diversity transmission (OPSD), $\mathbf{W}_{opsd}$, which is positioned in the receiver RF section. Hence,

$$G_{\rho,opsd} = \max_{\mathbf{W}\in S_p} \max_{\mathbf{u}} \max_{\|\mathbf{v}\|=1} G_\rho \tag{3.15}$$

The maximized SNR gain (3.15) is found through the following three steps.

3.3.1 Optimum vector v

In the first step, the SNR gain G_ρ is maximized on $\mathbf{v}$ subject to the constraint $\|\mathbf{v}\| = 1$, i.e.

$$G_{\rho,\mathbf{v}} = \max_{\|\mathbf{v}\|=1} G_\rho \tag{3.16}$$

The optimum vector $\mathbf{v}$ can be generally obtained based on four different schemes: MRT, Equal Gain Transmission (EGT), Selection Diversity Transmission (SDT), and Generalized Subset Selection (GSS) [8]. The following theorem provides $G_{\rho,\mathbf{v}}$ obtained based on the MRT method where the transmitter is fully informed by the receiver.

Theorem 3 *Assume that the channel matrix* $\mathbf{H}$*, the SAS matrix* $\mathbf{W}$ *and the vector* $\mathbf{u}$ *are known. Then, the SNR gain (3.16) maximized on* $\mathbf{v}$ *is given by*

$$G_{\rho,\mathbf{v}} = \frac{(1+\frac{\sigma^2_{\mathbf{n}_a}}{\sigma^2_{\mathbf{n}_s}})|\mathbf{u}^*\mathbf{W}\mathbf{H}\mathbf{H}^*\mathbf{W}^*\mathbf{u}|}{\|\mathbf{u}^*\mathbf{W}\|^2 + \frac{\sigma^2_{\mathbf{n}_a}}{\sigma^2_{\mathbf{n}_s}}\|\mathbf{u}^*\|^2} \tag{3.17}$$

associated with $\mathbf{v}_{opt} = \frac{\mathbf{H}^*\mathbf{W}^*\mathbf{u}}{\|\mathbf{H}^*\mathbf{W}^*\mathbf{u}\|}$.

proof 3 *The SNR gain G_ρ, defined in (3.14), can be rewritten as*

$$G_\rho = \frac{(1+\frac{\sigma^2_{\mathbf{n}_a}}{\sigma^2_{\mathbf{n}_s}})\,(\mathbf{v}^*\mathbf{H}^*\mathbf{W}^*\mathbf{u}\mathbf{u}^*\mathbf{W}\mathbf{H}\mathbf{v})}{\|\mathbf{u}^*\mathbf{W}\|^2+\frac{\sigma^2_{\mathbf{n}_a}}{\sigma^2_{\mathbf{n}_s}}\|\mathbf{u}^*\|^2} \tag{3.18}$$

Hence, the optimum solution for the maximization problem (3.16) is now given by

$$\mathbf{v}_{opt} = \arg\max_{\|\mathbf{v}\|=1} P_s \tag{3.19}$$

where $P_s = \mathbf{v}^*\mathbf{A}_\mathbf{v}\mathbf{v}$ and $\mathbf{A}_\mathbf{v} = \mathbf{H}^*\mathbf{W}^*\mathbf{u}\mathbf{u}^*\mathbf{W}\mathbf{H}$. Now, using the identity $\mathbf{x}^*\mathbf{A}\mathbf{x} \leq \lambda_{1,\mathbf{A}}\|\mathbf{x}\|^2$ where $\lambda_{1,\mathbf{A}}$ is the largest eigenvalue of $\mathbf{A}$ from the Rayleigh-Ritz theorem [42, Sec. 4.2.2] yields

$$\mathbf{v}^*\mathbf{A}_\mathbf{v}\mathbf{v} \leq \lambda_{1,\mathbf{A}_\mathbf{v}}\|\mathbf{v}\|^2 = \lambda_{1,\mathbf{A}_\mathbf{v}} \tag{3.20}$$

where the equality holds if and only if $\mathbf{v}$ is along the direction of the eigenvector corresponding to $\lambda_{1,\mathbf{A}_\mathbf{v}}$. The optimum SNR gain $G_{\rho,\mathbf{v}}$ is thus given by

$$G_{\rho,\mathbf{v}} = \frac{(1+\frac{\sigma^2_{\mathbf{n}_a}}{\sigma^2_{\mathbf{n}_s}})\lambda_{1,\mathbf{A}_\mathbf{v}}}{\|\mathbf{u}^*\mathbf{W}\|^2+\frac{\sigma^2_{\mathbf{n}_a}}{\sigma^2_{\mathbf{n}_s}}\|\mathbf{u}^*\|^2} \tag{3.21}$$

and the optimum vector $\mathbf{v}_{opt}$ is the corresponding eigenvector to $\lambda_{1,\mathbf{A}_\mathbf{v}}$. However, a non-trivial solution of $\mathbf{u}_{opt}$ can be obtained through the method used in [43]. From (3.20)

$$\mathbf{h}_\mathbf{A}\mathbf{h}^*_\mathbf{A}\mathbf{v}_{opt} = \lambda_{1,\mathbf{A}_\mathbf{v}}\mathbf{v}_{opt} \tag{3.22}$$

where $\mathbf{h}_\mathbf{A} = \mathbf{H}^*\mathbf{W}^*\mathbf{u}$. As seen, the matrix $\mathbf{A}_\mathbf{v} = \mathbf{h}_\mathbf{A}\mathbf{h}^*_\mathbf{A}$ is a rank one matrix as its all columns are linear combinations of the single vector $\mathbf{h}_\mathbf{A}$. Since the column space of the matrix $\mathbf{A}_\mathbf{v}$ consists of only one single vector, i.e. $\mathbf{h}_\mathbf{A}$, the only way to obtain a non-trivial solution is to have

$$\begin{aligned}\mathbf{v}_{opt} &= \frac{\mathbf{h}_\mathbf{A}}{\|\mathbf{h}_\mathbf{A}\|} = \frac{\mathbf{H}^*\mathbf{W}^*\mathbf{u}}{\|\mathbf{H}^*\mathbf{W}^*\mathbf{u}\|}\\ \lambda_{1,\mathbf{A}_\mathbf{v}} &= |\mathbf{u}^*\mathbf{W}\mathbf{H}\mathbf{H}^*\mathbf{W}^*\mathbf{u}|\end{aligned} \tag{3.23}$$

3.3.2 Optimum vector u

The result of the first step, i.e. $G_{\rho,\mathbf{v}}$, is then maximized on $\mathbf{u}$ via the MRC scheme assuming that all the information are available at the receiver side. Hence,

$$G_{\rho,\mathbf{v},\mathbf{u}} = \max_{\mathbf{u}} G_{\rho,\mathbf{v}} \tag{3.24}$$

The optimum SNR gain $G_{\rho,\mathbf{v},\mathbf{u}}$ is obtained by proving the following theorem.

Theorem 4 *For a known channel matrix* $\mathbf{H}$ *and a SAS matrix* $\mathbf{W}$*, the SNR gain* $G_{\rho,\mathbf{v},\mathbf{u}}$ *maximized on* $\mathbf{v}$ *and* $\mathbf{u}$ *is given by*

$$G_{\rho,\mathbf{v},\mathbf{u}} \;=\; (1+\frac{\sigma^2_{\mathbf{n}_a}}{\sigma^2_{\mathbf{n}_s}})\lambda_{1,\,\mathbf{A}} \tag{3.25}$$

where

$$\mathbf{A} \;=\; \mathbf{L}^{-1}\mathbf{W}\mathbf{H}\mathbf{H}^*\mathbf{W}^*(\mathbf{L}^{-1})^*$$

and the matrix $\mathbf{L}$ *comes from the Cholesky factorization [42] of* $\mathbf{L}\mathbf{L}^* = \mathbf{W}\mathbf{W}^* + \frac{\sigma^2_{\mathbf{n}_a}}{\sigma^2_{\mathbf{n}_s}}\mathbf{I}_{N_r}$*. This optimum SNR gain is associated with* $\mathbf{u}_{opt} = \beta_1\ (\mathbf{L}^{-1})^*\mathbf{u}_{1,\,\mathbf{A}}$ *where* $\beta_1 \neq 0$ *is an arbitrary constant which does not affect the SNR gain.*

proof 4 *We first find the optimum vector* $\mathbf{u}_{opt}$ *defined as*

$$\mathbf{u}_{opt} \;=\; \arg\ \max_{\mathbf{u}}\ G_{\rho,\mathbf{v}} \tag{3.26}$$

where

$$G_{\rho,\mathbf{v}} \;=\; \frac{(1+\frac{\sigma^2_{\mathbf{n}_a}}{\sigma^2_{\mathbf{n}_s}})|\mathbf{u}^*\mathbf{W}\mathbf{H}\mathbf{H}^*\mathbf{W}^*\mathbf{u}|}{\|\mathbf{u}^*\mathbf{W}\|^2+\frac{\sigma^2_{\mathbf{n}_a}}{\sigma^2_{\mathbf{n}_s}}\|\mathbf{u}^*\|^2} \tag{3.27}$$

The above-mentioned optimum solution can be obtained by taking the conjugate derivative [44] of (3.27), i.e. $G_{\rho,\mathbf{v}}$*, with respect to the vector* $\mathbf{u}$*. Hence,* $\partial G_{\rho,\mathbf{v}}/\partial\mathbf{u}' = 0$ *implies*

$$\mathbf{A}_{\mathbf{u}}\mathbf{u} \;=\; \tilde{\lambda}_{\mathbf{u}}\mathbf{B}_{\mathbf{u}}\mathbf{u} \tag{3.28}$$

where

$$\begin{aligned}
\mathbf{A}_{\mathbf{u}} &= \mathbf{W}\mathbf{H}\mathbf{H}^*\mathbf{W}^* \\
\mathbf{B}_{\mathbf{u}} &= \mathbf{W}\mathbf{W}^* + \frac{\sigma^2_{\mathbf{n}_a}}{\sigma^2_{\mathbf{n}_s}}\mathbf{I}_{N_r} \\
\tilde{\lambda}_{\mathbf{u}} &\triangleq \frac{|\mathbf{u}^*\mathbf{W}\mathbf{H}\mathbf{H}^*\mathbf{W}^*\mathbf{u}|}{\|\mathbf{u}^*\mathbf{W}\|^2+\frac{\sigma^2_{\mathbf{n}_a}}{\sigma^2_{\mathbf{n}_s}}\|\mathbf{u}^*\|^2}.
\end{aligned}$$

As seen, (3.28) is a generalized symmetric eigenproblem and can be converted to a standard for using the Cholesky factorization method proposed in [45]. Since $\mathbf{B}_{\mathbf{u}}$ *is a symmetric and positive definite matrix, we can define a Cholesky factorization of* $\mathbf{B}_{\mathbf{u}} = \mathbf{L}\mathbf{L}^*$*. Hence, (3.28) can be rewritten as*

$$\mathbf{A}\tilde{\mathbf{u}} \;=\; \tilde{\lambda}_{\mathbf{u}}\tilde{\mathbf{u}} \tag{3.29}$$

where $\mathbf{A} = \mathbf{L}^{-1}\mathbf{A}_{\mathbf{u}}(\mathbf{L}^{-1})^*$ *and* $\tilde{\mathbf{u}} = \mathbf{L}^*\mathbf{u}$. *As seen from (3.29),* $\tilde{\lambda}_{\mathbf{u}}$ *represents an eigenvalue of the matrix* $\mathbf{A}$ *[42] and therefore the eigenvector corresponding to* $\tilde{\lambda}_{\mathbf{u}}$ *can sub-maximize* $G_{\rho,\mathbf{v}}$. *On the other hand, we have* $G_{\rho,\mathbf{v}} = (1 + \frac{\sigma^2_{\mathbf{n}_a}}{\sigma^2_{\mathbf{n}_s}})\tilde{\lambda}_{\mathbf{u}}$. *This implies that the SNR gain* $G_{\rho,\mathbf{v}}$ *is maximized with the largest eigenvalue of* $\mathbf{A}$, *i.e.* $\lambda_{1,\mathbf{A}}$. *Hence, the optimum vector* $\tilde{\mathbf{u}}_{opt}$ *is along the direction of the eigenvector corresponding to the largest eigenvalue of the same matrix, i.e.* $\tilde{\mathbf{u}}_{opt} = \beta_1\ \mathbf{u}_{1,\mathbf{A}}$ *where* $\beta_1 \neq 0$ *is an arbitrary constant which does not affect the SNR gain. This yields* $\mathbf{u}_{opt} = \beta_1\ (\mathbf{L}^{-1})^*\mathbf{u}_{1,\mathbf{A}}$.

3.3.3 Optimum Pre-LNA SAS for Diversity Transmission

Assume that the optimal transceiver baseband design for diversity transmission, i.e. the optimal vectors $\mathbf{u}$ and $\mathbf{v}$, is given. Now, the OPSD matrix is given by

$$\mathbf{W}_{opsd} \;=\; \arg \max_{\mathbf{W} \in S_p} G_{\rho,\mathbf{v},\mathbf{u}} \tag{3.30}$$

This maximization problem does not also have a closed-form solution; however, to have an adaptive MIMO diversity system we can instead use a sub-OPSD which is shown later to have performance very close to the optimum one. To obtain the sub-OPSD matrix, we apply the procedure used for the spatial multiplexing problem (3.4) for the two practical states of the noise sources.

Sky Noise $\mathbf{n}_s$ Dominates

In this case, (3.12) is represented as $y = \mathbf{u}^*\mathbf{W}\mathbf{H}\mathbf{v}x + \mathbf{u}^*\mathbf{W}\mathbf{n}_s$. Hence, by substituting $\sigma^2_{\mathbf{n}_a} = 0$ into the aforementioned three-step procedure for maximum SNR gain finding, $G_{\rho,\mathbf{v},\mathbf{u}}$ reduces to $\lambda^2_{1,\mathbf{H}} = |||\mathbf{H}|||^2_2$ when

$$\beta_2\mathbf{W}^*_{opsd}\mathbf{u}_{opt,s} \;=\; \mathbf{u}_{1,\mathbf{H}_p}, \quad \mathbf{v}_{opt,s} \;=\; \mathbf{v}_{1,\mathbf{H}_p} \tag{3.31}$$

where $\mathbf{v}_{opt,s}$ and $\mathbf{u}_{opt,s}$ are the optimum vectors defined respectively in (3.17) and (3.25) for the particular case of the sky noise dominance, and $\beta_2 \neq 0$ is any arbitrary constant. Although the SNR gain $G_{\rho,\mathbf{v},\mathbf{u}}$ is herein $\mathbf{W}$-independent, for optimal diversity transmission we still need to meet the condition (3.31) on the $\mathbf{u}_{opt,s}$. Under this circumstance, the optimal SNR gain $G_{\rho,otsd} = G_{\rho,opsd} = \lambda^2_{1,\mathbf{H}} = |||\mathbf{H}|||^2_2$.

Amplifier Noise $\mathbf{n}_a$ Dominates

In this case, (3.12) is represented as $y = \mathbf{u}^*\mathbf{W}\mathbf{H}\mathbf{v}x + \mathbf{u}^*\mathbf{n}_a$. Hence, by substituting $\sigma^2_{\mathbf{n}_s} = 0$ into the aforementioned three-step procedure for optimal SNR gain finding, $G_{\rho,\mathbf{v},\mathbf{u}}$ is simplified to $\lambda^2_{1,\mathbf{WH}} = |||\mathbf{WH}|||^2_2$ when

$$\mathbf{u}_{opt,a} \;=\; \beta_3\mathbf{u}_{1,\mathbf{WH}}, \quad \mathbf{v}_{opt,a} \;=\; \mathbf{v}_{1,\mathbf{WH}} \tag{3.32}$$

where $\mathbf{v}_{opt,a}$ and $\mathbf{u}_{opt,a}$ are the optimum vectors defined respectively in (3.17) and (3.25) for the particular case of the amplifier noise dominance, and $\beta_3 \neq 0$ is any arbitrary constant. Now, we relax the constraint of the optimization problem (3.30) to $\mathbf{W} \in S_t$. In this case, the Optimum Trace-bounded SAS for Diversity transmission (OTSD) is given by

$$\mathbf{W}_{otsd} = \arg \max_{\mathbf{W} \in S_t} G_{\rho,\mathbf{v},\mathbf{u}} = \arg \max_{\mathbf{W} \in S_t} |||\mathbf{WH}|||_2^2 \tag{3.33}$$

The OTSD matrix thus obtained provides an upper-bound on the OPSD performance. To solve the maximization problem (3.33), we use of the spectral norm inequality [46] $|||\mathbf{WH}|||_2 \leq |||\mathbf{W}|||_2 \, |||\mathbf{H}|||_2, \forall \mathbf{W}, \mathbf{H}$ where the equality provides the general SAS matrix $\mathbf{W}$ which maximizes $|||\mathbf{WH}|||_2$ with a given $\mathbf{H}$. Now, define $S_s = \{\mathbf{W} | \; |||\mathbf{WH}|||_2^2 = |||\mathbf{W}|||_2^2 \; |||\mathbf{H}|||_2^2\}$, then we assume $S_t \cap S_s \neq \emptyset$. We later show this assumption is valid. Hence, the OTSD, as defined in (3.33), is now given by

$$\mathbf{W}_{otsd} = \arg \max_{\mathbf{W} \in S_t \cap S_s} \lambda_{1,\mathbf{W}}^2 \lambda_{1,\mathbf{H}}^2 = \arg \max_{\substack{tr(\mathbf{W}^*\mathbf{W}) \leq 1 \\ \mathbf{W} \in S_s}} \lambda_{1,\mathbf{W}}^2 \tag{3.34}$$

Theorem 5 *For a given channel matrix* $\mathbf{H}$*, the OTSD represented in (3.34) subject to the constraint* $\mathbf{W} \in S_t \cap S_s$ *is given by*

$$\mathbf{W}_{otsd} = \tilde{\mathbf{U}} \mathbf{\Pi} \tilde{\mathbf{V}}^* \tag{3.35}$$

where $\tilde{\mathbf{U}}$ *can be any* $N_r \times N_r$ *unitary matrix.* $\mathbf{\Pi} = [\mathbf{\Psi} | \mathbf{0}_{N_r \times (N_s - N_r)}]$ *where* $\mathbf{\Psi}$ *is a* $N_r \times N_r$ *diagonal matrix whose the only non-zero elements is with* $[\mathbf{\Psi}]_{1,1} = 1$*. Moreover,* $\tilde{\mathbf{V}} = [\mathbf{u}_{1,\mathbf{H}} | \mathbf{M}]$ *is a* $N_s \times N_s$ *unitary matrix where* $\mathbf{M}$ *is any* $N_s \times (N_s - 1)$ *matrix.*

proof 5 *Let* $\mathbf{W} = \mathbf{U}_w \mathbf{\Lambda}_w \mathbf{V}_w^*$ *as defined in proof 2. According to [46, Lemma 2.2], the spectral norm* $|||\mathbf{WH}|||$ *is maximized if the matrices* $\mathbf{W}^*\mathbf{W}$ *and* $\mathbf{HH}^*$ *have a common eigenvector which corresponds to their largest eigenvalue; i.e.* $\mathbf{u}_{1,\mathbf{W}^*} = \mathbf{u}_{1,\mathbf{H}}$*. This simply shows that* $\mathbf{V}_w = \tilde{\mathbf{V}}$*. Moreover, it does not put any condition on* $\mathbf{U}_w$ *and therefore* $\mathbf{U}_w$ *can be any* $N_r \times N_r$ *arbitrary unitary matrix. Now, (3.34) can be rewritten as*

$$\mathbf{W}_{otsd} = \arg \max_{tr(\mathbf{W}^*\mathbf{W}) \leq 1} \lambda_{1,\mathbf{W}}^2 \tag{3.36}$$

A solution to this maximization problem is $\lambda_{1,\mathbf{W}}^2 = 1$*, and* $\lambda_{i,\mathbf{W}}^2 = 0$ *for* $i = 2, 3, ..., N_r$*. Hence, the optimum* $\mathbf{\Lambda}_w$ *is* $\mathbf{\Pi}$*.*

This theorem shows that what we assumed earlier as $S_t \cap S_s \neq \emptyset$ was true. Hence, the optimum SNR gain subject to the constraint $\mathbf{W} \in S_t \cap S_s$ now becomes $G_{\rho,otsd} = \lambda_{1,\mathbf{H}}^2$.

As seen, when the sky noise $\mathbf{n}_s$ dominates the SAS matrix $\mathbf{W}$, which meets the condition (3.31), is OPSD. However, for when the amplifier noise $\mathbf{n}_a$ dominates the sub-optimum solution is obtained using OTSD as $\mathbf{W}_{sopsd} = \sqrt{\frac{1}{N_r N_s}}\mathbf{W}_{otsd}$ for when $\tilde{\mathbf{U}} = \mathbf{I}_{N_r}$.

3.4 Computer Simulations

The performance of the pre-LNA SAS applied on a MIMO diversity/spatial multiplexing system is compared against a full-complexity MIMO system via the simulations. The mutual information and the SNR gain are considered as the performance measures. A Rician-based statistical channel model is used to construct the realizations of the channel matrix $\mathbf{H}$ for a spatially correlated MIMO channel, e.g. an indoor wireless environment.

3.4.1 Channel Model

The statistical channel models are commonly used to evaluate the performance of the communications systems via simulation. A Rician-based statistical channel model is used here to realize the channel matrix, $\mathbf{H}$, for a spatially correlated MIMO channel. This model, in which there is a strong direct signal path, i.e. LOS, between the transmitter and the receiver, characterizes most of the wireless channels like indoor clustered wireless environment. In a Rician model, the channel matrix $\mathbf{H}$ can be represented as [47]

$$\mathbf{H} = \sqrt{\frac{K_f}{K_f+1}}\mathbf{H}_{LOS} + \sqrt{\frac{1}{K_f+1}}\mathbf{H}_{NLOS} \tag{3.37}$$

where $\mathbf{H}_{LOS}$ and $\mathbf{H}_{NLOS}$ respectively are the LOS and the NLOS channel components, and K_f represents the Rician K-factor. In the channel model (3.37), the LOS component is obtained by [48]

$$\mathbf{H}_{LOS} = \mathbf{a}(\Omega_{LOS,r}) \,.\, \mathbf{a}(\Omega_{LOS,t})^H$$

where $\mathbf{a}$ is the antenna array response, and $\Omega_{LOS,r}$ and $\Omega_{LOS,t}$ represent respectively the solid Angle Of Arrival (AOA) at the receive side and the solid Angle Of Departure (AOD) at the transmit side corresponding to the LOS component. The NLOS component of the channel matrix is given by the Kronecker model [48]:

$$\mathbf{H}_{NLOS} = \mathbf{R}_r^{1/2}\mathbf{H}_w\mathbf{R}_t^{1/2}$$

where $\mathbf{H}_w$ is a $N_t \times N_s$ matrix with complex Gaussian elements. Also, $\mathbf{R}_r$ and $\mathbf{R}_t$ are respectively the spatial covariance matrices at the receiver and transmitter, representing the receiver/transmitter signal correlation across the antenna elements. We

obtain the spatial covariance matrices, $\mathbf{R}_r$ and $\mathbf{R}_t$, based on the Two-Dimensional (2D) indoor clustered channel model proposed in [15] where only the azimuth angle is considered.

$$\mathbf{R} = \sum_{k=1}^{K}\sum_{l=1}^{L} \mathbf{a}\left(\Theta_k - \theta_{k,l}\right)\mathbf{a}^H\left(\Theta_k - \theta_{k,l}\right) \tag{3.38}$$

where Θ_k, $\theta_{k,l}$, K and L are the kth cluster mean/centre AOD/AOA, the lth ray AOD/AOA of the kth cluster, the number of clusters and the number of rays. The array response, $\mathbf{a}$, for such an antenna array is given by

$$\mathbf{a}(\theta) = \begin{bmatrix} 1 \\ e^{\frac{j2\pi}{\lambda_0}\Delta\sin(\theta)} \\ \vdots \\ e^{\frac{j2\pi}{\lambda_0}\Delta(N-1)\sin(\theta)} \end{bmatrix} \tag{3.39}$$

where Δ, λ_0 and N are respectively the antenna spacing, the wave-length and the number of antenna elements.

In our simulation study, the number of clusters and rays are considered as 10 and 20, respectively. Moreover, Θ_k is assumed to be uniformly distributed over $[0, 2\pi)$ and $\theta_{k,l}$ has a Laplacian distribution with 15° angular spread and mean Θ_k [15]. We produce 1000 channel matrix realizations with $N_s = 8$ and $N_t = 4$ where the transmit and receive antenna apertures, i.e. the ULA length, are respectively $5\lambda_0$ and $2\lambda_0$, and the number of RF chains, N_r, is also set to 4.

3.4.2 Systems under the test

The performances of the following MIMO systems, each having N_t transmit antennas (and N_t transmit RF chains), are compared

- A MIMO system with N_s receive antennas and N_s receive RF chains. As previously defined, this configuration is called full-complexity MIMO system.
- A MIMO system with N_s receive antennas, N_r receive RF chains, and a pure/subset selection matrix. The entries of this matrix are fixed As previously defined, this configuration is called MIMO system with receive pure antenna selection.
- A MIMO system with N_s receive antennas, N_r receive RF chains, and a post-LNA receive FFT-based Bulter matrix implemented by a $N_r \times N_s$ PLN. The entries of this matrix are fixed and their amplitudes and phases do not change. We call this system FFT-MIMO.

- A MIMO system with N_s receive antennas, N_r RF chains, and an optimum post-LNA receive SAS matrix realized by a $N_r \times N_s$ LN whose entries' phase and amplitude are fully adjustable with no-constraint.
- A MIMO system with N_s receive antennas, N_r RF chains, and a sub-optimum post-LNA receive SAS matrix realized by a $N_r \times N_s$ PLN with only adjustable phases.
- A MIMO system with N_r receive antennas and N_r receive RF chains. We call this configuration low-complexity MIMO in which the number of receive antenna terminals and receive RF chains are the same but equal to the number of receive RF chains used in SAS scheme.

3.4.3 Simulation Results

In Sections 3 and 4 the optimality of the pre-SAS scheme is discussed only for the two practical cases of noise dominance, i.e. when either the sky noise or the amplifier noise dominates. However, we show the behavior of the SAS method when both the aforementioned noise sources exist in the system. To evaluate this case, the mean mutual information (3.3) averaged on all channel matrix realizations is plotted versus the amplifier noise to the sky noise power ratio in Fig. 3.2 for the pre-LNA SAS against the full-complexity and post-LNA SAS. The plots are for $K_f = 20dB$ and $SNR = 10dB$. We have assumed that the total noise power is one, i.e. $\sigma^2_{\mathbf{n}_a} + \sigma^2_{\mathbf{n}_s} = 1$. We have plotted the mean mutual information (3.3) for the two particular cases of (3.6) and (3.10) for the SAS matrix $\mathbf{W}$ as *Upper-Bound 1* and *Upper-Bound 2*, respectively. As seen, this research presents an upper-bound for the optimum pre-LNA SAS when either the sky noise or the amplifier noise dominates and there is no closed-form solution for this upper-bound when both of the above noise sources contribute. However, one can simply realize that this upper-bound is lower-bounded by *Upper-Bound 1* and *Upper-Bound 2*, i.e.

$$I_u(\mathbf{W}_{otssm,s}),\ I_u(\mathbf{W}_{otssm,a}) \ \leq \ I_u(\mathbf{W}_{otssm})$$

where $\mathbf{W}_{otssm}$ denotes the upper-bound for the optimal solution when both the sky noise and the amplifier noise contribute. In other words, the *Upper-Bound 1* and/or *Upper-Bound 2* plots are still good measures to evaluate the pre-LNA SAS perfromace against a full-complexity MIMO and post-LNA SAS when both the noise sources contribute in $\mathbf{n}$. In Fig. 3.2, the mean mutual information (3.3) is also plotted for the sub-optimal solution taken of the *Upper-Bound 1*, i.e. $\mathbf{W}_{sotssm,a}$, and the *Upper-Bound 2*, i.e. $\mathbf{W}_{sotssm,s}$. In this figure, the sub-optimal solution for the post-LNA SAS is plotted based on the phase-shift-only algorithm proposed in [14]. As Fig. 3.2 shows the post-LNA SAS system always outperforms the pre-LNA SAS for the entire range of $\sigma^2_{\mathbf{n}_a}/\sigma^2_{\mathbf{n}_s}$, i.e. regardless of how the noise sources contribute in the system noise. This can be explained using the factor $\sqrt{\frac{1}{N_r N_s}}$ in the definition of $\mathbf{W}$ (see Chapter 2). In fact, this factor has no effect on a post-LNA

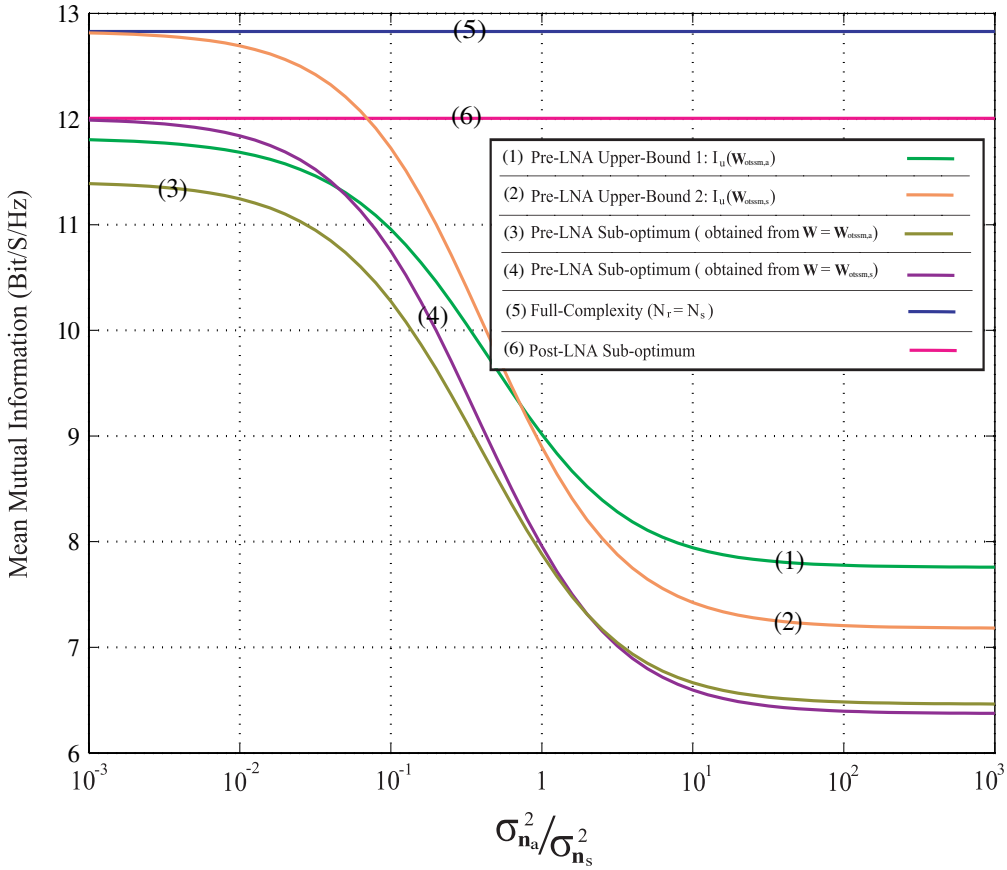

Figure 3.2: Mean mutual information versus the receiver/channel noise power ratio for different MIMO configurations.

SAS, and pre-LNA SAS when the sky noise dominates as in these case **W** is applied on both signal and noise. However, for a pre-LNA SAS when the amplifier noise dominates **W** is only applied on both signal and therefore the signal power reduces by the factor $\frac{1}{N_r N_s}$. The mean mutual information versus the SNR is also plotted in Fig. 3.3.

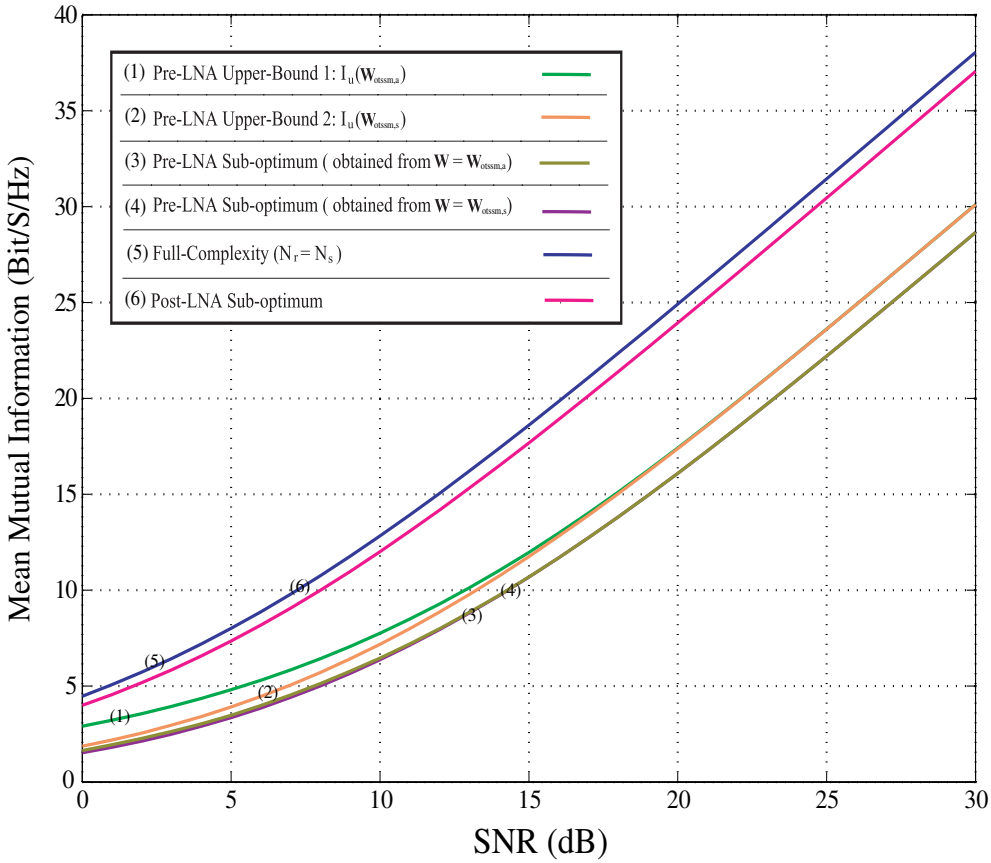

Figure 3.3: Mean mutual information versus the SNR for different MIMO configurations.

Chapter 4

SAS-MIMO for Interference Channels

In both [14] and [28], the SAS-MIMO system is only analyzed under a noise-dominated channel. However, in practice the noise is not the only impairment that limits the communication system performance. In many cases, e.g. wireless communications, the channel suffers from interference from other users and from fading due to destructive addition caused by multipath propagation as well. The interference has normally the following two important features which make it different than noise [49]:

- Power Angular Spectrum (PAS) of the received interference signals on each antenna element has a non-uniform spatial distribution. The interference PAS varies based on the location and transmit power of either the LOS interference sources or clusters/scatterers which reflect the rays coming from the NLOS interference sources.
- The interference covariance matrix is not diagonal.

By considering the interference channels with the above-mentioned characteristics for the interference, the solutions proposed in [14] and [28] for the MIMO system equipped with the receive SAS-MIMO, are no longer optimum. Indeed, the present work aims to derive the optimal solution for the SAS-MIMO system in presence of both noise and interference[1]. This optimization is performed for two transmission strategies, i.e. the spatial multiplexing and diversity. We consider two practical cases of either CSI is fully known at the transmitter side (CSIT) or

[1]In this chapter, we only consider the post-LNA SAS configuration as in Chapter 3 we showed that the post-LNA SAS always outperforms the pre-LNA SAS for both MIMO transmission schemes.

the transmitter is without CSI (CSIR). Although in both cases we assume that the channel is fully-known at the receiver side, we use CSIR to emphasize the case when the transmitter has no knowledge of CSI. Along with the optimal SAS solution, the closed-form optimum transceiver baseband structure is obtained under each of the above-mentioned transmission strategies. Moreover, the SAS optimality is investigated for two cases; one with no-constraint on the SAS module, and the other with the constraint that this module is built using PLN. Considering the aforementioned interference features, a 2D spatial model, which only includes the azimuth angle, is defined for the interference. In this model, the interference PAS is represented by a number of dominant interferers whose transmit power and AOA are assumed to be known at the receiver. Furthermore, we consider a zero-mean, i.i.d. circularly symmetric Gaussian random process vector for the noise. The performance of the optimum SAS-MIMO system is evaluated via computer simulation. The simulation results show that this SAS-MIMO system can achieve a full-complexity MIMO performance in terms of MI and Signal to Interference-plus-Noise Ratio (SINR) gain.

4.1 Baseband Interference-plus-Noise Model

Assume K narrow-band far-field interference signals, all centered at frequency f_0, impinge on the receive array from directions of $\{\theta_1, \theta_2, ..., \theta_K\}$ as shown in Fig. 4.1. We call these interference signals *interferers*. Due to multipath propagation (like in an indoor area), the interferers can be uncorrelated (like interferers s_1 and s_2, and/or s_3 and s_K in Fig. 4.1), partially correlated (like interferers s_3 and s_4) and/or fully-correlated (coherent) (like interferers s_k and s_K) with each other [49]. Each of the interferers is assumed to be Gaussian distributed where $s_k \sim \mathcal{CN}(0, \sigma^2_{s_k})$. The system noise $\mathbf{n}$, which is a combination of the external noise and the internal noise, is modeled at the LNA input as a zero-mean i.i.d. circularly symmetric Gaussian random process vector. This noise is assumed to be uncorrelated with the interferers. Hence, the interference-plus-noise, modeled as a vector at the receive antenna array, is given by

$$\mathbf{z} = \sum_{k=1}^{K} \mathbf{a}_k s_k + \mathbf{n} \tag{4.1}$$

where $\mathbf{n} \sim \mathcal{CN}(0, \sigma^2_{\mathbf{n}} \mathbf{I}_{N_s})$. The steering vector $\mathbf{a}_k$ of the receive antenna array in the direction of θ_k is given by

$$\mathbf{a}_k = \begin{bmatrix} 1 \\ e^{\frac{j2\pi}{\lambda_0}\Delta\cos(\theta_k)} \\ \vdots \\ e^{\frac{j2\pi}{\lambda_0}\Delta(N_s-1)\cos(\theta_k)} \end{bmatrix}$$

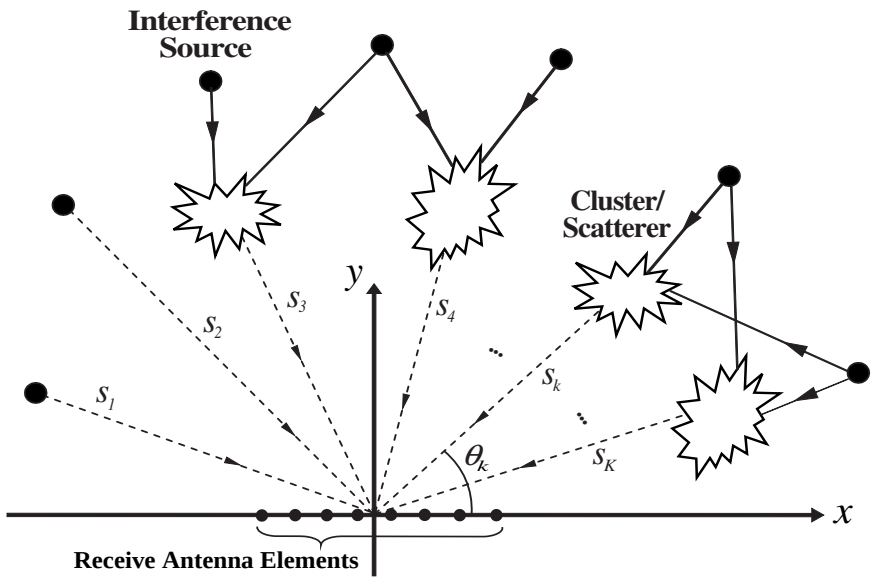

Figure 4.1: Interference Model.

where Δ and $\lambda_0 = 1/f_0$ are respectively the antenna spacing and the wave-length. Hence, the interference-plus-noise covariance matrix can be obtained as

$$\mathbf{K}_z = \mathbf{A}\mathbf{K}_s\mathbf{A}^* + \sigma_{\mathbf{n}}^2\mathbf{I}_{N_s} \tag{4.2}$$

where

$$\mathbf{A} = [\mathbf{a}_1, \mathbf{a}_2, ..., \mathbf{a}_K]^T$$

In (4.2), $\mathbf{K}_s = \mathcal{E}(\mathbf{s}\mathbf{s}^*)$ represents the interference covariance matrix where $\mathbf{s} = [s_1, s_2, ..., s_K]^T$. As seen, the covariance matrix $\mathbf{K}_z$ is always positive-definite due to the term $\sigma_{\mathbf{n}}^2\mathbf{I}_{N_s}$ in (4.2). In our optimization problem, we assume this covariance matrix, i.e. $\mathbf{K}_z$, is fully-known at the receiver side.

4.2 SAS-MIMO for Spatial Multiplexing Transmission

Figure 4.2-a shows the MIMO spatial multiplexing system. The $N_r \times 1$ received signal vector $\mathbf{y}$ is written as

$$\mathbf{y} = \mathbf{H}_a\mathbf{x} + \mathbf{W}\mathbf{z} \tag{4.3}$$

where $\mathbf{x}$ is a $N_t \times 1$ transmitted signal and $\mathbf{H}_a = \mathbf{W}\mathbf{H}$. Hence, the corresponding transmit-receive MI is given by [40]

$$I = \log\left[\det\left(\mathbf{W}\mathbf{H}\mathbf{K}_x\mathbf{H}^*\mathbf{W}^*(\mathbf{W}\mathbf{K}_z\mathbf{W}^*)^{-1} + \mathbf{I}_{N_r}\right)\right] \tag{4.4}$$

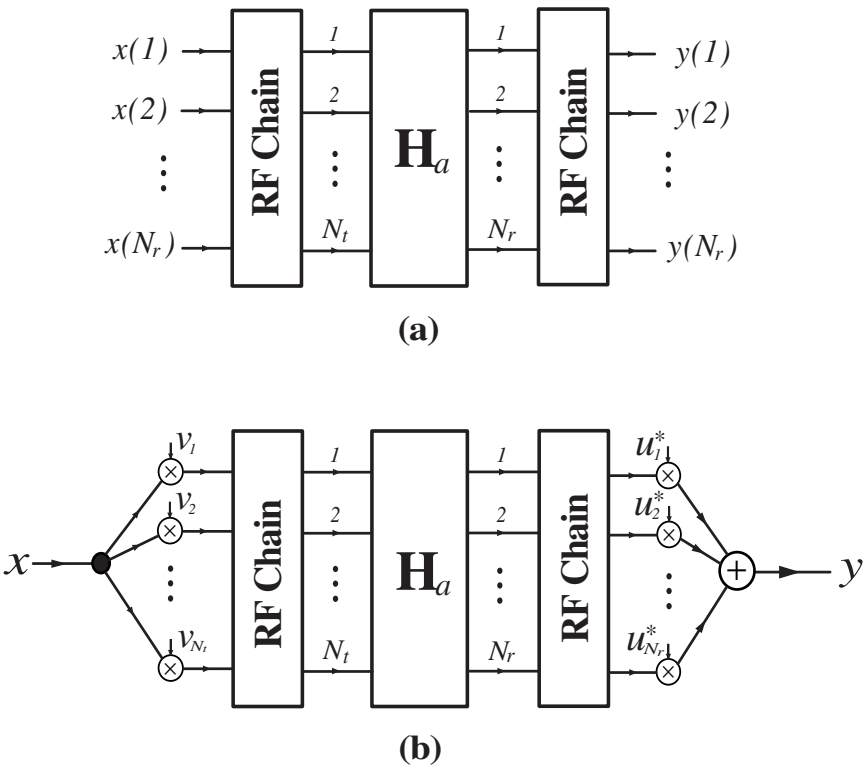

Figure 4.2: Baseband Models with $\mathbf{H}_a = \mathbf{WH}$ for (a) MIMO spatial multiplexing system (b) MIMO diversity system.

where $\mathbf{K}_x$ is the transmit signal covariance matrix. Now, by assuming that the channel matrix $\mathbf{H}$ and the interference covariance matrix $\mathbf{K}_z$ are given we solve the following optimization problem

$$I_M = \max_{\mathbf{K}_x \,:\, \mathrm{tr}(\mathbf{K}_x) \leq P_t} \; \max_{\mathbf{W} \in S_p} I \tag{4.5}$$

where the total average power available at the transmitter over a symbol period is given by P_t.

4.2.1 Optimum Pre-processing Matrix W

To maximize (4.4) on the pre-processing matrix $\mathbf{W}$, the solution is first found for the case when no constraint is imposed on W, i.e. $\mathbf{W} \in \mathcal{C}^{N_r \times N_s}$. A Phase Shift Based SAS (PSB-SAS) constraint $\mathbf{W} \in S_p$ is then applied. The latter is of practical interest, as it helps reduce the RF chain processing cost [14]. Hence, for the unconstrained case, the Optimum SAS for Spatial Multiplexing transmission (OSSM) is given by

$$\mathbf{W}_{ossm} = \arg \max_{\mathbf{W} \in \mathcal{C}^{N_r \times N_s}} I \tag{4.6}$$

The OSSM matrix, $\mathbf{W}_{ossm}$, is found through the following theorem.

Theorem 6 *For a given $N_s \times N_t$ channel matrix $\mathbf{H}$ and $N_s \times N_s$ interference covariance matrix $\mathbf{K}_z$, the $N_r \times N_s$ OSSM matrix represented in (4.6) is given by*

$$\mathbf{W}_{ossm} = \mathbf{M}\mathbf{\Omega}\mathbf{U}_A^*\mathbf{\Lambda}_z^{-1/2}\mathbf{U}_z^* \tag{4.7}$$

where $\mathbf{M}$ is any $N_r \times N_r$ non-singular matrix, and $\mathbf{\Omega} = [\mathbf{I}_{N_r}|\mathbf{0}_{N_r\times(N_s-N_r)}]$. The $N_s \times N_s$ unitary matrix $\mathbf{U}_z$ and $N_s \times N_s$ diagonal matrix $\mathbf{\Lambda}_z$ come from the Singular Value Decomposition (SVD) $\mathbf{K}_z = \mathbf{U}_z\mathbf{\Lambda}_z\mathbf{U}_z^*$, and $\mathbf{U}_A$ is a $N_s \times N_s$ unitary matrix coming from the SVD of $\mathbf{A} = \mathbf{U}_A\mathbf{\Lambda}_A\mathbf{U}_A^*$ where $\mathbf{A} = \mathbf{\Lambda}_z^{-1/2}\mathbf{U}_z^*\mathbf{H}\mathbf{K}_x\mathbf{H}^*\mathbf{U}_z\mathbf{\Lambda}_z^{-1/2}$.

proof 6 *For the proof of Theorem 6, we first convert the problem to [14, Theorem 2] and then use the techniques from [14, Appendix B] to complete the picture. To proceed this method, it is shown in [50, Theorem 8.7.1] that there exists a nonsingular $N_s \times N_s$ matrix $\mathbf{X}_1$ such that*

$$\begin{aligned} \mathbf{X}_1\mathbf{H}\mathbf{K}_x\mathbf{H}^*\mathbf{X}_1^* &= \mathbf{D}_1 \\ \mathbf{X}_1\mathbf{K}_z\mathbf{X}_1^* &= \mathbf{I}_{N_s} \end{aligned} \tag{4.8}$$

where $\mathbf{D}_1$ is a $N_s \times N_s$ diagonal matrix. Define $\mathbf{Y}_1 \triangleq \mathbf{W}\mathbf{X}_1^{-1}$. Substituting $\mathbf{W} = \mathbf{Y}_1\mathbf{X}_1$ into (4.4) yields

$$I_{u,csij}(\mathbf{Y}_1) = \log\left[\det\left(\frac{1}{N_t}\mathbf{Y}_1\mathbf{D}_1\mathbf{Y}_1^*(\mathbf{Y}_1\mathbf{Y}_1^*)^{-1} + \mathbf{I}_{N_r}\right)\right] \tag{4.9}$$

Now, the OSSM matrix is given by $\mathbf{W}_{ossmj} = \mathbf{Y}_{1,opt}\mathbf{X}_1$ where

$$\mathbf{Y}_{1,opt} = \arg \max_{\mathbf{Y}_1 \in \mathcal{C}^{N_r\times N_s}} I_{u,csij}(\mathbf{Y}_1) \tag{4.10}$$

According to [14, Theorem 2], the optimum matrix $\mathbf{Y}_{1,opt}$ is

$$\mathbf{Y}_{1,opt} = \mathbf{M}\mathbf{\Omega} \tag{4.11}$$

where $\mathbf{M}$ is an arbitrary $N_r \times N_r$ nonsingular matrix, and $\mathbf{\Omega} = [\mathbf{I}_{N_r}|\mathbf{0}_{N_r\times(N_s-N_r)}]$.

To find $\mathbf{X}_1$, let $\mathbf{X}_2 = \mathbf{\Lambda}_z^{-1/2}\mathbf{U}_z^*$ where $\mathbf{K}_z = \mathbf{U}_z\mathbf{\Lambda}_z\mathbf{U}_z^*$. Then, define $\mathbf{A} = \mathbf{X}_2\mathbf{H}\mathbf{K}_x\mathbf{H}^*\mathbf{X}_2^*$. Hence, $\mathbf{X}_1 = \mathbf{U}_A^*\mathbf{X}_2$, where $\mathbf{U}_A$ comes from the SVD of $\mathbf{A} = \mathbf{U}_A\mathbf{\Lambda}_A\mathbf{U}_A^*$, can meet the conditions in (4.8).

As seen, the optimum solution (4.7) depends on the availability of CSI. In the CSIT scenario, the optimal transmit covariance matrix must be found. This issue will be addressed shortly. However, before dealing with this problem, we turn our attention to the constraint optimization case where the SAS module is constructed by the pure phase-sifters. There is, unfortunately, no closed-form solution to this

problem. Hence, we resort to bounding techniques. To this end, a Sub-OSSM matrix ($\mathbf{W}_{sossm}$) is found using the following EGTS procedure:

Algorithm III: EGTS for Interference Channels

1- `Find the OSSM matrix using (4.7).`

2- `Set the magnitude of all elements of the found matrix to` $\sqrt{\frac{1}{N_r N_s}}$.

This procedure can be applied for both cases of CSIT and CSIR. Hence, MI corresponding to the Optimal PSB-SAS for Spatial Multiplexing transmission (OPSSM) is bounded as

$$I(\mathbf{W}_{sossm}) \leq I(\mathbf{W}_{opssm}) \leq I(\mathbf{W}_{ossm})$$

which reveals an optimality-region for $I(\mathbf{W}_{opssm})$.

4.2.2 Optimum Transmit Covariance Matrix $\mathbf{K}_x$

In this section, we obtain the optimal $\mathbf{K}_x$ for when either $\mathbf{W}_{ossm}$ or $\mathbf{W}_{sossm}$ is provided. Substituting (4.7) into (4.4) yields an upper-bound for (4.5) as

$$I_{u,M} = \max_{\mathrm{tr}(\mathbf{K}_x) \leq P_t} \log\left[\det\left(\mathbf{\Omega}\mathbf{\Lambda}_A\mathbf{\Omega}^* + \mathbf{I}_{N_r}\right)\right] \tag{4.12}$$

Similarly, using $\mathbf{W}_{sossm}$, resulted from EGTS procedure, the lower-bound for (4.5) is obtained as

$$I_{l,M} = \max_{\mathrm{tr}(\mathbf{K}_x) \leq P_t} \log\left[\det\left(\mathbf{W}_{sossm}\mathbf{H}\mathbf{K}_x\mathbf{H}^*\mathbf{W}^*_{sossm}(\mathbf{W}_{sossm}\mathbf{K}_z\mathbf{W}^*_{sossm})^{-1} + \mathbf{I}_{N_r}\right)\right] \tag{4.13}$$

To find the best transmit covariance matrix $\mathbf{K}_x$ for each of above bounds, we consider two practical cases of either CSIT or CSIR, separately.

CSIR

In this case, a reasonable choice for the transmit covariance matrix is $\mathbf{K}_{x,csir} = \frac{P_t}{N_t}\mathbf{I}_{N_t}$ [40]. Hence, the achieved MI upper- and lower-bounds, corresponding to (4.12) and (4.13), are respectively given by

$$I_{u,a} = \sum_{i=1}^{N_{min}} \log\left(1 + \frac{P_t}{N_t}\lambda^2_{i,\mathbf{A}_a}\right) \tag{4.14}$$

and

$$I_{l,a} = \log\left[\det\left(\frac{P_t}{N_t}\mathbf{W}_{sossm}\mathbf{H}\mathbf{H}^*\mathbf{W}^*_{sossm}(\mathbf{W}_{sossm}\mathbf{K}_z\mathbf{W}^*_{sossm})^{-1} + \mathbf{I}_{N_r}\right)\right] \quad (4.15)$$

where in (4.14), $N_{min} = min\{N_r, N_t\}$ and $\mathbf{A}_a = \mathbf{\Lambda}_z^{-1/2}\mathbf{U}_z^*\mathbf{H}\mathbf{H}^*\mathbf{U}_z\mathbf{\Lambda}_z^{-1/2}$.

CSIT

In this case, the optimal signaling based on the fed back information is applied. The following theorem provides the optimum $\mathbf{K}_x$ for the upper-bound of (4.12).

Theorem 7 *For a given $N_s \times N_t$ channel matrix $\mathbf{H}$ and the $N_s \times N_s$ interference covariance matrix $\mathbf{K}_z$ the optimal transmit signal covariance matrix $\mathbf{K}_x$ which maximizes $I(\mathbf{W}_{ossm})$, i.e. (4.12), is given by*

$$\mathbf{K}_{x,u,csit} = \mathbf{V}_B\mathbf{\Lambda}_{x,u,csit}\mathbf{V}_B^* \quad (4.16)$$

where $\mathbf{\Lambda}_{x,u,csit}$ is a $N_t \times N_t$ diagonal matrix whose non-zero elements are determined based on water-filling strategy as follows

$$[\mathbf{\Lambda}_{x,u,csit}]_{i,i} = \left(\gamma - \frac{1}{\lambda^2_{i,\mathbf{B}}}\right)^+$$

with γ chosen to satisfy the following constraint

$$\sum_{i=1}^{N_{min}}\left(\gamma - \frac{1}{\lambda^2_{i,\mathbf{B}}}\right)^+ \leq P_t$$

and $x^+ = max(0, x)$. Moreover, $\mathbf{V}_B$ is a $N_t \times N_t$ unitary matrix coming from the SVD of $\mathbf{B} = \mathbf{\Lambda}_z^{-1/2}\mathbf{U}_z^*\mathbf{H} = \mathbf{U}_B\mathbf{\Lambda}_B\mathbf{V}_B^*$.

proof 7 *Rewrite $\mathbf{A} = \mathbf{B}\mathbf{K}_x\mathbf{B}^*$ where $\mathbf{B} = \mathbf{\Lambda}_z^{-1/2}\mathbf{U}_z^*\mathbf{H}$. Now, consider the SVD of $\mathbf{B} = \mathbf{U}_B\mathbf{\Lambda}_B\mathbf{V}_B^*$ and $\mathbf{K}_x = \mathbf{U}_x\mathbf{\Lambda}_x\mathbf{U}_x^*$ where $\mathbf{U}_B$, $\mathbf{V}_B$, $\mathbf{\Lambda}_B$, $\mathbf{U}_x$ and $\mathbf{\Lambda}_x$ are respectively $N_s \times N_s$ unitary matrix, $N_t \times N_t$ unitary matrix ,$N_s \times N_t$ diagonal matrix, $N_t \times N_t$ unitary matrix and $N_t \times N_t$ diagonal matrix. Then, using the approach used in [41, Section IV] yields the best $\mathbf{U}_x$ as $\mathbf{U}_{x,u,csit} = \mathbf{V}_B$. Hence, (4.12) is rewritten as*

$$\begin{aligned} I_{u,M} &= \max_{\mathbf{\Lambda}_x\,:\,\mathrm{tr}(\mathbf{\Lambda}_x)\,\leq\,P_t} \log\left[\det\left(\mathbf{\Omega}\mathbf{\Lambda}_B\mathbf{\Lambda}_x\mathbf{\Lambda}_B^T\mathbf{\Omega}^T + \mathbf{I}_{N_r}\right)\right] \\ &= \max_{\lambda_{i,\mathbf{\Lambda}_x}\,:\,\mathrm{tr}(\mathbf{\Lambda}_x)\,\leq\,P_t} \sum_{i=1}^{N_{min}} \log\left(1 + \lambda_{i,\mathbf{\Lambda}_x}\lambda^2_{i,\mathbf{B}}\right) \end{aligned} \quad (4.17)$$

The water-filling approach is then employed to maximize (4.17). Hence, the best $\mathbf{\Lambda}_x$*, i.e.* $\mathbf{\Lambda}_{x,u,csit}$*, is found as*

$$\lambda_{i,\mathbf{\Lambda}_{x,u,csit}} = \left(\gamma - \frac{1}{\lambda_{i,\mathbf{B}}^2}\right)^+$$

with γ *chosen to satisfy the following constraint*

$$\sum_{i=1}^{N_{min}} \left(\gamma - \frac{1}{\lambda_{i,\mathbf{B}}^2}\right)^+ \leq P_t$$

Now, consider the lower bound of (4.13). Since the sub-optimal matrix $\mathbf{W}_{sossm}$ is a non-linear and complicated function of $\mathbf{K}_x$, finding a closed-form solution for the optimal $\mathbf{K}_x$ is a formidable task. Instead, we resort to an iterative approach to find the optimal $\mathbf{K}_x$. Suppose a SAS matrix $\mathbf{W}_{sossm}$ is given regardless how it is calculated. Then, the following theorem provides the optimum $\mathbf{K}_x$.

Theorem 8 *For a given* $N_s \times N_t$ *channel matrix* $\mathbf{H}$*, the* $N_s \times N_s$ *interference covariance matrix* $\mathbf{K}_z$ *and the SAS matrix* $\mathbf{W}_{ossm}$ *the optimal transmit signal covariance matrix* $\mathbf{K}_x$ *which maximizes* $I(\mathbf{W}_{sossm})$*, i.e. (4.13), is given by*[2]

$$\mathbf{K}_{x,l,csit} = \mathbf{V}_{\tilde{h}} \mathbf{\Lambda}_{x,l,csit} \mathbf{V}_{\tilde{h}}^* \tag{4.18}$$

where the entries of $\mathbf{\Lambda}_{x,l,csit}$ *are obtained based on water-filling strategy as follows*

$$[\mathbf{\Lambda}_{x,l,csit}]_{i,i} = \left(\mu - \frac{1}{\lambda_{i,\tilde{\mathbf{H}}}^2}\right)^+$$

with μ *chosen to satisfy the following constraint*

$$\sum_{i=1}^{N_{min}} \left(\mu - \frac{1}{\lambda_{i,\tilde{\mathbf{H}}}^2}\right)^+ \leq P_t$$

In (4.18), the $\mathbf{V}_{\tilde{h}}$ *is a* $N_t \times N_t$ *unitary matrix coming from the SVD of* $\tilde{\mathbf{H}} = \mathbf{L}_{wz}^{-1}\mathbf{W}_{sossm}\mathbf{H} = \mathbf{U}_{\tilde{h}}\mathbf{\Lambda}_{\tilde{h}}\mathbf{V}_{\tilde{h}}^*$*, with* $\mathbf{L}_{wz}$ *obtained from the Cholesky decomposition* $\mathbf{W}_{sossm}\mathbf{K}_z\mathbf{W}_{sossm}^* = \mathbf{L}_{wz}\mathbf{L}_{wz}^*$ *[42].*

proof 8 *Assume* $\mathbf{W}_{sossm}\mathbf{K}_z\mathbf{W}_{sossm}^*$ *is a positive-definite matrix*[3]*. Thus, there exists a Cholesky decomposition as*

$$\mathbf{W}_{sossm}\mathbf{K}_z\mathbf{W}_{sossm}^* = \mathbf{L}_{wz}\mathbf{L}_{wz}^* \tag{4.19}$$

[2]This theorem can be directly applied for the case in which the preprocessing matrix $\mathbf{W}$ is a FFT based Butler matrix used in [13] as $\mathbf{W}$ is fixed and known.

[3]Since $\mathbf{K}_z$ is positive-definite, this assumption is true when $\mathbf{W}_{sossm}$ is positive-definite too.

Substituting (4.19) into (4.13) yields

$$I_{l,M} = \max_{\mathbf{K}_x \,:\, \mathrm{tr}(\mathbf{K}_x) \,\leq\, P_t} \log\left[\det\left(\tilde{\mathbf{H}}\mathbf{K}_x\tilde{\mathbf{H}}^* + \mathbf{I}_{N_r}\right)\right] \tag{4.20}$$

where $\tilde{\mathbf{H}} = \mathbf{L}_{wz}^{-1}\mathbf{W}_{sossm}\mathbf{H}$. *Now, consider the SVD of* $\tilde{\mathbf{H}} = \mathbf{U}_{\tilde{h}}\mathbf{\Lambda}_{\tilde{h}}\mathbf{V}_{\tilde{h}}^*$ *where* $\mathbf{U}_{\tilde{h}}$, $\mathbf{V}_{\tilde{h}}$ *and* $\mathbf{\Lambda}_{\tilde{h}}$ *are respectively* $N_r \times N_r$ *unitary matrix,* $N_t \times N_t$ *unitary matrix ,*$N_r \times N_t$ *diagonal matrix. Similar to the proof of Theorem 2, applying the approach used in [41, Section IV] yields the best* $\mathbf{U}_x$ *as* $\mathbf{U}_{x,l,csit} = \mathbf{V}_{\tilde{h}}$. *Moreover, the best* $\mathbf{\Lambda}_x$, *i.e.* $\mathbf{\Lambda}_{x,l,csit}$, *is obtained using the water-filling optimization method as*

$$\lambda_{i,\mathbf{\Lambda}_{x,l,csit}} = \left(\mu - \frac{1}{\lambda_{i,\tilde{\mathbf{H}}}^2}\right)^+$$

for $i \in \{1, 2, ..., N_{min}\}$ *with* μ *chosen to satisfy the following constraint*

$$\sum_{i=1}^{N_{min}} \left(\mu - \frac{1}{\lambda_{i,\tilde{\mathbf{H}}}^2}\right)^+ \leq P_t$$

Hence, the following iterative algorithm provides the optimum $\mathbf{K}_x$, i.e. $\mathbf{K}_{x,l,csit}$, when $\mathbf{W}_{sossm}$ is $\mathbf{K}_x$-dependent. In this algorithm an initial value $\mathbf{K}_x = \frac{P_t}{N_t}\mathbf{I}_{N_t}$ is used.

Algorithm IV: Optimum $\mathbf{K}_x$ *when* $\mathbf{W}_{sossm}$ *is* $\mathbf{K}_x$*-dependent*

1- `Set` $I_{l,M} \leftarrow 0$ `and` $\mathbf{K}_x \leftarrow \frac{P_t}{N_t}\mathbf{I}_{N_t}$.

2- `Find` $\mathbf{W}_{ossm}$ `using (4.7).`

3- `Obtain` $\mathbf{W}_{sossm}$ `using Algorithm I (EGTS approach).`

4- `Calculate` $\mathbf{K}_{x,l,csit}$ `using (4.18).`

5- `Obtain MI` I `from (4.4) when` $\mathbf{W} = \mathbf{W}_{sossm}$.

6- `If` $I > I_{l,M}$`, then set` $I_{l,M} \leftarrow I$`,` $\mathbf{W} \leftarrow \mathbf{W}_{sossm}$ `and` $\mathbf{K}_x \leftarrow \mathbf{K}_{x,l,csit}$`, and then goto 2.`

7- `end`

4.3 SAS-MIMO for Diversity Transmission

The MIMO system equipped with SAS for the diversity transmission is depicted in Fig. 4.2-b. The input-output relationship for the signal transmission is given by

$$y = \mathbf{u}^*\mathbf{H}_a\mathbf{v}x + \mathbf{u}^*\mathbf{W}\mathbf{z} \tag{4.21}$$

where $\mathbf{u}$ and $\mathbf{v}$ are respectively $N_r \times 1$ and $N_t \times 1$ weighting vectors determined to optimize the diversity transmission. There is no constraint on the vectors $\mathbf{u}$ and $\mathbf{v}$ but for a total average transmit power P_t, it is required that $\|\mathbf{v}\| = 1$. To find the optimum solution for the diversity gain, we maximize the SINR gain for the two aforementioned cases: MIMO system with either CSIT or CSIR. Similar to the spatial multiplexing scheme, for each case we first find the optimal solution for the unconstrained case of $\mathbf{W} \in \mathcal{C}^{N_r \times N_s}$ and then a PSB-SAS constraint is applied. The SINR gain is generally defined as the ratio of the combiner output SINR to a reference system SINR [35, page 556]. From (4.21), the combiner output SINR is

$$\mathrm{SINR}_c = P_t \frac{|\mathbf{u}^*\mathbf{W}\mathbf{H}\mathbf{v}\mathbf{v}^*\mathbf{H}^*\mathbf{W}^*\mathbf{u}|}{|\mathbf{u}^*\mathbf{W}\mathbf{K}_z\mathbf{W}^*\mathbf{u}|} \tag{4.22}$$

In this chapter, we use the nominal receiver SINR, i.e. $\mathrm{SINR}_0 = \frac{P_t}{\|\mathbf{K}_s\|_1 + \sigma_{\mathbf{n}}^2}$ when $\mathcal{E}[|[\mathbf{H}]_{i,j}|] = 1$, as a reference. Hence, the SINR gain is given by

$$G_{\mathrm{SINR}} = \frac{\mathrm{SINR}_c}{\mathrm{SINR}_0} = (\|\mathbf{K}_s\|_1 + \sigma_{\mathbf{n}}^2)\frac{|\mathbf{u}^*\mathbf{W}\mathbf{H}\mathbf{v}\mathbf{v}^*\mathbf{H}^*\mathbf{W}^*\mathbf{u}|}{|\mathbf{u}^*\mathbf{W}\mathbf{K}_z\mathbf{W}^*\mathbf{u}|} \tag{4.23}$$

The SINR Gain G_{SINR} can be maximized through the optimal vectors $\mathbf{u}$ and $\mathbf{v}$ located in the transceiver baseband, and the Optimum SAS for Diversity transmission (OSD), $\mathbf{W}_{osd}$, which is positioned in the receiver RF section. Hence,

$$G_{\mathrm{SINR},osd} = \max_{\mathbf{W} \in S_p} \max_{\mathbf{u} \in \mathcal{C}^{N_r}} \max_{\|\mathbf{v}\|=1} G_{\mathrm{SINR}} \tag{4.24}$$

The maximized SINR gain (4.24) is found through the following three steps.

4.3.1 Optimum vector v

In the first step, the SINR gain G_{SINR} is maximized on $\mathbf{v}$ subject to the constraint $\|\mathbf{v}\| = 1$, i.e.

$$G_{\mathrm{SINR},\mathbf{v}} = \max_{\|\mathbf{v}\|=1} G_{\mathrm{SINR}} \tag{4.25}$$

Since the vector $\mathbf{v}$ is applied at the transmitter side, its optimum value depends on whether CSI exists at the transmitter side or not. In the following, we will find the optimum vector $\mathbf{v}$ for both cases of CSIT and CSIR. In case of CSIT, the optimum vector $\mathbf{v}$ is obtained based on the MRT strategy [8]. On the other hand, when CSI is not available at transmitter, i.e. CSIR case, the best transmit beamforming method is the GSS method [8], i.e. sending the signal through each of the transmit antennas with equal gain and phase. The following theorem provides the optimum SINR gain and its associated vector $\mathbf{v}$ for both cases of CSIR and CSIT.

Theorem 9 *Assume that the channel matrix* $\mathbf{H}$*, the SAS matrix* $\mathbf{W}$ *and the vector* $\mathbf{u}$ *are all known. Then, the SINR gain (4.25) maximized on* $\mathbf{v}$ *is given by*

$$G_{SINR,\mathbf{v},csij} = (\|\mathbf{K}_s\|_1 + \sigma_{\mathbf{n}}^2)\frac{|\mathbf{u}^*\mathbf{WHQH}^*\mathbf{W}^*\mathbf{u}|}{|\mathbf{u}^*\mathbf{WK}_z\mathbf{W}^*\mathbf{u}|} \tag{4.26}$$

where

$$\mathbf{Q} = \begin{cases} \mathbf{I}_{N_t} & \text{for } j = t \\ \frac{1}{N_t}\mathbf{1}_{N_t \times N_t} & \text{for } j = r \end{cases}$$

associated with

$$\mathbf{v}_{opt,csij} = \begin{cases} \frac{\mathbf{H}^*\mathbf{W}^*\mathbf{u}}{\|\mathbf{H}^*\mathbf{W}^*\mathbf{u}\|} & \text{for } j = t \\ \frac{1}{\sqrt{N_t}}\mathbf{1}_{N_t} & \text{for } j = r \end{cases}$$

proof 9 *The SINR gain* G_{SINR}*, defined in (4.23), can be rewritten as*

$$G_{SINR} = (\|\mathbf{K}_s\|_1 + \sigma_{\mathbf{n}}^2)\frac{|\mathbf{v}^*\mathbf{H}^*\mathbf{W}^*\mathbf{u}\mathbf{u}^*\mathbf{WHv}|}{|\mathbf{u}^*\mathbf{WK}_z\mathbf{W}^*\mathbf{u}|} \tag{4.27}$$

Hence, the optimum solution for the maximization problem (4.25) is now given by

$$\mathbf{v}_{opt} = \arg\max_{\|\mathbf{v}\|=1} P_s \tag{4.28}$$

where $P_s = \mathbf{v}^*\mathbf{A}_{\mathbf{v}}\mathbf{v}$ *and* $\mathbf{A}_{\mathbf{v}} = \mathbf{H}^*\mathbf{W}^*\mathbf{u}\mathbf{u}^*\mathbf{WH}$*. Now, from the Rayleigh-Ritz theorem [42, Sec. 4.2.2] we have*

$$\mathbf{v}^*\mathbf{A}_{\mathbf{v}}\mathbf{v} \leq \|\mathbf{v}\|^2\lambda_{1,\mathbf{A}_{\mathbf{v}}} = \lambda_{1,\mathbf{A}_{\mathbf{v}}} \tag{4.29}$$

where the equality holds if and only if $\mathbf{v}$ *is along the direction of the eigenvector corresponding to the largest eigenvalue of* $\mathbf{A}_{\mathbf{v}}$*, i.e.* $\lambda_{1,\mathbf{A}_{\mathbf{v}}}$*. Hence, for the CSIT case as the matrix* $\mathbf{A}_{\mathbf{v}}$ *is available at the transmitter side the optimum vector* $\mathbf{v}_{opt,csit}$ *is the eigenvector corresponding to* $\lambda_{1,\mathbf{A}_{\mathbf{v}}}$*. A non-trivial solution of* $\mathbf{v}_{opt,csit}$ *can be obtained using the method used in [43]. From (4.29)*

$$\mathbf{h}_{\mathbf{A}}\mathbf{h}_{\mathbf{A}}^*\mathbf{v}_{opt,csit} = \lambda_{1,\mathbf{A}_{\mathbf{v}}}\mathbf{v}_{opt,csit} \tag{4.30}$$

where $\mathbf{h}_{\mathbf{A}} = \mathbf{H}^*\mathbf{W}^*\mathbf{u}$*. As seen, the matrix* $\mathbf{A}_{\mathbf{v}} = \mathbf{h}_{\mathbf{A}}\mathbf{h}_{\mathbf{A}}^*$ *is a rank one matrix as its all the columns are linear combinations of the single vector* $\mathbf{h}_{\mathbf{A}}$*. Since the column space of the matrix* $\mathbf{A}_{\mathbf{v}}$ *consists of only one single vector, i.e.* $\mathbf{h}_{\mathbf{A}}$*, the only way to obtain a non-trivial solution is to have*

$$\begin{aligned} \mathbf{v}_{opt,csit} &= \frac{\mathbf{h}_{\mathbf{A}}}{\|\mathbf{h}_{\mathbf{A}}\|} = \frac{\mathbf{H}^*\mathbf{W}^*\mathbf{u}}{\|\mathbf{H}^*\mathbf{W}^*\mathbf{u}\|} \\ \lambda_{1,\mathbf{A}_{\mathbf{v}}} &= |\mathbf{u}^*\mathbf{WHH}^*\mathbf{W}^*\mathbf{u}| \end{aligned} \tag{4.31}$$

In the CSIR case, as the transmitter does not know the matrix $\mathbf{A_v}$ *the best method, i.e. GSS, is sending the signal through each of the transmitter terminals with equal gain and phase, i.e.* $\mathbf{v}_{opt,csir} = \frac{1}{\sqrt{N_t}}\mathbf{1}_{N_t}$.

The optimum SINR gain $G_{SINR,\mathbf{v}}$ *is thus given by*

$$G_{SINR,\mathbf{v},csij} = (\|\mathbf{K}_s\|_1 + \sigma_{\mathbf{n}}^2)\frac{|\mathbf{u}^*\mathbf{WHQH}^*\mathbf{W}^*\mathbf{u}|}{|\mathbf{u}^*\mathbf{WK}_z\mathbf{W}^*\mathbf{u}|} \tag{4.32}$$

where

$$\mathbf{Q} = \begin{cases} \mathbf{I}_{N_t} & \text{for } j = t \\ \frac{1}{N_t}\mathbf{1}_{N_t \times N_t} & \text{for } j = r \end{cases}$$

4.3.2 Optimum vector u and SAS matrix

The result of the first step, i.e. $G_{\text{SINR},\mathbf{v},csij}$, is then maximized on $\mathbf{u}$ and SAS matrix $\mathbf{W}$ for both cases of CSIT, i.e. $j = t$, and CSIR, i.e. $j = r$. Defining $\tilde{\mathbf{u}} = \mathbf{W}^*\mathbf{u}$ reduces (4.24) to

$$G_{\text{SINR},osd,csij} = \max_{\tilde{\mathbf{u}} \in \mathcal{C}^{N_s}} \tilde{G}_{\text{SINR},\mathbf{v},csij} \quad \text{for } j \in \{t, r\} \tag{4.33}$$

where

$$\tilde{G}_{\text{SINR},\mathbf{v},csij} = (\|\mathbf{K}_s\|_1 + \sigma_{\mathbf{n}}^2)\frac{|\tilde{\mathbf{u}}^*\mathbf{HQH}^*\tilde{\mathbf{u}}|}{|\tilde{\mathbf{u}}^*\mathbf{K}_z\tilde{\mathbf{u}}|} \tag{4.34}$$

As for both aforementioned cases CSI is assumed to be available at the receiver, the MRC strategy [8] is applied to find the best $\tilde{\mathbf{u}}$. The following theorem provides the optimum SINR gain $G_{\text{SINR},osd,csij}$ for $j \in \{t, r\}$ maximized on the vector $\tilde{\mathbf{u}}$.

Theorem 10 *For a known the channel matrix* $\mathbf{H}$*, the optimum SINR gain represented in (4.33) is given by*

$$G_{SINR,osd,csij} = (\|\mathbf{K}_s\|_1 + \sigma_{\mathbf{n}}^2)\lambda_{1,\mathbf{A}_L} \tag{4.35}$$

associated with

$$\mathbf{W}^*_{opt,csij}\mathbf{u}_{opt,csij} = \beta_4\ (\mathbf{L}_z^{-1})^*\mathbf{u}_{1,\mathbf{A}_L} \tag{4.36}$$

where

$$\mathbf{A}_L = \mathbf{L}_z^{-1}\mathbf{HQH}^*(\mathbf{L}_z^{-1})^*$$

with $\mathbf{L}_z$ *obtained from the Cholesky decomposition of the interference covariance matrix, i.e.* $\mathbf{K}_z$=$\mathbf{L}_z\mathbf{L}_z^*$. *In (4.36),* $\beta_4 \neq 0$ *is an arbitrary constant which does not affect the SINR gain.*

proof 10 *We first find the optimum vector* $\tilde{\mathbf{u}}_{opt,csij}$ *given by*

$$\tilde{\mathbf{u}}_{opt,csij} \;=\; \arg \max_{\mathbf{u} \in \mathcal{C}^{N_r}} \tilde{G}_{\mathrm{SINR},\mathbf{v},csij} \quad \text{for } j \in \{t, r\} \tag{4.37}$$

The above-mentioned optimum solution can be obtained by taking the conjugate derivative [44] of (4.34), i.e. $\tilde{G}_{SINR,\mathbf{v},csij}$*, with respect to the vector* $\tilde{\mathbf{u}}$*. Hence,* $\partial \tilde{G}_{SINR,\mathbf{v},csij}/\partial \tilde{\mathbf{u}}' = 0$ *implies*

$$\mathbf{HQH}^* \tilde{\mathbf{u}} \;=\; \tilde{\lambda}_{\tilde{\mathbf{u}}} \mathbf{K}_z \tilde{\mathbf{u}} \tag{4.38}$$

where

$$\tilde{\lambda}_{\tilde{\mathbf{u}}} \;=\; \frac{|\tilde{\mathbf{u}}^* \mathbf{HQH}^* \tilde{\mathbf{u}}|}{|\tilde{\mathbf{u}}^* \mathbf{K}_z \tilde{\mathbf{u}}|}$$

Substituting a Cholesky factorization $\mathbf{K}_z = \mathbf{L}_z \mathbf{L}_z^*$ *into (4.38) yields*

$$\mathbf{A}_L \tilde{\mathbf{u}}_L \;=\; \tilde{\lambda}_{\tilde{\mathbf{u}}} \tilde{\mathbf{u}}_L \tag{4.39}$$

where

$$\begin{aligned} \mathbf{A}_L &= \mathbf{L}_z^{-1} \mathbf{HQH}^* (\mathbf{L}_z^{-1})^* \\ \tilde{\mathbf{u}}_L &= \mathbf{L}_z^* \tilde{\mathbf{u}} \end{aligned} \tag{4.40}$$

As seen from (4.38), $\tilde{\lambda}_{\tilde{\mathbf{u}}}$ *represents an eigenvalue of the matrix* $\mathbf{A}_L$ *[42] and therefore the eigenvector corresponding to* $\tilde{\lambda}_{\tilde{\mathbf{u}}}$ *can sub-maximize* $\tilde{G}_{SINR,\mathbf{v},csij}$*. On the other hand, we have* $G_{SINR,\mathbf{v},csij} = (\|\mathbf{K}_s\|_1 + \sigma_{\mathbf{n}}^2)\tilde{\lambda}_{\tilde{\mathbf{u}}}$*. This implies that the SINR gain* $G_{SINR,\mathbf{v},csij}$ *is maximized with the largest eigenvalue of* $\mathbf{A}_L$*, i.e.* $\lambda_{1,\mathbf{A}_L}$*. Hence, the optimum vector* $\tilde{\mathbf{u}}_{opt,csij}$ *can be obtained based on the eigenvector corresponding to the largest eigenvalue of the same matrix, i.e.*

$$\tilde{\mathbf{u}}_{opt,csij} \;=\; \beta_4 \; (\mathbf{L}_z^*)^{-1} \mathbf{u}_{1,\mathbf{A}_L} \tag{4.41}$$

where $\beta_4 \neq 0$ *is an arbitrary constant which does not affect the SINR gain. We can assume that the optimum eigenvector (4.41) is associated with the optimum SAS matrix* $\mathbf{W}_{opt,csij}$ *and the optimum eigenvector* $\mathbf{u}_{opt,csij}$*, i.e.* $\tilde{\mathbf{u}}_{opt,csij} = \mathbf{W}_{opt,csij}^* \mathbf{u}_{opt,csij}$*.*

As Theorem 10 shows, there exist many solutions for $\mathbf{u}_{opt,csij}$ and $\mathbf{W}_{opt,csij}$ as they only need to meet the conditions (4.36). One of these solutions can be obtained using the procedure proposed in [14, Appendix A]. According to this method, if

$$\beta_4 \; (\mathbf{L}_z^{-1})^* \mathbf{u}_{1,\mathbf{A}_L} \;=\; [\alpha_1 e^{j\psi_1}, \alpha_2 e^{j\psi_2}, \cdots, \alpha_{N_s} e^{j\psi_{N_s}}]^T$$

where $\alpha_i \geq 0$, and $\psi_i \in \mathcal{R}$, then

$$\begin{aligned}
\mathbf{u}_{opt,csij} &= [u_1, u_2, 0, \cdots, 0]^T \\
\mathbf{W}_{opt,csij} &= \begin{bmatrix} e^{j\phi_{1,1}} & e^{j\phi_{1,2}} & \cdots & e^{j\phi_{1,N_s}} \\ e^{j\phi_{2,1}} & e^{j\phi_{2,2}} & \cdots & e^{j\phi_{2,N_s}} \\ 1 & 1 & \cdots & 1 \\ \vdots & \vdots & \ddots & \vdots \\ 1 & 1 & \cdots & 1 \end{bmatrix}
\end{aligned}$$

where

$$\begin{aligned}
u_1 &= \frac{\alpha_{max} + \alpha_{min}}{2} \\
u_2 &= \frac{\alpha_{max} - \alpha_{min}}{2} \\
\phi_{1,i} &= -\psi_i + \arccos \frac{\alpha_i^2 + \alpha_{max}\alpha_{min}}{\alpha_i(\alpha_{max} + \alpha_{min})} \\
\phi_{2,i} &= \psi_i + \arccos \frac{\alpha_i^2 - \alpha_{max}\alpha_{min}}{\alpha_i(\alpha_{max} - \alpha_{min})}
\end{aligned}$$

for $i \in \{1, 2, ..., N_s\}$.

4.4 Full-Complexity MIMO System in an Interference Channel

In order to assess SAS-MIMO against a full-complexity MIMO in an interference channel, in this section we derive the capacity and SNIR gain formulation for a full-complexity MIMO system[4], i.e. the MIMO system depicted in Fig. 1.1 when $N_T = N_t$ and $N_R = N_s$, in presence of the interference (4.1).

4.4.1 Spatial Multiplexing Transmission

In this case, the $N_s \times 1$ received signal vector $\mathbf{y}_f$ is written as

$$\mathbf{y}_f = \mathbf{H}\mathbf{x} + \mathbf{z} \tag{4.42}$$

and the channel capacity is given by [40]

$$C_f = \max_{\mathbf{K}_x \,:\, \mathrm{tr}(\mathbf{K}_x) \leq P_t} \log\left[\det\left(\mathbf{H}\mathbf{K}_x\mathbf{H}^*\mathbf{K}_z^{-1} + \mathbf{I}_{N_s}\right)\right] \tag{4.43}$$

[4]The formulation can be easily applied for a low-complexity MIMO system using N_r instead of N_s.

Hence, in case of CSIR a reasonable transmit signaling is the equi-power signaling with $\mathbf{K}_{x,csir} = \frac{P_t}{N_t}\mathbf{I}_{N_t}$. In this case, the achieved MI is given by

$$I_{af} = \log\left[\det\left(\frac{P_t}{N_t}\mathbf{H}\mathbf{H}^*\mathbf{K}_z^{-1} + \mathbf{I}_{N_s}\right)\right] \tag{4.44}$$

For CSIT the optimum transmit strategy is applied. In this case, to find the best $\mathbf{K}_x$, i.e. $\mathbf{K}_{x,csit}$, first we substitute the Cholesky decomposition $\mathbf{K}_z = \mathbf{L}_z\mathbf{L}_z^*$ into (4.43). Hence,

$$\mathbf{K}_{x,csit} = \arg \max_{\mathbf{K}_x \,:\, \mathrm{tr}(\mathbf{K}_x) \leq P_t} \log\left[\det\left(\mathbf{H}_L\mathbf{K}_x\mathbf{H}_L^* + \mathbf{I}_{N_s}\right)\right] \tag{4.45}$$

where $\mathbf{H}_L = \mathbf{L}_z^{-1}\mathbf{H}$. Now, consider the SVD of $\mathbf{H}_L = \mathbf{U}_{hl}\mathbf{\Lambda}_{hl}\mathbf{V}_{hl}^*$ where $\mathbf{U}_{hl}$, $\mathbf{V}_{hl}$ and $\mathbf{\Lambda}_{hl}$ are respectively $N_s \times N_s$ unitary matrix, $N_t \times N_t$ unitary matrix ,$N_s \times N_t$ diagonal matrix. Similar to the proof of Theorem 2, applying the approach used in [41, Section IV] yields the optimum $\mathbf{U}_x$ as $\mathbf{U}_{x,csit} = \mathbf{V}_{hl}$. Moreover, the best $\mathbf{\Lambda}_x$, i.e. $\mathbf{\Lambda}_{x,csit}$, is obtained using the water-filling optimization method as

$$\lambda_{i,\mathbf{\Lambda}_{x,csir}} = \left(\mu - \frac{1}{\lambda_{i,\mathbf{H}_L}^2}\right)^+$$

for $i \in \{1, 2, ..., N'_{min}\}$ where $N'_{min} = min\{N_t, N_s\}$ with μ chosen to satisfy the following constraint

$$\sum_{i=1}^{N_{min}} \left(\mu - \frac{1}{\lambda_{i,\mathbf{H}_L}^2}\right)^+ \leq P_t$$

4.4.2 Diversity Transmission

In this case, the input-output relationship at time instant k is given by

$$y_f = \mathbf{u}'^*\mathbf{H}\mathbf{v}'x + \mathbf{u}'^*\mathbf{z} \tag{4.46}$$

where $\mathbf{u}'$ and $\mathbf{v}'$ are respectively $N_s \times 1$ and $N_t \times 1$ weighting vectors determined to optimize the SINR gain. There is no constraint on the vectors $\mathbf{u}'$ and $\mathbf{v}'$ but $\|\mathbf{v}'\| = 1$. Similar to the definition (4.22) and then (4.23), the SINR gain in this case is given by

$$G'_{\text{SINR}} = (\|\mathbf{K}_s\|_1 + \sigma_{\mathbf{n}}^2)\frac{|\mathbf{u}'^*\mathbf{H}\mathbf{v}'\mathbf{v}'^*\mathbf{H}^*\mathbf{u}'|}{|\mathbf{u}'^*\mathbf{K}_z\mathbf{u}'|} \tag{4.47}$$

The SINR Gain G'_{SINR} can be maximized through the optimal vectors $\mathbf{u}'$ and $\mathbf{v}'$

located in the transceiver baseband as

$$G'_{\text{SINR},opt} = \max_{\mathbf{u}' \in \mathcal{C}^{N_s}} \max_{\|\mathbf{v}'\|=1} G'_{\text{SINR}} \tag{4.48}$$

the SINR gain G_{SINR} is first maximized on $\mathbf{v}'$ subject to the constraint $\|\mathbf{v}'\| = 1$. The optimum vector $\mathbf{v}'$ is found for both cases of CSIT and CSIR, respectively using MRT and GSS schemes. Then, the optimum vector $\mathbf{u}'$ is obtained based on MRC method. Similar to the procedure (4.25) to (4.35), the optimum $\mathbf{v}'$ and $\mathbf{u}'$ are given by

$$\mathbf{v}'_{opt,csij} = \begin{cases} \frac{\mathbf{H}^*\mathbf{u}'}{\|\mathbf{H}^*\mathbf{u}'\|} & \text{for } j = t \\ \frac{1}{\sqrt{N_t}}\mathbf{1}_{N_t} & \text{for } j = r \end{cases}$$

and

$$\mathbf{u}'_{opt,csij} = \beta' \, (\mathbf{L}_z^{-1})^* \mathbf{u}'_{1,\mathbf{A}'_L} \quad \text{for } j \in \{t, r\}$$

where

$$\mathbf{A}'_L = \begin{cases} \mathbf{L}_z^{-1}\mathbf{H}\mathbf{H}^*(\mathbf{L}_z^{-1})^* & \text{for } j = t \\ \frac{1}{N_t}\mathbf{L}_z^{-1}\mathbf{H}\mathbf{1}_{N_t \times N_t}\mathbf{H}^*(\mathbf{L}_z^{-1})^* & \text{for } j = r \end{cases}$$

and $\beta' \neq 0$ is an arbitrary constant which does not affect the SINR gain.

4.5 Computer Simulations

In this section, we provide simulation results in order to uphold our theoretical analysis. In our simulations, the spatial multiplexing and diversity transmission scenarios are considered for both cases of CSIR and CSIT.

The statistical channel model defined in Section 3.4.1 is used for the computer simulations. In our simulation study, 1000 channel matrix realizations are produced with $N_t = 4$. The arbitrary non-singular matrix $\mathbf{M}$ is also chosen as a $N_r \times N_r$ identity matrix, $\mathbf{M} = \mathbf{I}_{N_r}$. In the modeled interference, we assume the kth major interferer, the receive angle θ_k and the interferers covariance matrix, $\mathbf{K}_s$, are given. Moreover, the noise power, i.e. $\sigma^2_{\mathbf{n}}$, is also given.

4.5.1 Interference Dominance Effect on Mutual Information/SNR Gain

To study the dominance effect of interference, we use a measure called Interference Dominance Ratio (IDR). This measure is defined based on the received interference power by a single element reference antenna when the total interference-plus-noise

power is assumed to be constant. From (4.2), for such an antenna the received interference power is given by

$$P_{IN} = \|\mathbf{K}_s\|_1 + \sigma_{\mathbf{n}}^2 \tag{4.49}$$

Hence, for $P_{IN} = cte$. IDR is defined as

$$\text{IDR} = \frac{\|\mathbf{K}_s\|_1}{\sigma_{\mathbf{n}}^2} \tag{4.50}$$

The mean MI (4.3), averaged on all channel matrix realizations, is plotted versus IDR in Fig. 4.3. In this figure $\text{SINR}_0 = 10dB$, the number of interferers is 2, and $K_f = 5dB$. The results for the both cases of having either CSIT or CSIR are plotted in this figure. The curves with solid lines and dashed lines correspond to the CSIT and CSIR cases, respectively. As this figure shows, the optimum SAS-MIMO achieves the full-complexity MIMO performance regardless of either interference or noise dominance. However, there is a significant difference between the optimum SAS and the sub-optimum PSB-SAS performances at high IDRs. This difference shows how the beamforming capability of un-constrained SAS improves the performance compared to the PSB-SAS method and recommends using the variable gain amplifiers in the SAS implementation. Moreover, a SAS-MIMO, regardless of being optimum or sub-optimum, always outperforms both the FFT-MIMO and the low-complexity MIMO systems. Another fact revealed in this figure is the outperforming of the FFT-MIMO system compared to the low-complexity MIMO one for all IDRs. However, this merit reduces to a insignificant improvement at low IDRs.

We also observe that the channel knowledge at the transmitter does not affect the MI of the SAS-MIMO strategy, for both optimum and sub-optimum cases. This is in line with earlier findings that when the number of received antennas is more than the transmit ones, providing CSIT has no significant improvement on the capacity [51, Chapter 8].

To study the SAS-MIMO system under diversity transmission, the mean SINR gain (4.23), averaged on all channel matrix realizations is plotted versus IDR in Fig. 4.4 (2 interferers and $K_f = 5dB$). The similar results, as the multiplexing transmission case, are drawn from this figure too, i.e. the optimum SAS-MIMO achieves the full-complexity MIMO performance in terms of SINR gain for all IDRs, and it always outperforms the FFT-MIMO and low-complexity MIMO systems. It is interesting to observe that the SAS-MIMO SINR gain increases linearly with IDR while it saturates at high IDRs for FFT-MIMO. The reason is simply because of the effectiveness of the adaptive beamforming capability of the SAS-MIMO in suppressing the interference. In contrast to the spatial multiplexing case, Fig. 4.4 shows that providing CSIT improves the performance of the diversity transmission system for the whole range of IDR.

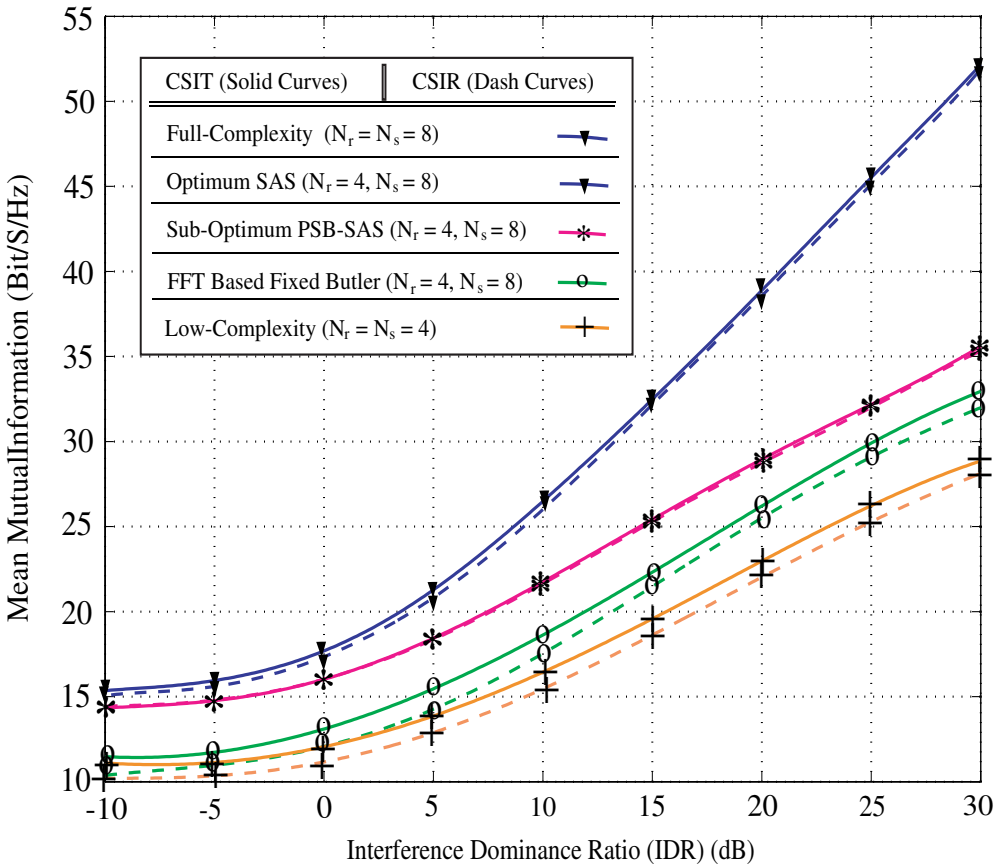

Figure 4.3: MI versus IDR when $\mathrm{SINR}_0 = 10dB$, the number of interferers is 2 and $K_f = 5dB$.

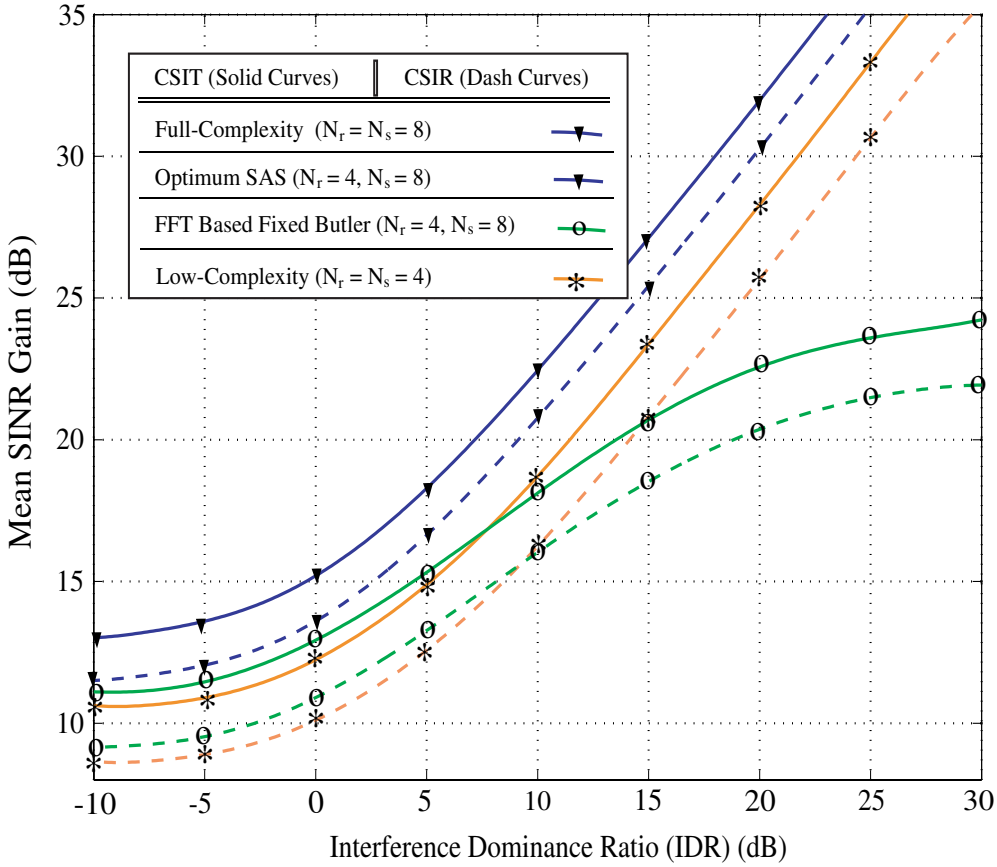

Figure 4.4: SINR gain versus IDR when the number of interferers is 2 and $K_f = 5dB$.

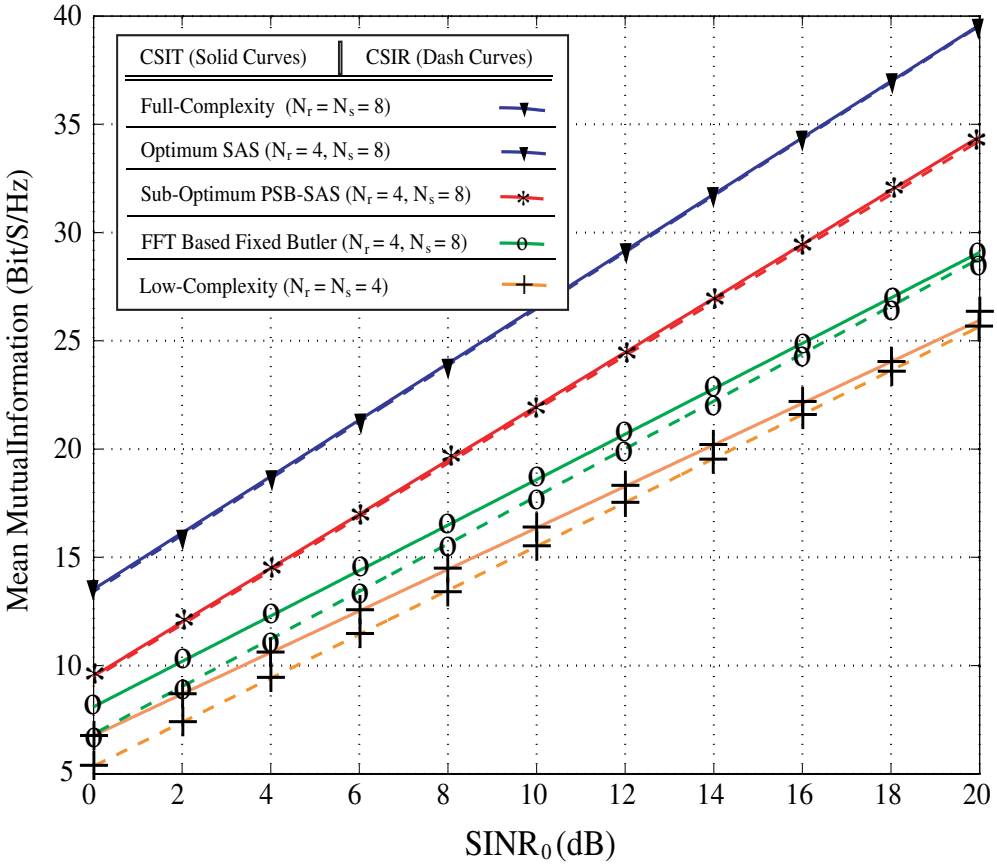

Figure 4.5: MI versus nominal Signal to Nominal Interference-plus-Noise Ratio (SINR_0) when the number of interferers is 2, IDR $= 10dB$ and $K_f = 5dB$.

4.5.2 Signal to Interference-plus-Noise Ratio Effect on Mutual Information

Fig. 4.5 shows the mean MI for different SINR_0s, i.e. P_t/P_{IN}, when the number of interferers is 2, IDR $= 10dB$ and $K_f = 5dB$. This figure shows that the optimum SAS achieves the full-complexity MIMO performance for all SINR_0s. Moreover, although the performance for all MIMO schemes increases almost linearly with SINR, the improvement using SAS-MIMO schemes compared to the other ones is more significant at high SINR_0s, owing to the interference suppressing capability of these schemes.

4.5.3 Number of Interferers Effect on Mutual Information/SNR Gain

To investigate how the number of interferers affects the system performance, the mean MI and SNIR gain are plotted in Fig. 4.6 versus the number of interferers. The simulation is performed only for the CSIR case, IDR $= 10dB$ and $K_f =$

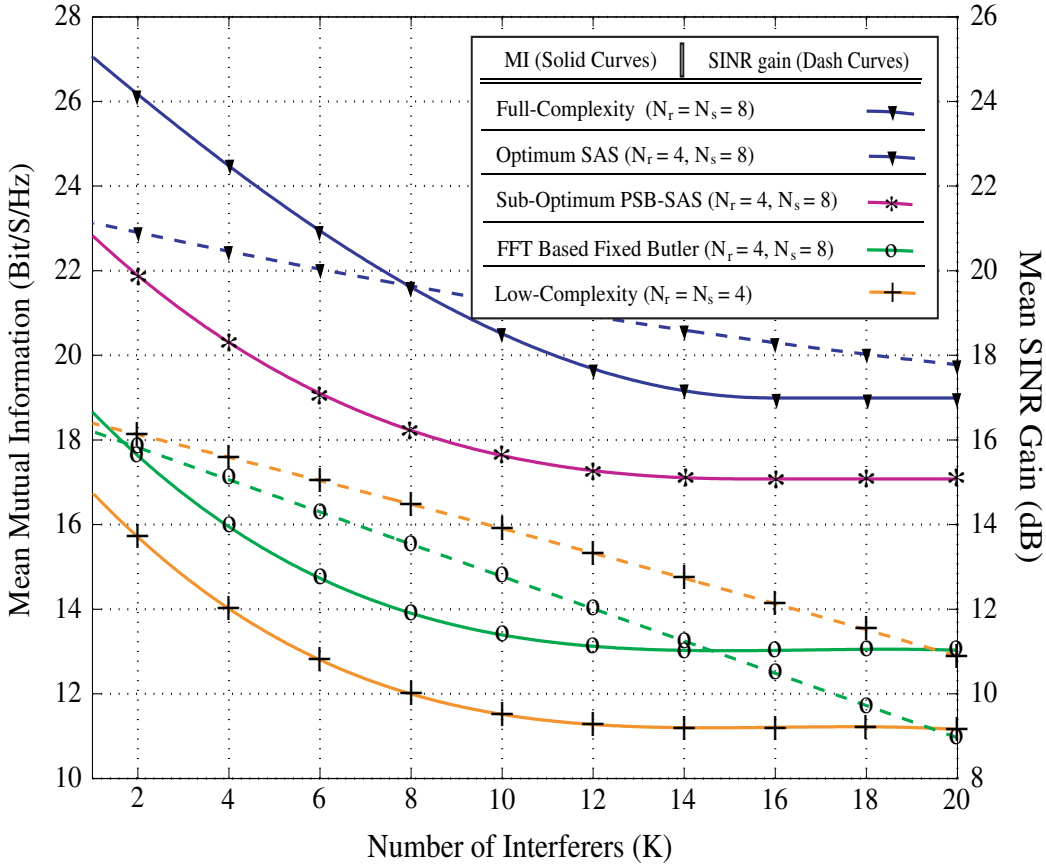

Figure 4.6: MI and SNIR gain versus Number of Interferers when IDR $= 10dB$, $K_f = 5dB$ and CSIR case. For MI plot $\text{SINR}_0 = 10dB$.

$5dB$. For the mean MI the signal to interference-plus-noise ratio is set to $10dB$. As this figure indicates, for both spatial multiplexing and diversity transmissions the optimum SAS still achieves the full-complexity MIMO performance regardless of how many interferers exist in the channel. As expected the mean MI of the MIMO systems degrades with increasing number of interferers. However, it remains constant when the number of the interferers goes beyond a limit. This limit is 16 for full-complexity MIMO and optimum SAS-MIMO; 14 for sub-optimum SAS-MIMO; and 12 for FFT-MIMO and low-complexity MIMO. On the other hand, as Fig. 4.6 reveals, the SINR gain for all methods decreases linearly with the increasing of the number of the interferers. However, full-complexity MIMO/optimum SAS-MIMO significantly outperforms FFT-MIMO and low-complexity MIMO for any number of interferers in the channel.

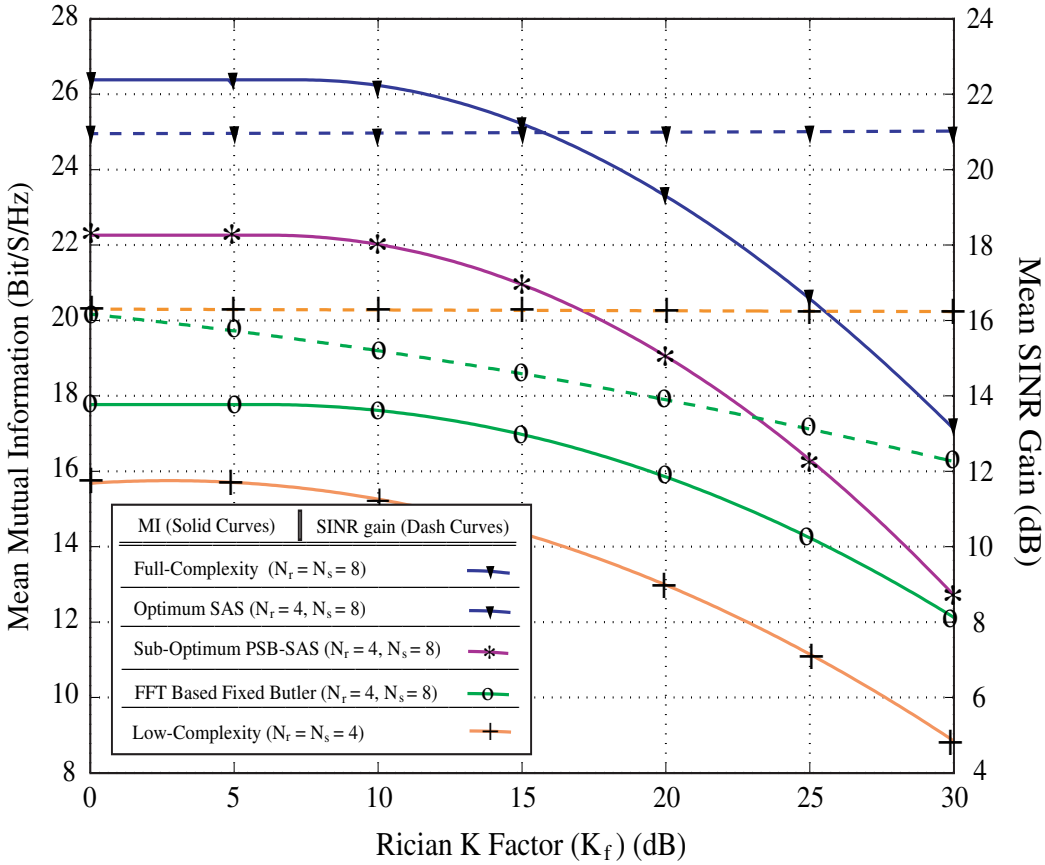

Figure 4.7: MI and SNIR gain versus Rician K factor (K_f) when IDR $= 10dB$, the number of interferers is 2 and CSIR case. For MI plot $\text{SINR}_0 = 10dB$.

4.5.4 Rician K-Factor Effect on Mutual Information/SNR Gain

In this sub-section, we study the effect of LOS link dominance on the SAS-MIMO system performance. The Rician K-factor is used as measure in this regard. As observed from Fig. 4.7 the mean MI decreases as the K-factor increases (when the LOS link dominates). This is expected as increasing the LOS component leads to less multipath effect and hence less capacity improvement.

This figure also shows that the optimum SAS-MIMO always achieves the full-complexity SINR gain. Moreover, the SINR gain remains constant for the whole range of K-factors for all MIMO methods except FFT-MIMO, which is expected too due to fixed and uncontrollable beams produced by the Butler matrix.

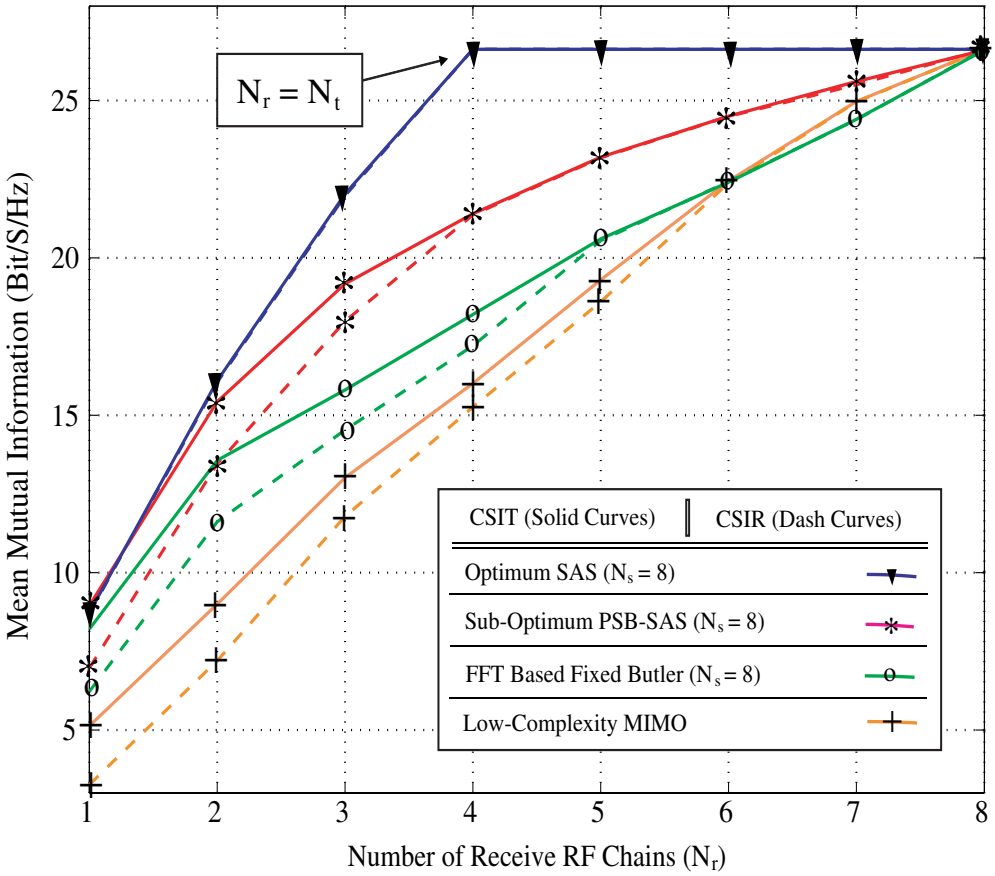

Figure 4.8: MI versus number of receive RF chains (N_r) when $\text{SINR}_0 = 10dB$, the number of interferers is 2, IDR $= 10dB$ and $K_f = 5dB$.

4.5.5 Number of RF chains Effect on Mutual Information/SNR Gain

As stated in previous sections, one of the significant benefits derived from the SAS method is the reduced system complexity and cost via lowering the number of RF chains. In this section, we evaluate how the number of receive RF chains N_r can affect the performance in both spatial multiplexing and diversity transmissions. Fig. 4.8 and Fig. 4.9 respectively show the mean MI and mean SINR gain versus N_r. Again the number of interferers is 2, IDR $= 10dB$, $K_f = 5dB$, and $\text{SINR}_0 = 10dB$ (for MI results only). Obviously, N_r is upper-bounded by N_s which shows the full-complexity case, i.e. $N_r = N_s$. Inspecting these figure some conclusions can be drawn as follows

1. All MIMO methods have the same performance at $N_r = N_s$. This observation reveals that no beamforming technique can improve the performance of a full-complexity system even in the presence of interference.

2. Fig. 4.8 shows that for the spatial multiplexing transmission an optimum

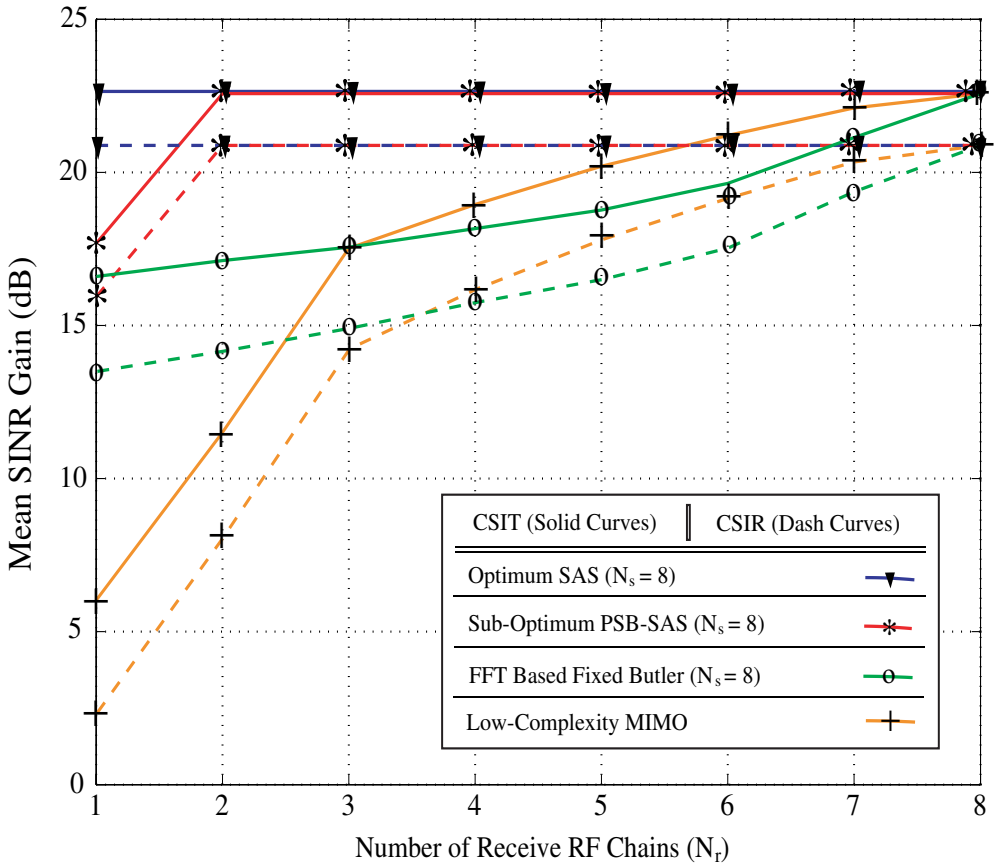

Figure 4.9: SNIR gain versus number of receive RF chains (N_r) when the number of interferers is 2, IDR $= 10dB$ and $K_f = 5dB$.

SAS-MIMO can achieve the full-complexity performance only if the number of receive antennas is more than the transmit ones, i.e. $N_r \geq N_t$. However, in a diversity transmission an optimum SAS-MIMO can achieve the full-complexity performance (SNIR gain) only when the number of receive antennas is more than one, i.e. $N_r > 1$ (as indicated in Fig. 4.9).

3. The FFT-MIMO basically outperforms the low-complexity MIMO for low N_r, whereas low-complexity MIMO is superior to FFT-MIMO for the N_r close to N_s.

Chapter 5

Channel Estimation for SAS-MIMO System

The SAS-MIMO technique like most of the antenna selection strategies employs CSI at the receiver side for performance optimization, e.g. to maximize the capacity. CSIR is typically obtained via channel estimation. Pilot or training based channel estimation schemes are the conventional methods which are employed for MIMO channel estimation [52] and [53]. The conventional channel estimation schemes usually use Least-Square (LS) and Minimum-Mean-Square-Error (MMSE) estimators. These estimators are implemented in baseband section based on the information which are directly obtained from the receive antennas and corresponding RF-chains. In a SAS-MIMO system the number of receive antennas is much more than the number of RF-chains. In other words, the conventional channel estimators find an estimate of $\mathbf{WH}$. This issue implies that if even a predefined $\mathbf{W}$ is available, due to size of matrices $\mathbf{W}$ and $\mathbf{H}$ finding the whole entries of $\mathbf{H}$ is impractical.

In this chapter a feasible channel estimation scheme is proposed for the SAS-MIMO system. A two-step RF-baseband co-operative method is employed for this purpose. The general idea is similar to the technique used in [54]; however, we propose a new channel estimation procedure designed for the SAS-MIMO system. Moreover, our proposed channel estimation method is applied on an IEEE 802.16 framing standard. To this end, we evaluate the performance of the proposed channel estimation technique using an Orthogonal Frequency-Division Multiplexing (OFDM)-based SAS-MIMO simulation model. In this study, both the LS and MMSE estimators are employed and evaluated as the baseband part of the channel estimator.

5.1 Frequency Domain Representation of OFDM based SAS-MIMO System

We assume that the SAS-MIMO system is operating in a frequency-selective quasi-static fading environment, meaning that the channel affects different frequency components of the transmitted signal differently and remains constant during a packet transmission. Moreover, suppose that the maximum length of the channel impulse response (maximum delay spread obtained from the propagation environment) is L_c. At each transmit chain/antenna, the data is first converted into time domain by Inverse Fast-Fourier Transform (IFFT) then a Cyclic Prefix (CP) of length L_g is added (see Fig. 5.2). In order to combat Inter-Symbol Interference (ISI), we let $L_g \geq L_c - 1$. At receiver, the CP is removed from the received symbol. Then the time domain received data are converted into frequency domain by FFT. We define N_{sub} as the number of subcarriers in OFDM. N_{sub} is also the number of subcarriers for channel estimation. The frequency domain expression of the received vector can be expressed as

$$\mathbf{Y}_f(k) \;=\; \mathbf{H}_a(k)\mathbf{X}_f(k) + \mathbf{N}_f(k) \tag{5.1}$$

where the index k represents the data symbol number in the time sequence and

- $\mathbf{H}_a$ is herein $N_r \times N_t$ channel transfer function matrix with the entries $[\mathbf{H}_a]_{i,j} = \mathbf{h}^*(i,j)$ where $\mathbf{h}(i,j)$ are vectors of size N_{sub}, and $i \in \{1, 2, ..., N_r\}$ and $j \in \{1, 2, ..., N_t\}$ are the ith receiver and the jth transmitter indices, respectively.
- $\mathbf{Y}_f$ is the $N_r \times 1$ received signal with the entries $[\mathbf{Y}_f]_i = \mathbf{y}_f^*(i)$ where $\mathbf{y}_f(i)$ are vectors of size N_{sub}.
- $\mathbf{X}_f$ is the $N_t \times 1$ transmitted signal with the entries $[\mathbf{X}_f]_j = \mathbf{X}_f^{(d)}(j)$ which are diagonal matrices of size N_{sub}.
- $\mathbf{N}_f$ is the $N_r \times 1$ noise vector with the entries $[\mathbf{N}_f]_i = \mathbf{n}_f^*(i)$ where $\mathbf{n}_f(i)$ are vectors of size N_{sub}. $\mathbf{N}_f$ is a zero mean AWGN process whose entries are correlated, i.e. $\mathcal{CN}(0, \mathbf{K}_{\mathbf{n}_f})$, due to applying $\mathbf{W}$ on the i.i.d. noise.

5.2 Channel Estimation Method

The channel estimation mechanism includes two stages: *measurement* and *estimation*. At the first step, we measure the received signal on N_s antennas by controlling the SAS matrix $\mathbf{W}$. We then estimate $\mathbf{H}$ using the measured received signal in the next stage. This strategy is fully applicable to WLAN IEEE 802.11a/b/g/n and Wireless Metropolitan Area Network (WMAN) IEEE 802.16-2004/e standards, where the first stage can be done at the preamble section of each data frame. The second stage is however performed when a complete measurement, which may take

some frames, is finalized. Hence, optimum $\mathbf{W}$ will be updated when an estimation becomes complete[1]. In the following we provide the measurement setup for the channel estimation.

5.2.1 Measurement Approach

The proposed approach for the channel measurement consists of three stages. First a preamble structure is designed. Then, the efficient training sequences are proposed and finally the SAS matrix $\mathbf{W}$ is set properly to measure the channel matrix $\mathbf{H}$.

Preamble Structure

To employ the standards WLAN and WMAN for the transmit data framing, we need to design a proper preamble for the MIMO channel estimation. Indeed, the preambles on different transmit antennas should be orthogonal and shift-orthogonal for at least the channel length [55]. Regarding the preamble design for MIMO channel estimation several methods are proposed in the literature [53] and [56]. In [56], a simple preamble structure is proposed in which the time orthogonality is used for the preamble design. Figure 5.1 shows the structure of the preamble for N_t transmit antennas in an IEEE 802.16 framing standard.

[1] Obviously, the proposed estimation method works well for the slow-fading channels like indoor environments.

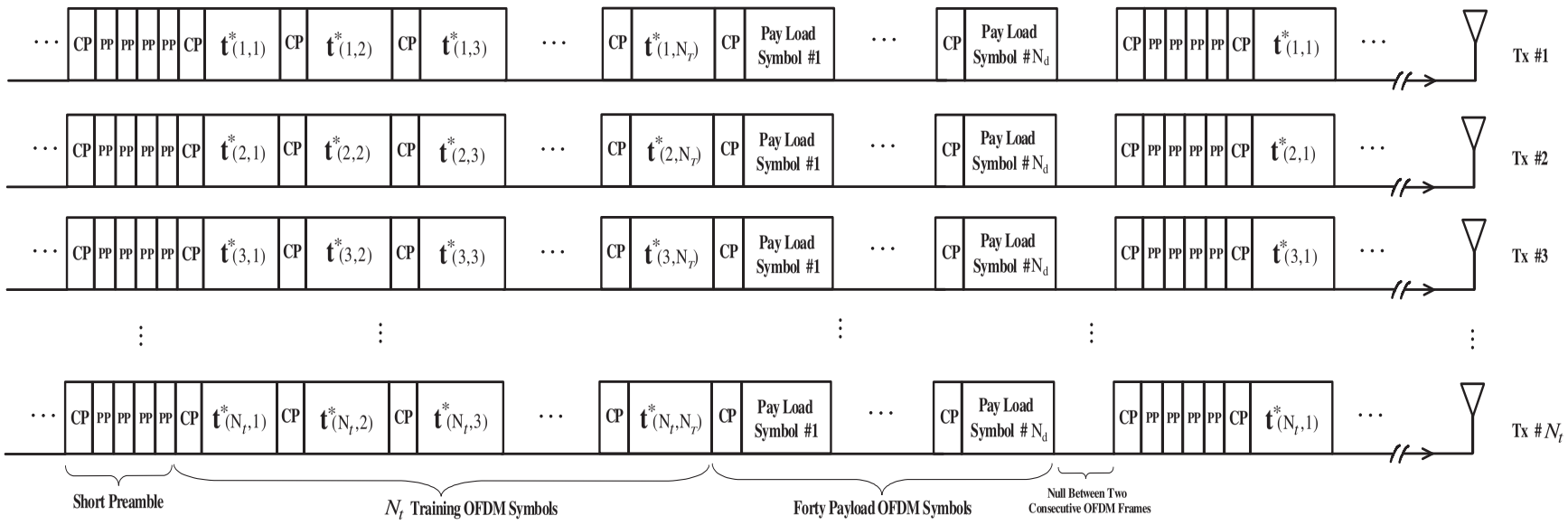

Figure 5.1: Framing structure for SAS-MIMO channel estimation.

The preamble consists of a short training sequence (an OFDM symbol) of four 64-sample Preamble-Patterns (PP) and N_{Tr} 256-sample long training sequences (OFDM symbols). Each long training sequence is composed of two repetitions of a 128-sample fragment. The short training sequence and the long training sequences are separated by a 64-sample CP. The number of the long training sequences N_{Tr} is determined based on the number of unknown parameters which are herein $N_s N_t$ entries of $\mathbf{H}$. The estimation theory [57] says that to estimate all these parameters we need at least N_s training symbols. Hence, there exist two strategies to set N_{Tr}:

1. $N_{Tr} = N_s$, in this case the measurement period is completed at the end of the preamble and therefore the estimated channel can be updated in each frame sequence.

2. $N_{Tr} = N_t$, in this case $N_f = \lceil N_s/N_r \rceil$ frames are needed to complete the measurement period. Thus, the estimated channel can be updated after each N_f-frame-sequence period.

We choose the second method due to its low computational complexity and its high feasibility in $\mathbf{W}$ setting during the measurement period. Hence, for the measurement period (5.1), can be written as

$$\mathbf{Y} = \mathbf{WHX} + \mathbf{N} \tag{5.2}$$

where

- $\mathbf{H}$ is $N_s \times N_t$ channel transfer function matrix with the entries $[\mathbf{H}]_{i,m} = \mathbf{h}^*(i,m)$ where $\mathbf{h}(i,m)$ are vectors of size N_{sub} and $m \in \{1, 2, ..., N_s\}$ is the mth actual receive antenna index.

- $\mathbf{Y}$ is $N_r \times N_t$ received signal matrix with the entries $[\mathbf{Y}]_{i,n} = \mathbf{y}_f^*(i,n)$ where $n \in \{1, 2, ..., N_t\}$ is the nth training symbol index.

- $\mathbf{X}$ is $N_t \times N_t$ transmitted training matrix with the entries $[\mathbf{X}]_{j,m} = \mathbf{T}(j,m)$. $\mathbf{T}(j,m)$ itself is a diagonal matrix with the entries $[\mathbf{T}(j,m)]_{l,l} = [\mathbf{t}(j,m)]_l$ where $\mathbf{t}^*(j,m)$ is the (j,m) training sequence (See Figure 5.1).

- $\mathbf{N}$ is $N_r \times N_t$ noise vector with the entries $[\mathbf{N}]_{i,n} = \mathbf{n}_f^*(i,n)$.

Efficient Training Sequence

To design the training symbols, first we decompose the transmitted training matrix as

$$\mathbf{X} = \mathbf{X}^{(1)}\mathbf{T} \tag{5.3}$$

where $\mathbf{X}^{(1)} = \text{diag}(\mathbf{T}_1^{(1)}, \mathbf{T}_2^{(1)}, ..., \mathbf{T}_{N_t}^{(1)})$ and $\mathbf{T}_n^{(1)}$ are diagonal matrices of size N_{sub} with equal power called as the elementary training sequences. In this thesis, we

choose $\mathbf{T}_n^{(1)} = \mathbf{T}_0$ where $\mathbf{T}_0$ is a diagonal matrix whose entries are one of the 256 samples of the long training sequence used in IEEE 802.16 standard. Also, $\mathbf{T} = \mathbf{\Gamma}_{N_t} \otimes \mathbf{I}_N$ where $N_t \times N_t$ training sequence pattern matrix $\mathbf{\Gamma}$ is defined such that $[\mathbf{\Gamma}_{N_t}]^*_{j,n}[\mathbf{\Gamma}_{N_t}]_{j,n} = 1$ to keep the pilots at different times and different antennas have equal energy and $\otimes$ represents the Kronecker product. Generally, we design $\mathbf{T}$ to be invertible. For instance, for $N_t = 4$,

$$\mathbf{\Gamma}_4 = \begin{bmatrix} 1 & 1 & 1 & 1 \\ 1 & -1 & 1 & -1 \\ 1 & 1 & -1 & -1 \\ 1 & -1 & -1 & 1 \end{bmatrix}$$

Hence, (5.2) is rewritten as

$$\mathbf{Y}^{(1)} = \mathbf{WHX}^{(1)} + \mathbf{N}^{(1)} \tag{5.4}$$

where $\mathbf{Y}^{(1)} = \mathbf{YT}^{-1}$ and $\mathbf{N}^{(1)} = \mathbf{NT}^{-1}$.

Now, to represent a complete measurement period which includes N_f frames, we need to extend (5.4) for all frames as

$$\mathbf{Y}^{(c)} = \mathbf{W}^{(c)}\mathbf{HX}^{(1)} + \mathbf{N}^{(c)} \tag{5.5}$$

where

$$\mathbf{Y}^{(c)} = \begin{bmatrix} \mathbf{Y}(1) \\ \mathbf{Y}(2) \\ \vdots \\ \mathbf{Y}(N_f) \end{bmatrix} \mathbf{T}^{-1}, \quad \mathbf{W}^{(c)} = \begin{bmatrix} \mathbf{W}(1) \\ \mathbf{W}(2) \\ \vdots \\ \mathbf{W}(N_f) \end{bmatrix},$$

$$\mathbf{N}^{(c)} = \begin{bmatrix} \mathbf{N}(1) \\ \mathbf{N}(2) \\ \vdots \\ \mathbf{N}(N_f) \end{bmatrix} \mathbf{T}^{-1}$$

where $\mathbf{Y}^{(1)}(l)$, $\mathbf{W}(l)$ and $\mathbf{N}^{(1)}(l)$ show the value of matrices $\mathbf{Y}^{(1)}$, $\mathbf{W}$ and $\mathbf{N}^{(1)}$ respectively for the lth frame ($l \in \{1, 2, ..., N_f\}$). Note that in (5.5) we assumed that the channel matrix $\mathbf{H}$ is fixed during N_f frames measurement period.

SAS Module Setting

In this stage, $\mathbf{W}$ is set properly for measuring the whole N_sN_t entries of $\mathbf{H}$ from (5.5). There are some constraints in designing the weighting matrix $\mathbf{W}$. From the mathematical point of view, $\mathbf{W}^{(c)}$ must be invertible. On the other hand, we need to consider the practical aspects. For example, if we implement $\mathbf{W}$ using the phase-shifter-only components, the structure will imply some limitations (like

non-zero components) which must be considered in the design. Herein, we choose $\mathbf{W}^{(c)} = \sqrt{\frac{1}{N_r N_s}}\mathbf{\Gamma}_{N_s}$ where for $N_s = 8$,

$$\mathbf{W}^{(c)} = \sqrt{\frac{1}{N_r N_s}} \begin{bmatrix} 1 & 1 & 1 & 1 & 1 & 1 & 1 & 1 \\ 1 & -1 & 1 & -1 & 1 & -1 & 1 & -1 \\ 1 & 1 & -1 & -1 & 1 & 1 & -1 & -1 \\ 1 & -1 & -1 & 1 & 1 & -1 & -1 & 1 \\ 1 & 1 & 1 & 1 & -1 & -1 & -1 & -1 \\ 1 & -1 & 1 & -1 & -1 & 1 & -1 & 1 \\ 1 & 1 & -1 & -1 & -1 & -1 & 1 & 1 \\ 1 & -1 & -1 & 1 & -1 & 1 & 1 & -1 \end{bmatrix}$$

Hence, (5.5) becomes

$$\mathbf{Y}^{(2)} = \mathbf{H}\mathbf{X}^{(1)} + \mathbf{N}^{(2)} \tag{5.6}$$

where

$$\mathbf{Y}^{(2)} = \mathbf{W}^{(c)^{-1}}\mathbf{Y}^{(c)}, \qquad \mathbf{N}^{(2)} = \mathbf{W}^{(c)^{-1}}\mathbf{N}^{(c)}.$$

As (5.6) shows, by measuring $\mathbf{Y}^{(2)}$ we can estimate $\mathbf{H}$ in the presence of noise $\mathbf{N}^{(2)}$. In the next section, we estimate $\mathbf{H}$ using different methods.

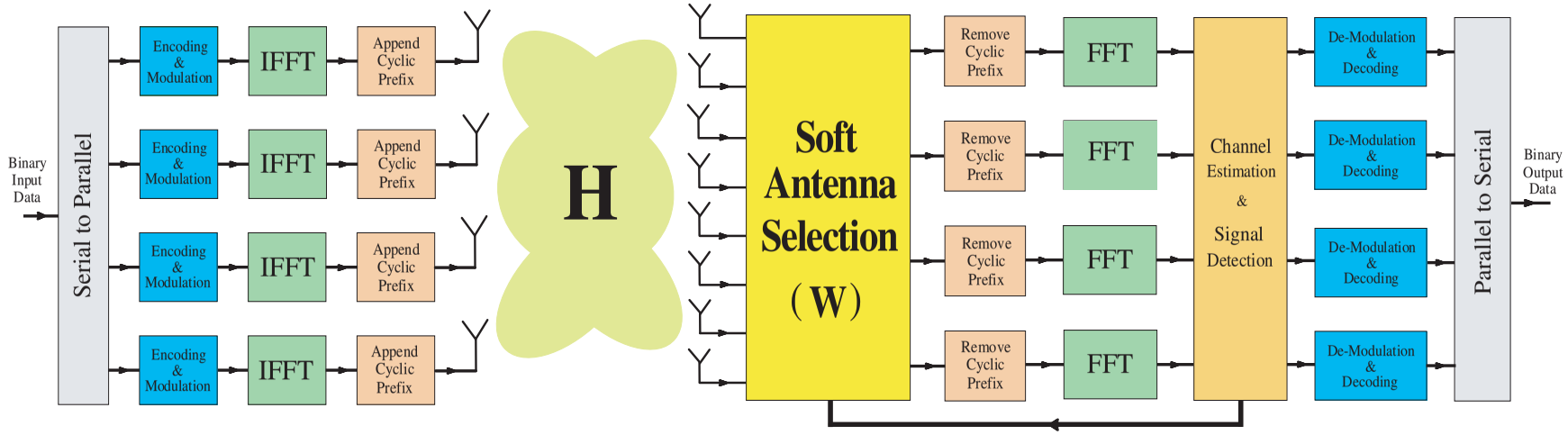

Figure 5.2: OFDM-based 4×4 SAS-MIMO with $N_s = 8$ simulation model.

5.2.2 H Estimation

To estimate the channel matrix $\mathbf{H}$, we use two estimators: LS and MMSE.

LS Estimator

According to this estimator the estimated channel matrix $\mathbf{H}$ is given by [58]:

$$\hat{\mathbf{H}}_{\text{LS}} = \mathbf{Y}^{(2)}\mathbf{X}^{(1)^{-1}} \tag{5.7}$$

MMSE Estimator

To derive an expression for the MMSE estimation of the channel, we first rewrite (5.6) as

$$\tilde{\mathbf{Y}} = \tilde{\mathbf{H}} + \tilde{\mathbf{N}} \tag{5.8}$$

where

$$\begin{aligned} \tilde{\mathbf{Y}} &= \text{vec}\left(\mathbf{Y}^{(2)}\mathbf{X}^{(1)^{-1}}\right), \quad \tilde{\mathbf{N}} = \text{vec}\left(\mathbf{N}^{(2)}\mathbf{X}^{(1)^{-1}}\right) \\ \tilde{\mathbf{H}} &= \text{vec}\left(\mathbf{H}\right) \end{aligned}$$

with vec(.) as the matrix vector transformation[2].

Hence, an MMSE estimate of the channel can be expressed as [59]:

$$\hat{\tilde{\mathbf{H}}}_{\text{MMSE}} = \mathcal{E}(\tilde{\mathbf{H}}\tilde{\mathbf{Y}}^*|\mathbf{X}^{(1)})\mathcal{E}(\tilde{\mathbf{Y}}\tilde{\mathbf{Y}}^*|\mathbf{X}^{(1)})^{-1}\tilde{\mathbf{Y}}. \tag{5.9}$$

Substituting (5.8) into (5.9) gives

$$\hat{\tilde{\mathbf{H}}}_{\text{MMSE}} = \mathcal{E}(\tilde{\mathbf{H}}\tilde{\mathbf{H}}^*)\left(\mathcal{E}(\tilde{\mathbf{H}}\tilde{\mathbf{H}}^*) + \mathcal{E}(\tilde{\mathbf{N}}\tilde{\mathbf{N}}^*|\mathbf{X}^{(1)})\right)^{-1}\tilde{\mathbf{Y}} \tag{5.10}$$

where $\mathcal{E}(\tilde{\mathbf{H}}\tilde{\mathbf{H}}^*)$ and the nominal SNR_0 are a priori known.

5.3 Proposed Method Evaluation via Simulation

To evaluate the proposed channel estimation approach, we use the simulation model for the transmitter and receiver shown in Figure 5.2. In this model:

- $N_t = 4$, $N_s = 8$, and $N_r = 4$.

[2]This transformation stacks the columns of the matrix argument into a single column vector.

- Modulation: QPSK .
- IEEE 802.16 OFDM transmission standard used in [60]: 200 subcarriers, OFDM symbol size of 320 (256-point FFT and the cyclic prefix size of 64), and the number of the payloads, N_d, is set to 40.
- Preamble: modeled as 4×4 long training sequences (i.e. $N_{Tr} = 4$)(see Figure 5.1). In this preamble, $[\mathbf{T}(j,m)]_{l,l}$ entries are the same and are chosen based on the IEEE 802.16 long training sequence [61].
- Coding: Convolutional.
- Phase-Shifter-Only SAS is used for $\mathbf{W}$.
- The transmitter employs VBLAST system in order to send data through different antennas.
- At the receiver, the channel parameters are estimated based on an LS or MMSE method.
- Detection of the VBLAST signals is performed using a combination of nulling and symbol cancellation.
- The Indoor clustered MIMO channel model presented in Section 3.4.1 is used to demonstrate the channel.

5.3.1 Performance Evaluation Results

The performance of the proposed channel estimation method with two employed estimators: LS and MMSE, is evaluated in terms of BER as shown in Figure 5.3. To measure this parameter 10^6 IEEE 802.16 frames are produced. The channel matrix is generated randomly according to the model described above for each two frames and during the transmission of each two frames the channel is kept unchanged. According to the figure, the proposed method works well for both LS and MMSE estimators. However, the MMSE estimator provides a better performance than the LS estimator as expected.

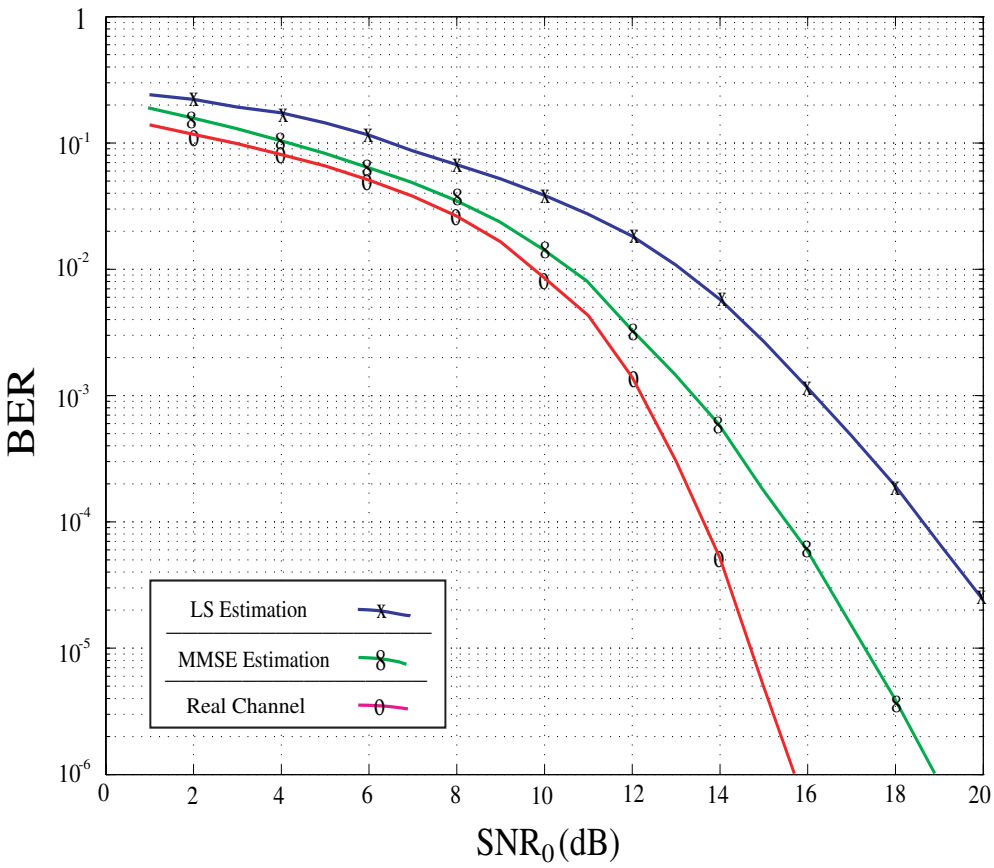

Figure 5.3: BER versus different nominal SNRs.

Chapter 6

Signal Coverage

In this chapter, we evaluate the SAS-MIMO system in terms of signal coverage issues. A SNR analysis is first performed for a reference point which is the mixer input, i.e. the input of Receiver Block Chain (RBC) shown in Fig. 6.1. Then, the different systems are compared based on a standard receiver settings. In this thesis, we use WLAN 802.11b standard. Settings for a typical 802.11b receiver is given in Table 6.1. Moreover, to implement the SAS module we use the components shown in Table 6.2.

6.1 SNR Analysis

In this section three difference receiver architectures are analyzed. (1) A single RF chain receiver as a reference. (2) SAS-MIMO receiver with active phased array, i.e. post-LNA SAS-MIMO. (3) SAS-MIMO receiver with passive phased array, i.e. pre-LNA. The SAS module in the last two ones is a phase only LN built by the component given in Table 6.2. In this analysis, we assume that there is no dominant sky noise, and the antenna temperature is the same as room temperature $T_A = T_0$, e.g. in terrestrial mobile communications [35, page 457].

Table 6.1: A Typical Receiver for WLAN 802.11b Standard [62]

Operating Frequency	$2.4GHz$
Bandwidth	$11MHz$
Receiver Sensitivity	$-76dBm$
Total Noise Figure	$8.3dB$
Transmission Line Gain G_{TL}	$-1.7dB$
LNA Gain G_{LNA}	$20dB$
LNA Noise Figure G_{LNA}	$3.5dB$

Table 6.2: SAS Module Components

Type	**Frequency**	**Loss**	Reference
Phase Shifter	$2-4GHz$	$3.5dB$	[63]
Power Splitter	$2-4GHz$	$6+0.6dB$	[64]
Power Combiner	$0.8-2.5GHz$	$1dB$	[65]

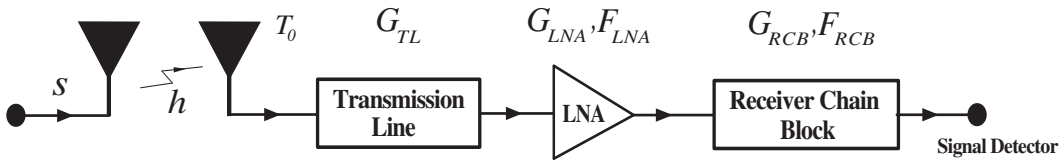

Figure 6.1: Single RF chain Transceiver.

6.1.1 Reference Single RF Channel Receiver

Consider a regular transceiver with single antenna connected to the RF chain depicted in Fig. 6.1. Such a structure is used in common MIMO structures like a low/full-complexity MIMO system. Now, assuming that the receiver noise dominates, i.e. no sky noise, the noise power at the input of the mixer is given by

$$\begin{aligned} N_{Single} &= (N_A + N_{TL})G_{TL}G_{LNA} + N_{LNA}G_{LNA} \\ &= F_{LNA}G_{LNA}KT_0B_\omega \end{aligned} \tag{6.1}$$

Moreover, the signal power at the input of the mixer is given by

$$S_{Single} = |h.s|^2 G_{TL}G_{LNA} \tag{6.2}$$

where h and s are the channel and transmitted signal, respectively. Hence, the resulting SNR, called SNR_0, is given by

$$\text{SNR}_0 = \frac{S_{single}}{N_{single}} = \frac{G_{TL}|h.s|^2}{F_{LNA}KT_0B_\omega} \tag{6.3}$$

Moreover, for a low/full-complexity MIMO system where we have an array of size N_t at the transmitter side (see Fig. 6.2)

$$S_{LF} = |\sum_{k=1}^{N_t} h_k s_k|^2 G_{TL}G_{LNA} \tag{6.4}$$

Hence,

$$\text{SNR}_{LF} = \frac{S_{LF}}{N_{single}} = \frac{G_{TL}|\sum_{k=1}^{N_t} h_k s_k|^2}{F_{LNA}KT_0B_\omega} \tag{6.5}$$

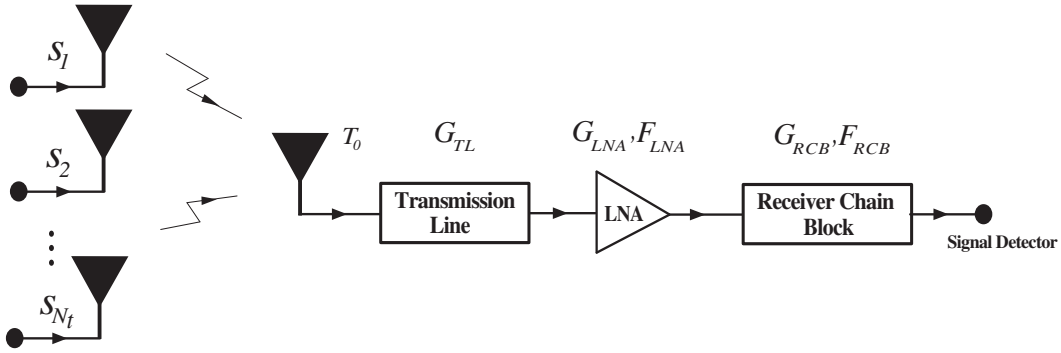

Figure 6.2: Low/Full complexity MIMO RF chain Transceiver.

6.1.2 Active Phased Array Receiver

To calculate SNR for a SAS module with an active phased array, we consider one out of N_r input receiver branches depicted in Fig. 6.3. As mentioned before, in a perfect match condition the noise power coming from LNA is divided by N_r but we only add up $1/N_s$ noise power of input ports at the combiner output . As shown in the figure, the phase-shifter has a gain G_ϕ, and the power splitter and combiner have an insertion loss $1/G_S$ and $1/G_C$, respectively. Hence, that the receiver noise dominates, i.e. no sky noise, the noise power at the input of the ith (out of N_r) mixer is given by

$$\begin{aligned} N_{Active_i} &= \frac{G_{C_i}}{N_s}\sum_{j=1}^{N_s}\Bigg((N_A+N_{TL_j})\frac{G_{TL_j}G_{LNA_j}G_{S_j}G_{\phi_{ij}}}{N_r} \\ &\quad +N_{LNA_j}\frac{G_{LNA_j}G_{S_j}G_{\phi_{ij}}}{N_r}+N_{S_j}\frac{G_{S_j}G_{\phi_{ij}}}{N_r}+N_{\phi_{ij}}G_{\phi_{ij}}+N_{C_i}\Bigg) \\ &= KT_0B_\omega\sum_{j=1}^{N_s}\Bigg((F_{LNA_j}G_{LNA_j}-1)\frac{G_{S_j}G_{\phi_{ij}}G_{C_i}}{N_r}+1\Bigg) \end{aligned} \tag{6.6}$$

Note that we have normalized (divided) the total noise power by the factor N_s due to this assumption that the power divider is reciprocal, i.e. $|S_{io}|^2 = |S_{oi}|^2 = \frac{1}{N_s}$ where the scattering parameters S_{io} and S_{oi} are associated with the ith input port and the output port, and this fact that noise on each input branch is uncorrelated to the others [29, page 446].

The signal power is also given by

$$S_{Active_i} = \frac{G_{C_i}}{N_rN_s}|\sum_{j=1}^{N_s}\sum_{k=1}^{N_t}\sqrt{G_{TL_j}G_{LNA_j}G_{S_j}G_{\phi_{ij}}}e^{j\phi_{ij}}h_{kj}s_k|^2 \tag{6.7}$$

In (6.7), the signal power is also normalized to N_s since the signal power at the combiner output is the summation of the powers of the input branches, i.e. the

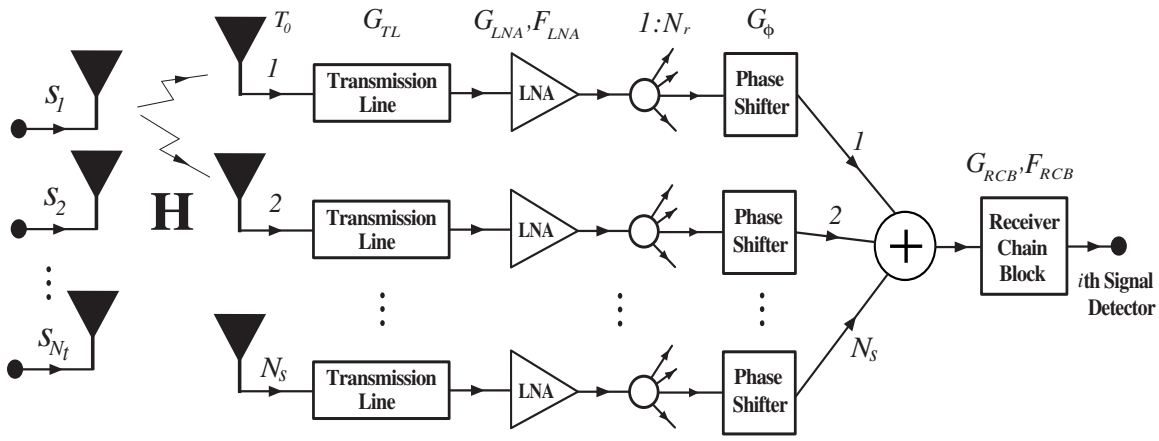

Figure 6.3: ith (out of N_r) receiver input for a SAS-MIMO with active phased array.

law of conservation of energy [30]. Now, we perform the practical assumptions to simplify the above formulas in two steps:

1. Assuming the phased array is uniform, i.e. the same electronics are used on the array branches, yields

$$\begin{aligned} N_{Active_i} &= KT_0B_\omega\Big((F_{LNA}G_{LNA}-1)\frac{G_SG_\phi G_C}{N_r}+1\Big) \\ S_{Active_i} &= \frac{G_CG_{TL}G_{LNA}G_SG_\phi}{N_rN_s}|\sum_{j=1}^{N_s}\sum_{k=1}^{N_t}e^{j\phi_{ij}}h_{kj}s_k|^2 \end{aligned} \tag{6.8}$$

2. Further, if we assume the ideal case $G_{TL}=G_C=G_\phi=G_S=1$ then

$$\begin{aligned} N_{Active_i} &= KT_0B_\omega\Big((F_{LNA}G_{LNA}-1)\frac{1}{N_r}+1\Big) \\ S_{Active_i} &= \frac{G_{LNA}}{N_rN_s}|\sum_{j=1}^{N_s}\sum_{k=1}^{N_t}e^{j\phi_{ij}}h_{kj}s_k|^2 \end{aligned} \tag{6.9}$$

Thus, SNR at the ith mixer input is given by

$$\mathrm{SNR}_{Active_i} = \frac{S_{Active_i}}{N_{Active_i}} \tag{6.10}$$

where S_{Active_i} and N_{Active_i} are obtained based on one of above-mentioned assumptions' results (6.8) and (6.9).

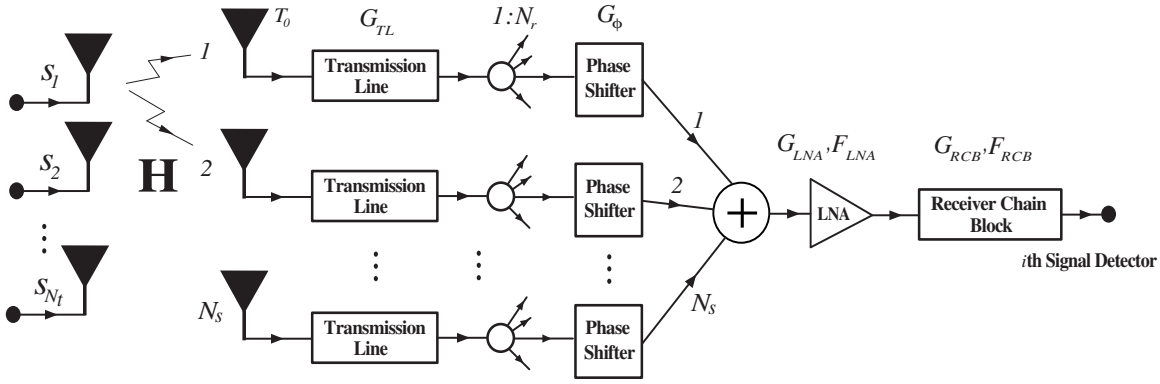

Figure 6.4: ith (out of N_r) receiver input for a SAS-MIMO with passive phased array.

6.1.3 Passive Phased Array Receiver

A noise analysis for a pre-LNA SAS module is herein investigated by considering one out of N_r input receiver branches depicted in Fig. 6.4. In this configuration, the noise power at the input of the ith (out of N_r) mixer is given by

$$\begin{aligned} N_{Passive_i} &= \frac{G_{C_i}G_{LNA_i}}{N_s}\sum_{j=1}^{N_s}\Big((N_A+N_{TL_j})\frac{G_{TL_j}G_{S_j}G_{\phi_{ij}}}{N_r}+N_{S_j}\frac{G_{S_j}G_{\phi_{ij}}}{N_r} \\ &\quad +N_{\phi_{ij}}G_{\phi_{ij}}+N_{C_i}\Big)+N_{LNA_i}G_{LNA_i} \\ &= KT_0B_\omega F_{LNA_i}G_{LNA_i} \end{aligned} \tag{6.11}$$

Moreover, the signal power is given by

$$S_{Passive_i} = \frac{G_{C_i}G_{LNA_i}}{N_rN_s}\Big|\sum_{j=1}^{N_s}\sum_{k=1}^{N_t}\sqrt{G_{TL_j}G_{S_j}G_{\phi_{ij}}}e^{j\phi_{ij}}h_{kj}s_k\Big|^2 \tag{6.12}$$

The same practical assumptions applied for the active phased array are performed here for the pre-LNA SAS.

1. Assuming the phased array is uniform yields

$$\begin{aligned} N_{Passive_i} &= KT_0B_\omega F_{LNA}G_{LNA} \\ S_{Passive_i} &= \frac{G_CG_{TL}G_{LNA}G_SG_\phi}{N_rN_s}\Big|\sum_{j=1}^{N_s}\sum_{k=1}^{N_t}e^{j\phi_{ij}}h_{kj}s_k\Big|^2 \end{aligned} \tag{6.13}$$

2. Further, if we assume the ideal case $G_{TL} = G_C = G_\phi = G_S = 1$ then

$$\begin{aligned} N_{Passive_i} &= KT_0B_\omega F_{LNA}G_{LNA} \\ S_{Passive_i} &= \frac{G_{LNA}}{N_rN_s}|\sum_{j=1}^{N_s}\sum_{k=1}^{N_t} e^{j\phi_{ij}}h_{kj}s_k|^2 \end{aligned} \tag{6.14}$$

Thus, SNR at the ith mixer input is given by

$$\mathrm{SNR}_{Passive_i} = \frac{S_{Passive_i}}{N_{Passive_i}} \tag{6.15}$$

where $S_{Passive_i}$ and $N_{Passive_i}$ are obtained based on one of above-mentioned assumptions' results (6.13) and (6.14).

6.1.4 Discussion on Analytical Derivations

In this discussion, we two by two compare the results of the SNR calculations for all three above-mentioned configurations.

Low/Full Complexity versus Active Phased Array

To compare these two configurations, we define the following SNR gain

$$\mathrm{G}_1 = \frac{\mathrm{SNR}_{Active_i}}{\mathrm{SNR}_{LF}} \tag{6.16}$$

where for SNR_{Active_i} we employ (6.8). Hence,

$$\mathrm{G}_1 = \frac{\frac{G_CG_SG_\phi}{N_rN_s}|\sum_{j=1}^{N_s}\sum_{k=1}^{N_t} e^{j\phi_{ij}}h_{kj}s_k|^2}{|\sum_{k=1}^{N_t} h_ks_k|^2}\frac{F_{LNA}G_{LNA}}{\left((F_{LNA}G_{LNA}-1)\frac{G_SG_\phi G_C}{N_r}+1\right)} \tag{6.17}$$

Now $F_{LNA}G_{LNA} >> 1$ yields

$$1 < \mathrm{G}_1 = \frac{|\sum_{j=1}^{N_s}\sum_{k=1}^{N_t} e^{j\phi_{ij}}h_{kj}s_k|^2}{N_s|\sum_{k=1}^{N_t} h_ks_k|^2} < N_s \tag{6.18}$$

Hence, we have an improvement for the provided SNR to the baseband while using an active phase array. Note that this improvement is independent of the insertion loss of the phase array components.

Low/Full Complexity versus Passive Phased Array

To compare these two configurations, we define the following SNR gain

$$\mathrm{G}_2 \;=\; \frac{\mathrm{SNR}_{Passive_i}}{\mathrm{SNR}_{LF}} \tag{6.19}$$

where for SNR_{Pctive_i} we employ (6.13). Hence,

$$\mathrm{G}_2 \;=\; \frac{G_C G_S G_\phi |\sum_{j=1}^{N_s}\sum_{k=1}^{N_t} e^{j\phi_{ij}} h_{kj} s_k|^2}{N_r N_s |\sum_{k=1}^{N_t} h_k s_k|^2} \;<\; \frac{G_C G_S G_\phi N_s}{N_r} \tag{6.20}$$

The upperbound for G_2 can be less than one for very lossy passive phased array. Hence, in comparison to the active phased array although this structure is employing a lower number of LNAs, the active phased array always outperforms the passive one in terms of providing SNR to the baseband, i.e. even though the passive phased array is made of no insertion loss components.

In the next section, we will demonstrate the above mentioned mathematical achievements through a ray tracing simulation.

6.2 Ray-tracing Modeling

The performance of the SAS-MIMO system is studied via a *ray-tracing* simulation in this chapter. Although in a ray tracing model many real parameters are ignored or simplified due to the time consuming and fundamental limits which this kind of simulation has, it works much better than the traditional channel models, e.g. statistical models, to show the propagation characteristics in a site specific case. In this type of channel modeling, the source of errors which make the ray tracing inaccurate against the measurement are categorized as follows

1. This kind of channel modeling is employing geometrical models which are inaccurate and simplified. Hence, many details in the environment are not considered and may cause inaccuracy in final results.

2. Although Electro-Magnetic (EM) parameters are considered in the ray-tracing modeling, they are not very precise and in fact an averaged measured values are imported and used. This issue may also cause uncertainty in the results.

3. Ray tracing softwares usually consider all the EM processes including reflection, refraction, diffraction theories. However, a simplified edition of them are employed due to being time-consuming. Hence, the final results may be affected by this simplification.

Moreover, although the statistical models are more general than site specific models, i.e. ray tracing, they can not be useful when the temporal variation of the

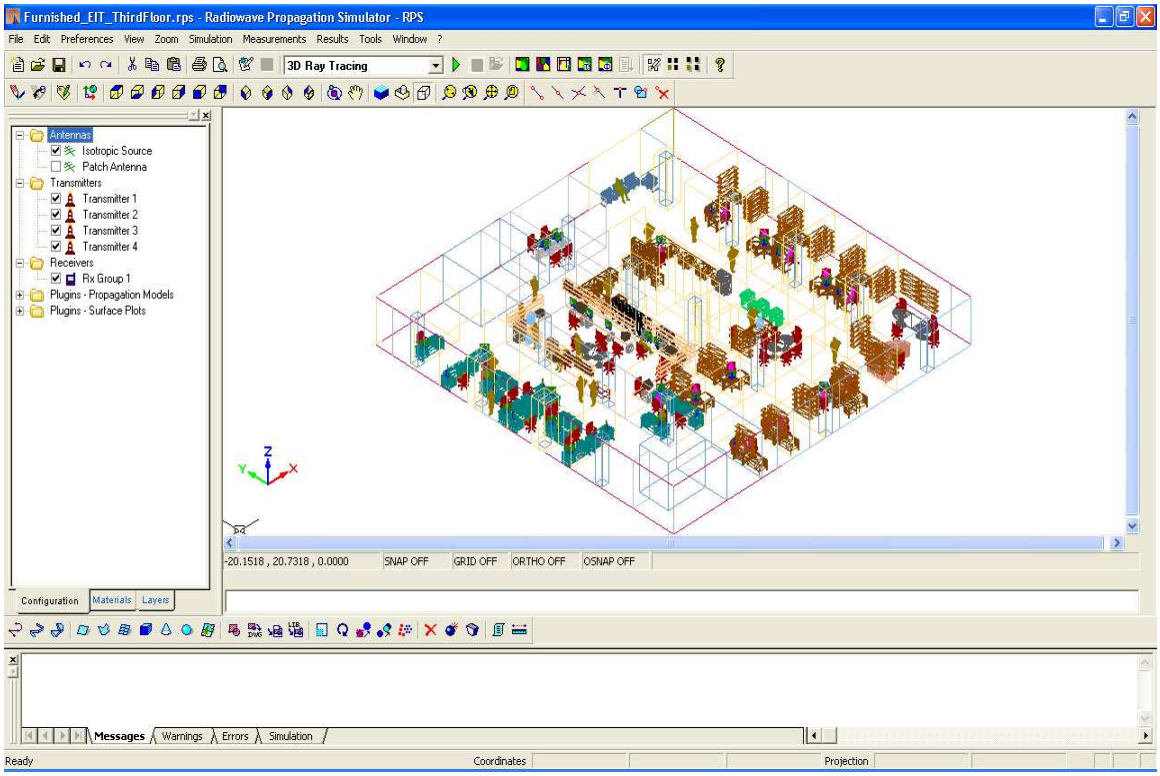

Figure 6.5: RPS software appearance.

channel, which is due the movement, is important. Hence, a ray tracing simulation can be helpful when an adaptive system is under evaluation. There exist many ray-tracing tools for the deterministic modeling of the waves propagation environments. Among them, Radiowave Propagation Simulator (RPS) [66] has been shown to be accurate in terms of statistical properties and is widely used for the wave propagation simulations. The student version of this software is free for public. Fig. 6.5 shows the software main screen.

6.2.1 Propagation Environment

In this thesis, we employ a Three-Dimensional (3D) ray-tracing modeling to assess the signal coverage for a $2.4GHz$ wireless communication example. The Intelligent Multi-Antenna radio Systems (iMARS) laboratory located in the third floor map of the EIT building at University of Waterloo is used as a typical indoor wireless environment (see Fig. 6.6 and 6.7). This laboratory is structured by different wall materials including concrete, wood etc., and furnished with tables, chairs and shelves mostly built by wooden and plastic materials. Moreover, there exist various electronic equipments like computers, printers and test devices in this lab. The reflection coefficients for the employed materials in $2.4GHz$ operating frequency are reported in [67], [68] and [69]. Moreover, to evaluate the human body shadowing effect we use the measured permittivity data for human skin in [70]. Table 6.3

Table 6.3: Measured Permittivity of Indoor Materials at 2.4 GHz

Type	**Thickness (mm)**	**Complex ϵ_r**
Plexiglass I	2.5	$2.5 - j0.0235$
Plexiglass II	7.1	$2.74 - j8.76 \times 10^{-4}$
Blinds (closed)	0.5	$3.49 - j2.08 \times 10^{-4}$
Blinds (open)	22	$1.96 - j1.1682 \times 10^{-4}$
Red Brick	102	$5.821 - j0.6753$
Carpet	7.75	$1.32 - j7.8672 \times 10^{-5}$
Fabric	1.13	$1.49 - j8.8804 \times 10^{-5}$
Fiberglass	890	$1.02 - j9.3942 \times 10^{-4}$
Glass	2.5	$6.3778 - j0.1659$
Drywall I	12.8	$2.1899 - j0.0243$
Drywall II	9	$2.49 - j0.0105$
Linoleum	1.61	$3.08 - j0.0043$
Fir	37.7	$2.5299 - j0.506$
Particle-Board	19	$2.6838 - j0.2953$
Plywood	18.5	$2.4503 - j0.3111$
Stucco	25.75	$0.9833 - j0.4219$
Tiles	21.2	$3.0747 - j0.1807$
Light Cover	2.5	$1.66 - j0.0115$
Tar Paper	1.7	$2.4682 - j0.0953$
Human Skin	5	$39.5161 - j6.2029$

summarizes the measured permittivity data at 2.4GHz used in this thesis.

6.3 Wireless Communication Link Settings

In our simulation study, the transmitter antenna array is located at the corner of Hallway 1 and 2 (see Fig. 6.6). The transmitter array consists of 4 patch antenna elements facing toward the iMARS lab (45° rotation relative to Hallway 1 and 2), facing down with a small tilt of 8°, and $20cm$ off from the ceiling. Each of transmitter elements has $0.1mW$ transmitting power. The transmitter settings considered in our ray-tracing simulation through the RPS software are shown in Fig. 6.8.

A nominal patch beam pattern added to Fig. 6.6 to demonstrate the transmitter antenna orientation. The patch antenna employed for the transmitter has a gain $5.5dB$ with a pattern shown in Fig. 6.9-(a). We have considered an array spacing $\lambda/2$ for the transmitter.

The receiver antenna array consists of an 8-element array of dipoles ($\lambda/2$ length) with 0.1λ element spacing located in the iMARS lab. The dipole antenna employed for the receiver has a gain $2dB$ with a pattern shown in Fig. 6.9-(b). These array elements are chosen from a line of receiving points from locations A to B as shown in Fig. 6.6. The antenna array moving steps are $5mm$ apart through the line

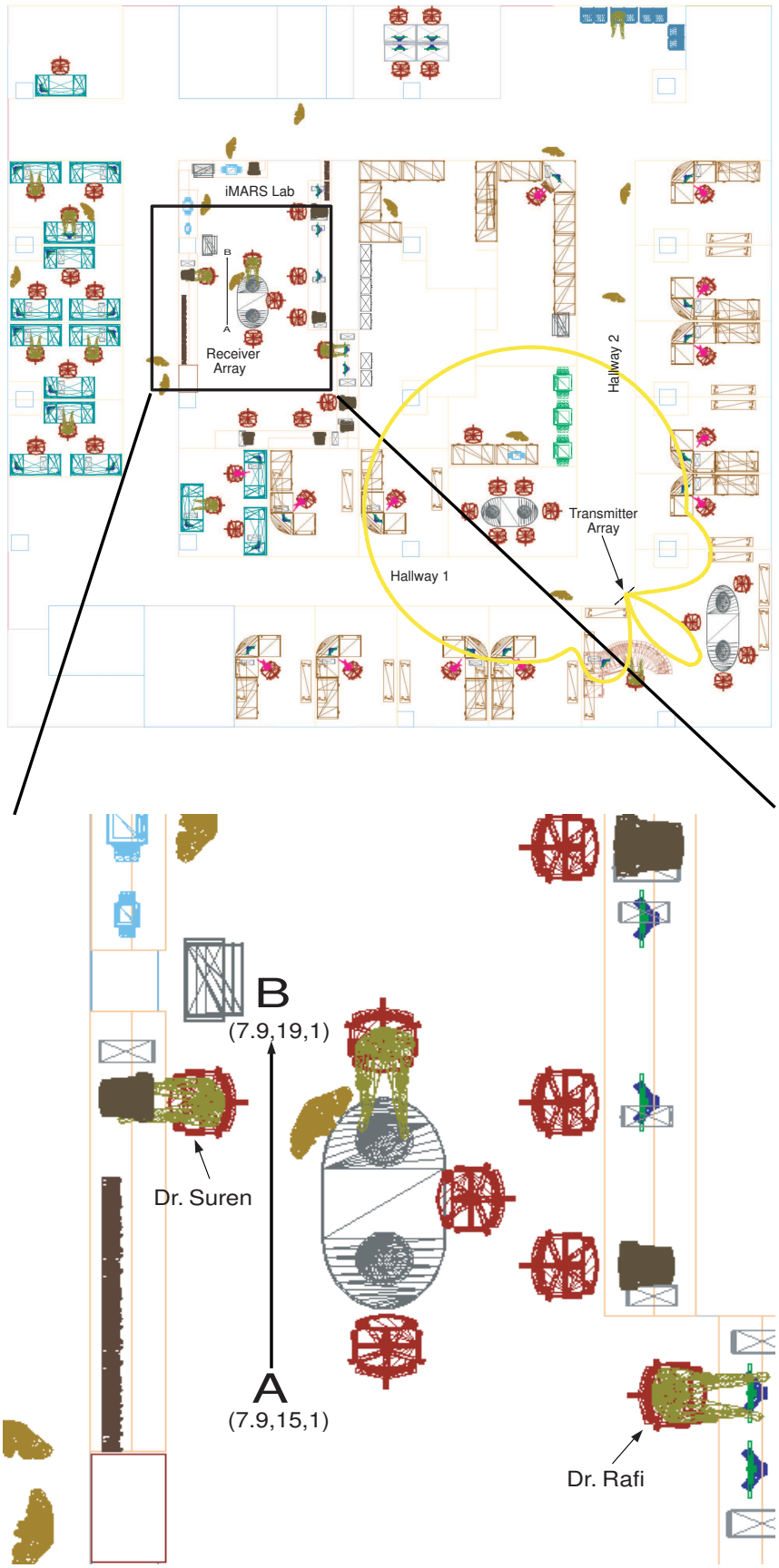

Figure 6.6: The third floor map of EIT building, University of Waterloo.

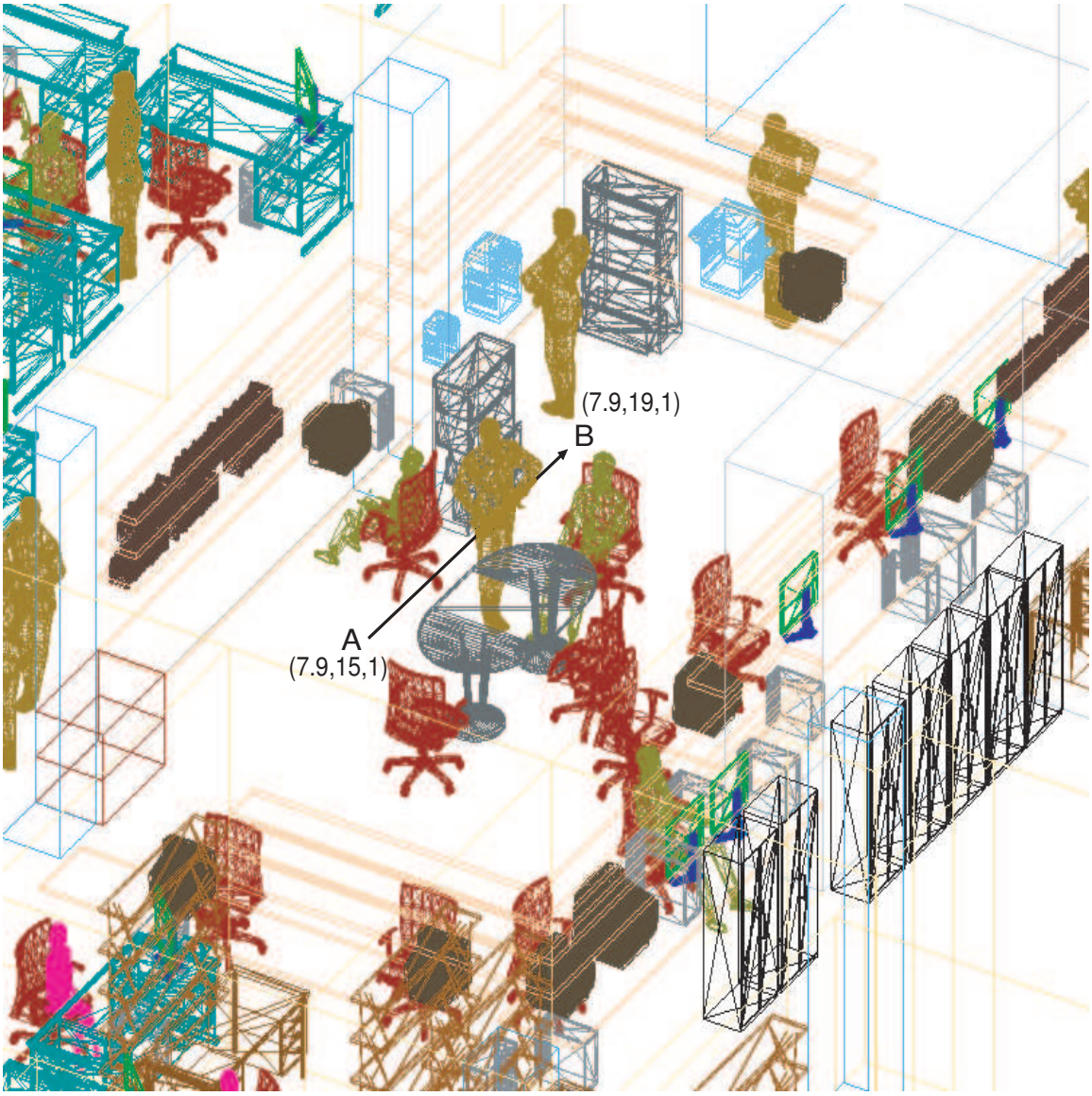

Figure 6.7: A 3D view of simulated environment (the third floor of EIT building, University of Waterloo).

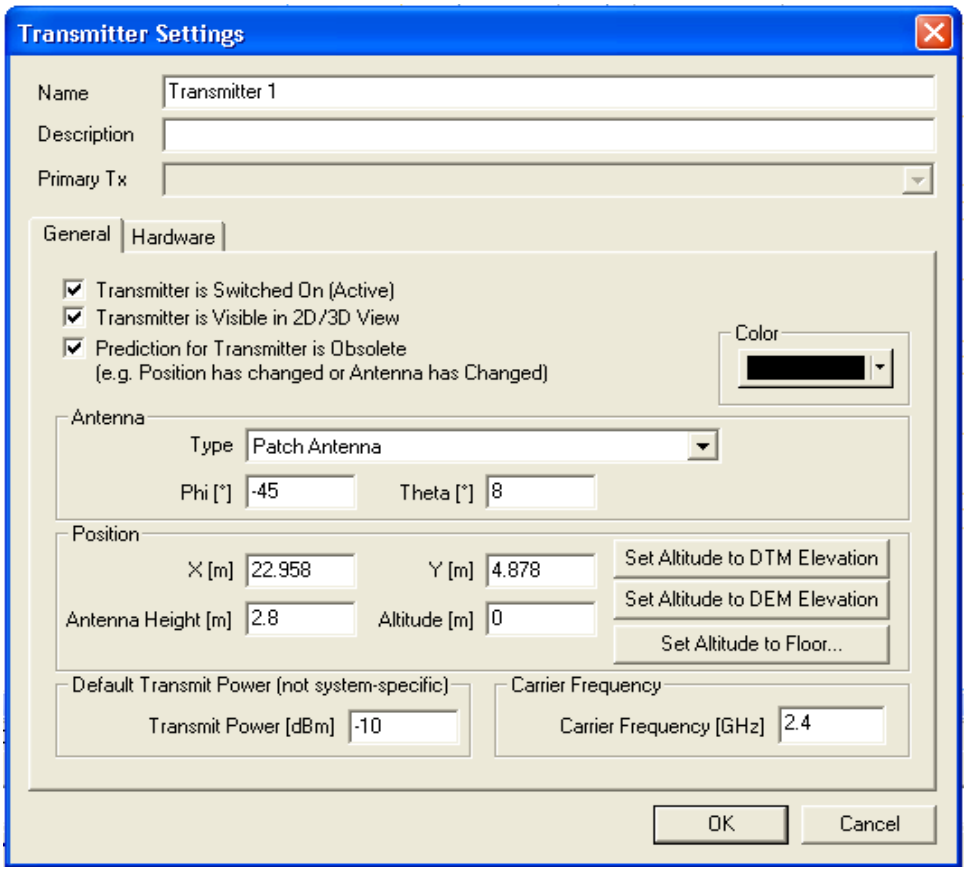

Figure 6.8: The overall settings for each transmitter elements.

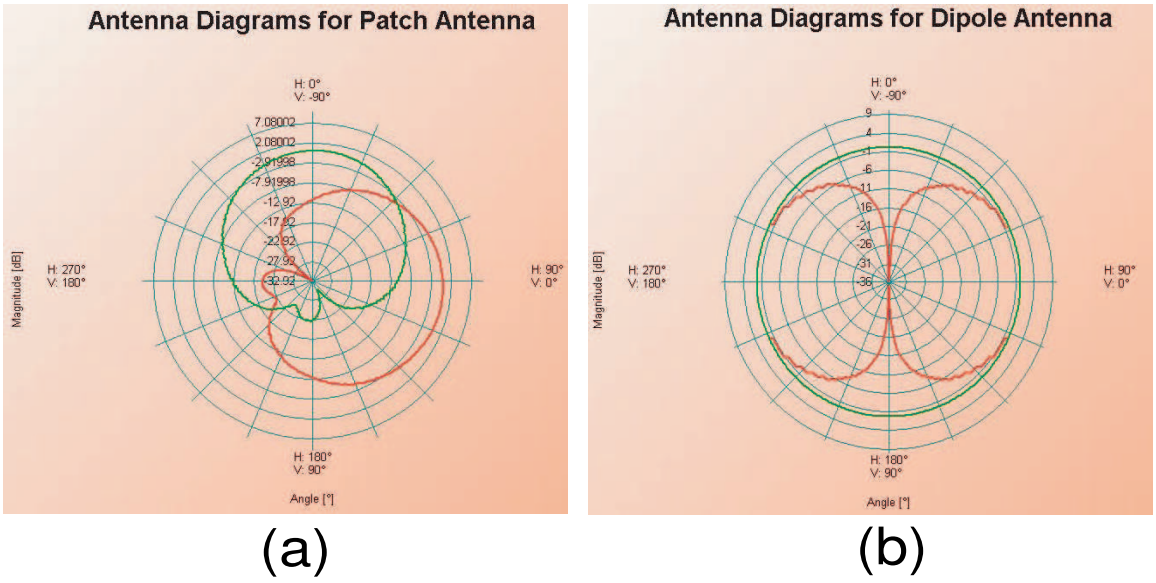

(a) (b)

Figure 6.9: Beam pattern of the transmitter (a) and the receiver (b) antenna elements.

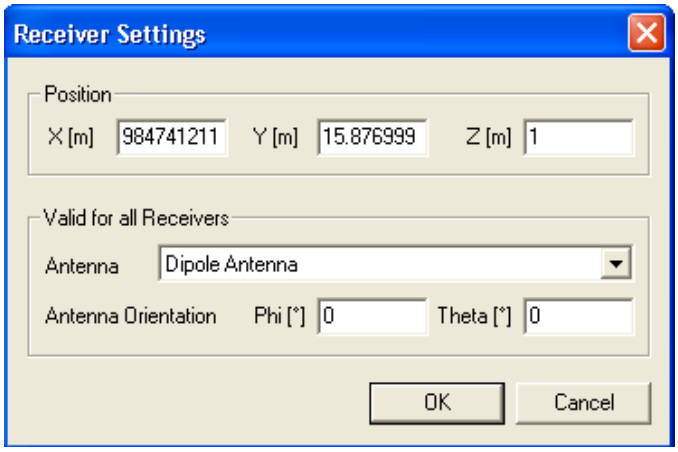

Figure 6.10: The overall settings for each transmitter elements.

of receiving points which are at $1m$ height from the lab floor. To simulate the shadowing effect, a human-body blocks the LOS path between the transmitter and the receiver. The receiver settings (for a chosen receiver point) considered in our ray-tracing simulation through the RPS software are shown in Fig. 6.10.

6.4 Simulation Results

As stated before, we perform the simulations on a 802.11b (direct sequence WiFi) system architecture for all of under the test configurations. Assume this system provides a receiver sensitivity of $-76dBm$ (see Table 6.1). Starting with the $-174dBm/Hz$ background thermal noise and adding $70dB$ corresponding to the $11MHz$ channel bandwidth we obtain $-104dBm$ for the antenna noise. Subtracting this number from the required $-76dBm$ receiver sensitivity (minimum antenna signal), we calculate an input SNR of $28dB$. If we assume the transmission line TL (see Fig. 2.5), including the filters, duplexer etc., has a maximum $1.7dB$ noise figure (see Table 6.1), LNA provides $3.5dB$ noise figure and everything else being ideal, a minimum $22.8dB$ SNR is needed at the input of the mixer.

To show the effect of the SAS processing on the signal coverage, SNR at the mixer input along the path A-B for different architectures are shown in Fig. 6.11. In this study, we assume that the same receiver electronic components are used for all of configurations. As the figure shows, a full-complexity MIMO even fails to receive signal in a deep-fading areas like human body shadowing. However, when an active/passive array is used in the front end, due to beamforming capability the received power can be improved even $10dB$. Note that if we apply the inaccuracy effect of the ray tracing modeling, i.e. $\pm 4dB$, we will still have improvement at the worst case. The post-SAS method gives the receiver an opportunity to receive the power even in a deep fading shown in the plot even with the loss in the implemented PLN. In terms of the signal coverage analysis, the post-LNA SAS configuration also

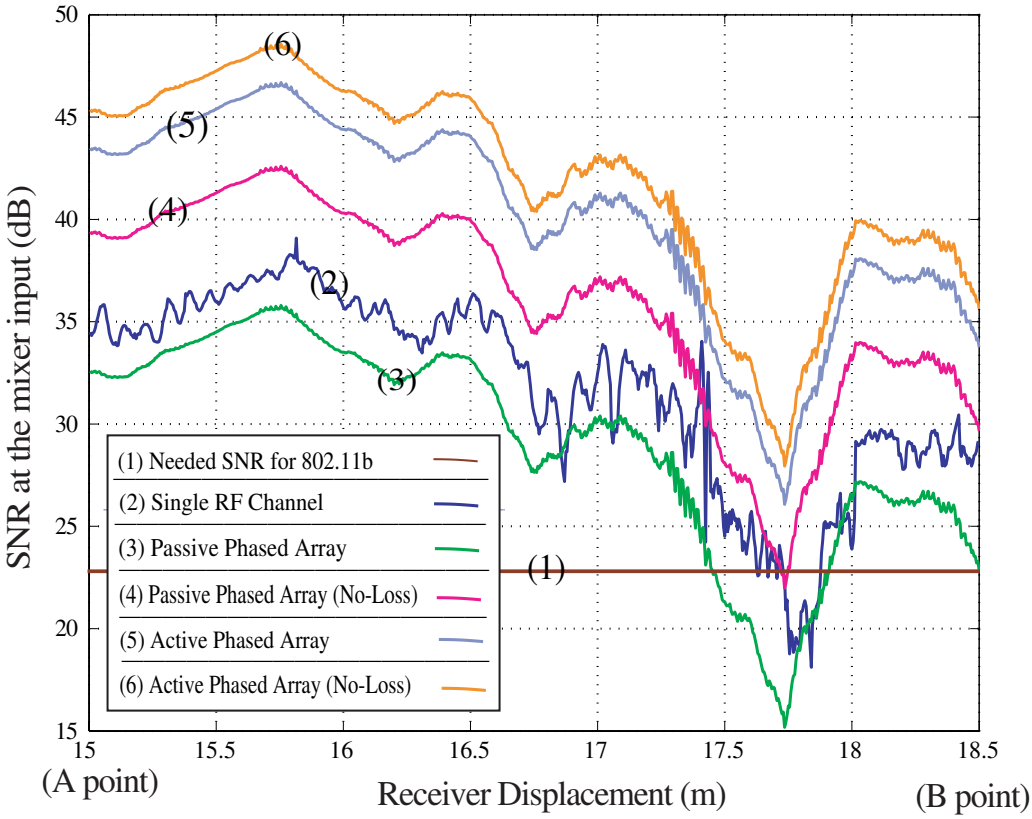

Figure 6.11: Signal coverage from A to B points.

shows a better performance than pre-LNA SAS. A pre-LAN SAS with loss in the implemented PLN, though it gains a beamforming capability, even works worse than a regular full complexity MIMO in terms of provided SNR to the baseband.

Chapter 7

Conclusion and Future Work

In this thesis, the following tasks have been done

- The pre-LNA SAS-MIMO spatial multiplexing/diversity transmission systems are investigated in the noise-limited channels. An upper-bound for the optimum pre-LNA SAS module plus a sub-optimum solution is derived. The simulation results using a general MIMO channel model show that the post-LNA configuration always outperforms the pre-LNA SAS.
- The optimum post-LNA SAS-MIMO is found in an interference channel where both noise and interference exist. The optimum solutions are provided for both aforementioned transmission strategies in CSIR and CSIT cases. The simulation results reveal that the post-LNA SAS-MIMO is also upper-bounded by a full-complexity MIMO in the interference channels.
- We proposed a channel estimation method for SAS-MIMO.
- A signal coverage analysis is performed for the pre/post-LNA SAS to investigate on the provided SNR to the baseband. We have employed an operational WLAN (802.11b) system settings applied on a ray-tracing channel model. The results for a case study show that although the optimum post-LNA SAS works like a full-complexity MIMO in spatial multiplexing/diversity transmission strategies, it provides even a better SNR to the baseband. This issue becomes more important when a deep fading occurs and a full-complexity MIMO built by the regular receiver components, i.e. 802.11b here in this thesis, can not afford the fading.

As future work, we propose the followings:

- Finding the optimum solution for post-LNA SAS-MIMO with the constraints, e.g. based on the phase-shift-only SAS, for both spatial multiplexing and diversity transmission strategies.

- Interference estimation including the interference received power and AOA estimations. Instead, a directily estimate of the interference covariance matrix $\mathbf{K}_z$ also works.
- Signal coverage analysis and simulation for when the interference exists in the channel.
- Implementing the pre/post-LNA SAS-MIMO, e.g. using a FPGA based Software Defined Radio (SDR) system (being done).

Publications resulting from this research

[1] J. Ahmadi-Shokouh, S. H. Jamali and S. Safavi-Naeini, "Enhanced Receiver Sensitivity in MIMO System with Soft Antenna Selection" *Submitted to Antenna Propagation Letters. (2008)*

[2] J. Ahmadi-Shokouh, S. H. Jamali and S. Safavi-Naeini, "Optimal Receive Soft Antenna Selection for MIMO Interference Channels" *Submitted to Transactions on Wireless Communications. (2008)*

[3] J. Ahmadi-Shokouh, S. H. Jamali and S. Safavi-Naeini, "Switch On the Optimal Receive Soft Antenna Selection for Reliable Communications in MIMO Interference Channels" *Accepted in 68th IEEE Vehicular Technology Conference. Sep. 21-24, 2008.*

[4] J. Ahmadi-Shokouh, S. H. Jamali and S. Safavi-Naeini, "Switch Loss and Antenna Directivity Effects on MIMO Antenna Selection" *21th IEEE Canadian Conf. on Electrical and Computer Eng.* pp. 641-646, 2008.

[5] J. Ahmadi-Shokouh, S. H. Jamali and S. Safavi-Naeini, "Receive Soft Antenna Selection for Spatial- Multiplexing MIMO Systems in Interference-Dominated Channels" *21th IEEE Canadian Conf. on Electrical and Computer Eng.* pp. 627- 630, 2008.

[6] J. Ahmadi-Shokouh, S. H. Jamali and S. Safavi-Naeini, "On the Optimality of SPRAS-MIMO for Spatial Multiplexing Transmission," *IEEE Radio and Wireless Symposium,* pp. 531-534, 2007.

[7] J. Ahmadi-Shokouh, S. H. Jamali and S. Safavi-Naeini, "Channel Estimation for OFDM-Based SPRASMIMO System," *IEEE Global Telecommunications Conference,* pp. 1-5, 2006.

[8] J. Ahmadi-Shokouh, S. Nikneshan, S. H. Jamali and S. Safavi-Naeini, "Performance Study of the VBLAST-Based MIMO System with Smart Passive Receive Antennas," IEEE 23rd Biennial Symposium on Communications, pp. 295- 298, 2006.

[9] J. Ahmadi-Shokouh, S. H. Jamali and S. Safavi-Naeini, "Capacity of SPRAS-MIMO System with MMSE Channel Estimation," *IEEE Vehicular Technology Conference,* pp. 1-5, Fall 2006.

[10] J. Ahmadi-Shokouh, S. Nikneshan, S. H. Jamali and S. Safavi-Naeini, "MIMO Testbed with SPRAS Approach," Discovery 2006.

List of Figures

[1] J. Winters, "On the Capacity of Radio Communication Systems with Diversity in a Rayleigh Fading Environment," *IEEE Journal of Selected Areas on Communications*, vol. 5, no. 5, pp. 871878, June 1987.

[2] G. J. Foschini and M. J. Gans, "On Limits of Wireless Communications in a Fading Environment When Using Multiple Antennas," *Wireless Personal Commun.*, no. 6, pp. 311-335, Mar. 1998.

[3] G. G. Raleigh and J. M. Cioffi, "Spatio-Temporal Coding for Wireless Communication," *IEEE Transactions on Communications*, vol. 46, no. 3, pp. 357366, March 1998.

[4] I. E. Telatar, "Capacity of multi-antenna Gaussian channels," *European Trans. on Commun.*, vol. 10, no. 6, pp. 585-595, Nov./Dec. 1999.

[5] T. Marzetta and B. Hochwald, "Capacity of a Mobile Multiple-Antenna Communication Link in Rayleigh Flat Fading," *IEEE Transactions on Information Theory*, vol. 45, no. 1, pp. 139157, January 1999.

[6] S. M. Alamouti, "A Simple Transmit Diversity Technique for Wireless Communications," *IEEE Journal on Selected Areas in Communications*, vol. 16, no. 8, pp. 14511458, Oct. 1998.

[7] T. K. Y. Lo, "Maximum ratio transmission," *IEEE Trans. Commun.*, vol. 47, pp. 14581461, Oct. 1999.

[8] D. J. Love and R. W. Heath Jr., "Grassmannian beamforming for multiple-input multiple-output wireless systems," *IEEE Trans. Inform. Theory*, vol. 49, no. 10, pp. 2735-2747, Oct. 2003.

[9] A. F. Molisch and M. Z. Win, "MIMO systems with antenna selection-an overview," *IEEE Microwave Mag.*, vol. 5, no. 1, pp. 46-56, Mar. 2004.

[10] A. F. Molisch, M. Z. Win and J. H. Winters, "Capacity of MIMO Systems with Antenna Selection," *IEEE Int. Conf. on Commun.*, pp. 570574, 2001.

[11] R.W. Heath Jr., S. Sandhu and A. J. Paulraj, "Antenna Selection for Spatial Multiplexing Systems with Linear Receivers," *IEEE Commun. Lett.*, vol. 5, no. 4, pp. 142144, Apr. 2001.

[12] D. Gore, R. Nabar and A. J. Paulraj, "Selection of an optimal set of transmit antennas for a low rank matrix channel," *IEEE Int. Conf. on Acous. Spee. and Sign. Process.*, pp. 2785-2788, 2000.

[13] A. F. Molisch and X. Zhang, "FFT-Based Hybrid Antenna Selection Schemes for Spatially Correlated MIMO Channels," *IEEE Commun. Letters*, vol. 8, no. 1, pp. 36-38, Jan. 2004.

[14] X. Zhang, A. F. Molisch and S.-Y. Kung, "Variable-Phase-Shift-Based RF-Baseband Codesign for MIMO Antenna Selection," *IEEE Trans. on Sig. Process.*, vol. 53, no. 11, pp. 4091-4103, Nov. 2005.

[15] A. Forenza and R. W. Heath Jr., "Impact of Antenna Geometry on MIMO Communication in Indoor Clustered Channels," *IEEE Ant. and Propag. Society Symp.*, pp. 1700-1703, 2004.

[16] M. A. Jensen and J. W. Wallace, "A Review of Antennas and Propagation for MIMO Wireless Communications," *IEEE Transactions on Antennas and Propagation*, vol. 52, no. 11, pp. 2810-2824, November 2004.

[17] S. Sandhu, R. U. Nabar, D. A. Gore and A. Paulraj,"Near-Optimal Selection of Transmit Antennas for a MIMO Channel Based on Shannon Capacity," *IEEE Asilomar Conference Signals, Systems and Computers*, pp. 567571, 2000.

[18] D. Gore and A. Paulraj, "Space-Time Block Coding with Optimal Antenna Selection," *IEEE International Conference Acoustics, Speech, and Signal Processing*, pp. 24412444, 2001.

[19] D. A. Gore, R. W. Heath and A. J. Paulraj, "Transmit Selection in Spatial Multiplexing Systems," *IEEE Communication Letter*, vol. 6, no. 11, pp. 491493, November 2002.

[20] D. A. Gore and A. J. Paulraj, "MIMO Antenna Subset Selection with Space-Time Coding," *IEEE Transactions on Signal Processing*, vol. 50, no. 10, pp. 25802588, October 2002.

[21] M. A. Jensen and M. L. Morris, "Efficient Capacity-Based Antenna Selection for MIMO Systems," *IEEE Transactions on Information Theory*, vol. 54, no. 1, pp. 110-116, January 2005.

[22] D. Gore, R. Nabar and A. Paulraj, "Selection of an Optimal Set of Transmit Antennas for a Low Rank Matrix Channel," *IEEE International Conference on Acoustics, Speech, and Signal Processing*, pp. 27852788, 2000.

[23] R. B. Ertel, P. Cardieri, K. W. Sowerby, T. S. Rappaport and J. H. Reed, "Overview of Spatial Channel Models for Antenna Array Communication Systems," *IEEE Personal Communications*, vol. 5, no. 1, pp. 1022, February 1998.

[24] R. Janaswamy, "Effect of Element Mutual Coupling on the Capacity of Fixed Length Linear Arrays," *IEEE Antennas Wireless Propagation Letter*, vol. 1, no. 1, pp. 157160, 2002.

[25] A. F. Molisch, M. Z. Win and J. H. Winters, "Reduced-Complexity Transmit/Receive-Diversity Systems," *IEEE Transactions on Signal Processing*, vol. 51, pp. 27292738, November 2003.

[26] A. F. Molisch, X. Zhang, S. Y. Kung and J. Zhang, "DFT-Based Hybrid Antenna Selection Schemes for Spatially Correlated MIMO Channels," *IEEE Int. Symp. on Persona1, Indoor Mobile Radio Commun.*, pp. 1119-1123, 2003.

[27] X. Zhang, A. F. Molisch and S. Y. Kung, "Phase-Shift-Based Antenna Selection for MIMO Channels," *IEEE Global Telecommun. Conf.*, pp. 1089-1093, 2003.

[28] P. Sudarshan, N. B. Mehta, A. F. Molisch and J. Zhang, "Channel Statistics-Based RF Pre-Processing with Antenna Selection," *IEEE Trans. Wireless Commun.*, vol. 5, no. 12, pp. 3501-3511, Dec. 2006.

[29] A. Bahattacharyya, *Phased Array Antennas*, John Wiley & Sons, Hoboken NJ, USA, 2006.

[30] J. J. Lee, "G/T and Noise Figure of Active Array Antennas," *IEEE Trans. Ant. and Propag.*, vol. 41, no. 2, pp. 241-244, Feb. 1993.

[31] H. Santos, *RF MEMS Circuit Design for Wireless Communications*, Artech House, 2002.

[32] Z. J. Yao, S. Chen, S. Eshelman, D. Denniston and C. Goldsmith, "Micromachined Low-Loss Microwave Switches," *J. MEMS*, vol. 8, no. 2, pp. 12934. Jun. 1999.

[33] B. A. Cetiner, H. Jafarkhani, J.-Y. Qian, H. J. Yoo, A. Grau and F. D. Flaviis, "Multifunctional Reconfigurable MEMS Integrated Antennas for Adaptive MIMO Systems", *IEEE Commun. Mag.*, vol. 42, no. 12, pp. 62-70, Dec. 2004.

[34] S. Hara, U. Irie, U. Nakaya, T. Toda and A. Oishi, "Acceleration of Beamfonning Speed for RF MEMS-Implemented Phased Array Antenna", *IEEE Topical Conf. on Wireless Commun. Tech.*, pp. 400-401, 2003.

[35] R. Vaughan and J. B. Andersen, *Channels, Propag. and Ant.s for Mobile Commun.*, London, United Kingdom: IEE, 2003.

[36] M. J. Gans, "Channel Capacity Between Antenna Arrays– Part I: Sky Noise Dominates," *IEEE Trans. Commun.*, vol. 54, no. 9, pp. 1586-1592, Sep. 2006.

[37] J. Engberg and T. Larsen, *Noise Theory of Linear and Nonlinear Circuits*, John Wiley and Sons: New York USA, 1995.

[38] M. J. Gans, "Channel Capacity Between Antenna Arrays– Part I: Amplifier Noise Dominates," *IEEE Trans. Commun.*, vol. 54, no. 11, pp. 1983-1992, Nov. 2006.

[39] A. F. Molisch, *Wireless Communications*, John Wiley and Sons, IEEE Press: The Atrium, Southern Gate, Chichester, West Essex, England, 2005.

[40] A. J. Paulraj, D. A. Gore, R. U. Nabar and H. Bolsckei, "An Overview of MIMO Communications – A Key to Gigabit Wireless," *Proc. of the IEEE*, vol. 92, no. 2, pp. 198-218, Feb. 2004.

[41] S. A. Jafar, S. Vishwanath and A. Goldsmith, "Channel Capacity and Beamforming for Multiple Transmit and Receive Antennas with Covariance Feedback," *IEEE Int. Conf. Commun.*, pp. 2266-2270, 2001.

[42] R. A. Horn and C. R. Johnson, *Matrix Analysis*, Cambridge University Press, Cambridge U. K., 1994.

[43] B. Holter and G. E. Oien, "The optimal Weights of Maximum Ratio Combiner Using an Eigenfilter Approach", *IEEE Nordic Signal Processing Symp.*, 2002.

[44] S. Haykin, *Adaptive Filter Theory*, Prentice Hall, USA, 2001.

[45] R. S. Martin and J. H. Wilkinson, "Reduction of the Symmetric Eigenproblem $\mathbf{Ax} = \lambda\mathbf{x}$ and Related Problems of Standard Form" , *Journal of Numerische Mathematik.*, vol. 11, pp. 99110, 1968.

[46] H. K. Wimmer, "Extremal Problems for Holder Norms of Matrices and Realizations of Linear Systems," *SIAM J. Matrix Anal. Appl.*, vol. 9, no. 3, July 1988.

[47] A. J. Paulraj, R. Nabar and D. Gore, *Introduction to Space-Time Wireless Communications*, New York: Cambridge Univ. Press, 2003.

[48] A. Forenza and R. W. Heath, Jr., "Benefit of Pattern Diversity via Two-Element Array of Circular Patch Antennas in Indoor Clustered MIMO Channels," *IEEE Trans. Commun.*, vol. 54, no. 5, pp. 943-954, May 2006.

[49] T.-J. Shan, M. Wax and T. Kailath, "On spatial smoothing for directional-of-arrival estimation of coherent signals" *IEEE Trans. Acoust., Speech, Signal Proces.*, vol. ASSP-33, no. 4, pp. 806-811, Aug. 1985.

[50] G. H. Golub and C. F. Van Loan, *Matrix Computations*, John Hopkins University Press, Baltimore MA, 1989.

[51] D. Tse and P. Viswanath, *Fundamentals of Wireless Communication,* Cambridge University Press, Cambridge U. K., May 2005.

[52] B. Hassibi and B. Hochwald, "How much training is needed in multiple-antenna wireless links?" *IEEE Trans. Inform. Theory*, vol. 49, pp. 951963, Apr. 2003.

[53] S. Yang, Y. Zhaot, "Channel Estimation Method for 802.11a WLAN with Multiple-Antenna," *10th Asia-Pacific Conf. on Commun. and 5th Inter. Symp. on Multi-Dimensional Mobile Commun.*, pp. 297-300, 2004.

[54] Y. Nakaya., T. Toda., S. Hara and Y. Oishi, "MIMO Receiver Using an RF-Adaptive Array Antenna with a Novel Control Method," *IEEE Inter. Conf. on Commun.*, pp. 2568-2572, 2004.

[55] I. Barhumi, G. Leus, and M. Moonen, "Optimal Training Sequences for Channel Estimation in MIMO OFDM Systems in Mobile Wireless Channels," *Int. Zurich Seminar Broadband Commun., Zurich, Switzerland*, pp. (441)(446), 2002.

[56] A. V. Zelst and T. C. W. Schenk, "Implementation of a MIMO OFDM-Based Wireless LAN System" *IEEE Trans. Sign. Process.*, vol. 52, no. 2, pp. 483-494, Feb. 2004.

[57] S. M. Kay, *Fundamentals of Statistical Signal Processing: Estimation Theory*, Upper Saddle River, N.J., USA: Prentice Hall, 1993.

[58] O. Edfors, M. Sandell, J.-J. van de Beek, S. K. Wilson and P. O. Borjesson, "OFDM Channel Estimation by Singular Value Decomposition" *IEEE Trans. Commun.*, vol. 46, no. 7, pp. 931939, July 1998.

[59] J. J. van de Beek, O. Edfors, M. Sandell, S. K. Wilson, and P. O. Borjesson, "On channel estimation in OFDM systems," *IEEE Vehi. Tech. Conf.*, pp. 815819, 1995.

[60] W. Xiang, D. Waters, T. G. Pratt, J. Barry and B. Walkenhorst, "Implementation and Experimental Results of a Three-Transmitter Three-Receiver OFDM/BLAST Testbed" *IEEE Commun. Mag.*, vol. 42, no. 12, pp. 88-95, Dec. 2004.

[61] IEEE P802.16a/D4-2002, "Part 16: Air Interface for Fixed Broadband Wireless Access Systems."

[62] G. Andrijevic, H. Magnusson, A. Klimpe and H. Olsson, "Multistandard Receiver for Home Networking and Digital Media," *IEEE Norchip Conf.*, pp. 131-134, 2004.

[63] Digital Control 5-Bit Phase shifter, part No. RFPSHT0204D *RF-LAMBDA: www.rflambda.com*

[64] SMA Power Divider 4-Way 2-4 GHz, part No. MP8204-4 *S. M. Electronics L.L.C.: www.smelectronics.us*

[65] SMA Power Divider 8-Way 0.8-2.5 GHz, part No. MP8209-8 *S. M. Electronics L.L.C.: www.smelectronics.us*

[66] Radiowave Propagation Simulator (RPS). *Radioplan: www.radioplan.com*

[67] R. Wilson, "Propagation Losses Through Common Building Materials 2.4 GHz vs 5 GHz," *Magic Networks, Inc.*, Aug. 2002.

[68] J. Jemai, R. Piesiewicz and T. Krner, "Calibration of an Indoor Radio Propagation Prediction Model at 2.4 GHz by Measurements of the IEEE 802.11b Preamble," *IEEE Vehi. Tech. Conf.*, pp. 111-115, Spring 2005.

[69] T. Hult and A. Mohammed, "Assessment of Multipath Propagation for a 2.4 GHz Short-Range Wireless Communication System," *IEEE Vehi. Tech. Conf.*, pp. 544-548, Spring 2007.

[70] L. Roelens, W. Joseph and L. Martens, "Comparison of Path Loss near Homogeneous Medium, Layered Medium and Anatomically Correct Human Model," *IEEE Ant. Propag. Conf.*, pp. 672-675, 2006.